Technical Report Documentation Page

1. Report No.	2. Government Accession No.	3. Recipient's Catalog No.
FHWA/TX-01/1856-2		

4. Title and Subtitle	5. Report Date
LATERAL CONNECTIONS FOR DOUBLE TEE BRIDGES	April 2001
	6. Performing Organization Code

7. Author(s)	8. Performing Organization Report No.
Harry L. Jones	Report 1856-2

9. Performing Organization Name and Address	10. Work Unit No. (TRAIS)
Texas Transportation Institute The Texas A&M University System College Station, Texas 77843-3135	11. Contract or Grant No. Project No. 0-1856

12. Sponsoring Agency Name and Address	13. Type of Report and Period Covered
Texas Department of Transportation Research and Technology Implementation Office P. O. Box 5080 Austin Texas 78763-5080	Research: September 1998-August 2000
	14. Sponsoring Agency Code

15. Supplementary Notes

Research performed in cooperation with the Texas Department of Transportation and the U.S. Department of Transportation, Federal Highway Administration.
Research Project Title: Develop a Method To Tie Double "T" Flanges Together To Get Proper Lateral Load Transfer

16. Abstract

This project developed, analyzed, and tested a method for laterally connecting the edges of double tee members in a bridge. Load tests were conducted on a 27 ft span, two-tee bridge in the laboratory. Static and cyclic loadings were applied. No distress or failures were found in the connections during the testing program. The report reviews connection methods that have been used in the past and recommends a detail for use in TxDOT bridges. Appropriate lateral distribution factors for TxDOT bridges built with the recommended connection are addressed.

17. Key Words	18. Distribution Statement
Restressed, Concrete, Double, Tee, Lateral, Connection, Multibeam, Multi-Beam, Bridge	No Restrictions. This document is available to the public through NTIS: National Technical Information Service 5285 Port Royal Road Springfield, Virginia 22161

19. Security Classif.(of this report)	20. Security Classif.(of this page)	21. No. of Pages	22. Price
Unclassified	Unclassified	114	

LATERAL CONNECTIONS FOR DOUBLE TEE BRIDGES

by

Harry L. Jones
Associate Research Engineer
Texas Transportation Institute

Report 1856-2
Project Number 0-1856
Research Project Title: Develop a Method To Tie Double "T" Flanges Together To Get Proper Lateral Load Transfer

Sponsored by the
Texas Department of Transportation
In Cooperation with the
U.S. Department of Transportation
Federal Highway Administration

April 2001

TEXAS TRANSPORTATION INSTITUTE
The Texas A&M University System
College Station, Texas 77843-3135

DISCLAIMER

The contents of this report reflect the views of the author, who is responsible for the facts and the accuracy of the data presented herein. The contents do not necessarily reflect the official view or policies of the Federal Highway Administration or the Texas Department of Transportation (TxDOT). This report does not constitute a standard, specification, or regulation. Not intended for construction, bidding, or permit purposes. The engineer in charge of the project was Harry L. Jones, P.E. #35066.

ACKNOWLEDGMENTS

This project was sponsored by the Texas Department of Transportation in cooperation with the U.S. Department of Transportation, Federal Highway Administration. The assistance of Jeff Cotham, TxDOT project director, is gratefully acknowledged. The bridge inspections cited in Chapter 1 of this report were performed by Mr. Cotham, who also provided numerous and useful insights into the performance of double tee bridges.

TABLE OF CONTENTS

LIST OF FIGURES viii
LIST OF TABLES xi

CHAPTER 1. INTRODUCTION 1
- REFLECTIVE CRACKING 1
- LATERAL LOAD DISTRIBUTION 4
- CONNECTION COST 5
- EXPERIENCE WITH THE CURRENT TXDOT CONNECTION 5
- IN SEARCH OF A BETTER CONNECTION 5
- REPORT ORGANIZATION 12

CHAPTER 2. METHODS FOR LATERAL CONNECTION OF DOUBLE TEES 13
- SURVEY OF CONNECTION DETAILS 13
  - Parking Structures 13
  - State DOT Bridges 15
- NEW CONNECTION METHOD RECOMMENDATIONS 27
- RECOMMENDED “SIMPLE” CONNECTION DETAIL 28
- RECOMMENDED “CONTINUOUS” CONNECTION DETAIL 30

CHAPTER 3. PILOT TESTS 33
- DOUBLE TEE BRIDGE TESTS 33
- CONNECTION BEAM TESTS 48

CHAPTER 4. NUMERICAL SIMULATION 57
- MULTI-BEAM BRIDGE MODEL 57
- DOUBLE TEE BRIDGE TESTS ON THE PILOT BRIDGE 62
- ASSESSMENT OF ANALYTICAL MODEL PREDICTIONS 68

CHAPTER 5. ADDITIONAL BRIDGE MODEL TESTS 69
- DOUBLE TEE BRIDGE MODEL DESCRIPTION 69
- INSTRUMENTATION 71
- PROOF TESTS 71
- “SIMPLE” CONNECTION STIFFNESS DETERMINATION 78
- CYCLIC LOAD TESTING 81
- ULTIMATE LOAD TESTS 86

CHAPTER 6. APPLICATION TO TXDOT BRIDGES 87
- LIVE LOAD LATERAL DISTRIBUTION FACTOR 87
- LATERAL CONNECTION DESIGN FORCES 94

REFERENCES 101

LIST OF FIGURES

Figure **Page**

1 Original TxDOT Lateral Connection 2
2 Modified TxDOT Lateral Connection 2
3 Differential Rotation of Tee Flanges 3
4 "Pumping" of Asphalt into Gap 3
5 Deck Cracking – Draw Bridge 8
6 Asphalt Surface Cracking – Quinta Creek Bridge 8
7 Deck Cracking – Oso Creek/SH 44 Bridge 9
8 Asphalt Surface Cracking – Oso Creek/SH 286 Bridge (Overall View) 9
9 Asphalt Surface Cracking – Oso Creek/SH 286 Bridge (Zoomed View) 10
10 Deck Cracking – Morris and Cummings Cut Bridge (Zoomed View) 10
11 Deck Cracking – Morris and Cummings Cut Bridge (Overall View) 11
12 Deck Cracking – Redfish Bay Bridge 11
13 Connection Detail Developed by Martin et al. (First of Two Versions) 14
14 Connection Detail Developed by Martin et al. (Second of Two Versions) 14
15 Connection Detail Developed by PCI 15
16 Connection Detail Used by Nebraska DOT 16
17 Connection Detail Developed by Florida DOT 16
18 Welded Plate Detail by Martin 17
19 Connection Details for Joining of Flanges in Double Tees 18
20 Methodologies for Connecting Multi-Stemmed Precast Members (48 in. Centers) 20
21 Methodologies for Connecting Multi-Stemmed Precast Members (96 in. Centers) 21
22 Methodologies for Connecting Multi-Stemmed Precast Members (60 in. Centers) 22
23 Methodologies for Connecting Multi-Stemmed Precast Members (55 in. Centers) 23
24 Connector Details of Specimens 1A, 1B, and 1C 24
25 Connector Details of Specimen 2A 25
26 Connector Details of Specimens 3A and 3B 26
27 Proposed "Simple" Connection Detail 29
28 Proposed "Continuous" Connection Detail 31
29 Closure Pour in "Continuous" Connection 31
30 Plan View of Double Tee Laboratory Bridge 34
31 Double Tee Laboratory Bridge 34
32 Strain Gages on Connection Plates 35
33 Location of Strain Gages on Connection Plates 36
34 Shear Key 36
35 Loading Points for Tests 46
36 Simulated Wheel Load Applied at Connection II 47

LIST OF FIGURES (Continued)

Figure **Page**

37 Loading at Outside Edge of Tee 49
38 Failed Flange from Loading Outside Flange Edge 50
39 Loading at Center Edge of Tee 50
40 Failed Flange from Center Edge Loading 51
41 “Simple” Connection Test Specimens 51
42 Details of Beam Test Specimens 52
43 Details of “Simple” Connection Used in Beams 53
44 Beam Connection Test in Progress 53
45 Pull-Out of Weld Plate in Beam Connection Test 55
46 Spalling of Cover Concrete in Beam Connection Test 56
47 Typical Multi-Beam Double Tee Bridge 58
48 Modeling of Double Tee Supports 60
49 Force Components Developed is Discrete Connection 60
50 Spring Stiffnesses Used in Modeling Discrete Connection 61
51 Compression Data for Bearing Pad Used in Lab Bridge 63
52 Best Fit Line for Bearing Pad Data 63
53 Plan View of Lab Bridge Model 70
54 Embedded Plate before Connection Made 70
55 Steel Frame Supporting Bridge Model 72
56 Steel Bar Welded into Connection 72
57 Schematic of Load Cell Support System 73
58 Photograph of Load Cell 73
59 Location of Load Cells and Displacement Transducers 74
60 Position of Strain Gages on Shear Key 74
61 Loading Positions for Proof Tests 77
62 Reaction Error Versus Stiffness k_z, Load Position 1 80
63 Reaction Error Versus Stiffness k_z, Load Position 1, with Shear Key 82
64 Shear Key Stress Versus Cycles of Load 84
65 Bar/Plate Connection after Cyclic Loading 85
66 Edge of Flange after Shear Key Removal 85
67 Section of Shear Key 86
68 Load Distribution Factor for Exterior 6 ft. Tees 90
69 Load Distribution Factor for Interior 6 ft. Tees 93
70 Load Distribution Factor for Interior 7 ft. Tees 93
71 Comparison of AASHTO and Multi-Beam Theory Distribution Factors 94
72 Force Components in Bar/Plate Discrete Connection 95
73 Force Components in Shear Key 95
74 Shear Key Moment M_c along Span 97
75 Shear Key Shear F_z along Span 97
76 Maximum M_c in Connection Versus Span 98

LIST OF FIGURES (Continued)

Figure **Page**

77 Maximum F_z in Connection Versus Span.....99
78 Maximum M_c in Shear Key Versus Span.....99
79 Maximum F_z in Shear Key Versus Span 100

LIST OF TABLES

Table **Page**

1 Construction and Inspection Results for Bridges 6
2 Total Shear Strength 27
3 Stresses in Connection Plates for Load Position A 38
4 Stresses in Connection Plates for Load Position B 39
5 Stresses in Connection Plates for Load Position C 40
6 Stresses in Connection Plates for Load Position D 41
7 Stresses in Connection Plates with Shear Key for Load Position A 42
8 Stresses in Connection Plates with Shear Key for Load Position B 43
9 Stresses in Connection Plates with Shear Key for Load Position C 44
10 Stresses in Connection Plates with Shear Key for Load Position D 45
11 Summary of Test Results 54
12 Section Properties of TxDOT Standard Double Tees with 6 in. Thick Flange 58
13 Comparison of Computed and Measured Plate Stress, Load Position A 64
14 Comparison of Computed and Measured Plate Stress, Load Position B 65
15 Comparison of Computed and Measured Plate Stress, Load Position C 66
16 Comparison of Computed and Measured Plate Stress, Load Position D 67
17 Predicted and Measured Reaction Forces of Individual Tees 76
18 Variation of Reactions with Load Position 78
19 Computed K_z of Discrete Connection by Load Case 80
20 Computed Kphi of Shear Key by Load Case 82
21 Bridges Used in Analyses 89
22 Span Lengths Used in Analyses 90
23 Computed Lateral Distribution Factors 91
24 Maximum Connection and Shear Key Forces 98
25 Recommended Connection and Shear Key Design Forces 100

CHAPTER 1. INTRODUCTION

The prestressed concrete double tee bridge is a potentially attractive structure for short to medium range spans where speed of construction is an issue. Additionally, it may be a viable alternative to the pan form bridge for use on off-system roads as the cost of this labor-intensive type of construction escalates. The Texas Department of Transportation currently has a set of standard double tee cross sections that can be produced by some Texas fabricators. These standards are under review and revision by TxDOT, and the research reported herein was carried out to assist TxDOT in developing more economical and efficient double tee bridge designs. Specifically, the research addresses methods of connecting the flanges of adjacent tees which enable them to share and distribute wheel loads.

Figs. 1 and 2 show the two connection details that have been used by TxDOT, with that in Fig. 2 being a more recent variation on the vertical plate detail in the first figure. Both connection types are grouted after the connecting plates or angles are field welded in place. These connections were originally spaced longitudinally along the flange edges at 10 ft. centers, and more recently the spacing has been reduced to 5 ft. on center. While the connections seem to have performed as intended, with no particular problems reported in the connections themselves, there remain several issues this research attempts to address, which are summarized below.

REFLECTIVE CRACKING

Reflective cracking is the formation of longitudinal cracks in the bridge riding surface over the juncture of adjacent double tee flanges. It can occur in either an asphalt wearing surface or composite concrete deck, with cracks tending to run the full length of the span. In the case of an asphalt surface, the primary mechanism driving the formation of these cracks is differential transverse rotation between the flanges of adjacent tees. Fig. 3 depicts the effect, drawn to an exaggerated scale. Rotations like either (a) or (b) occur in a typical structure due to vehicular loads, although at different locations in a bridge. A lateral connection like those in Figs. 1 and 2 is incapable of providing any significant reduction in the differential rotation, and longitudinal cracks are formed along the joint. In addition, the gap between abutting flange edges presents a recess into which the asphalt is “pumped” under the pressure of tires on passing trucks (see Fig. 4), with wider gaps producing more severe cracking and deterioration.

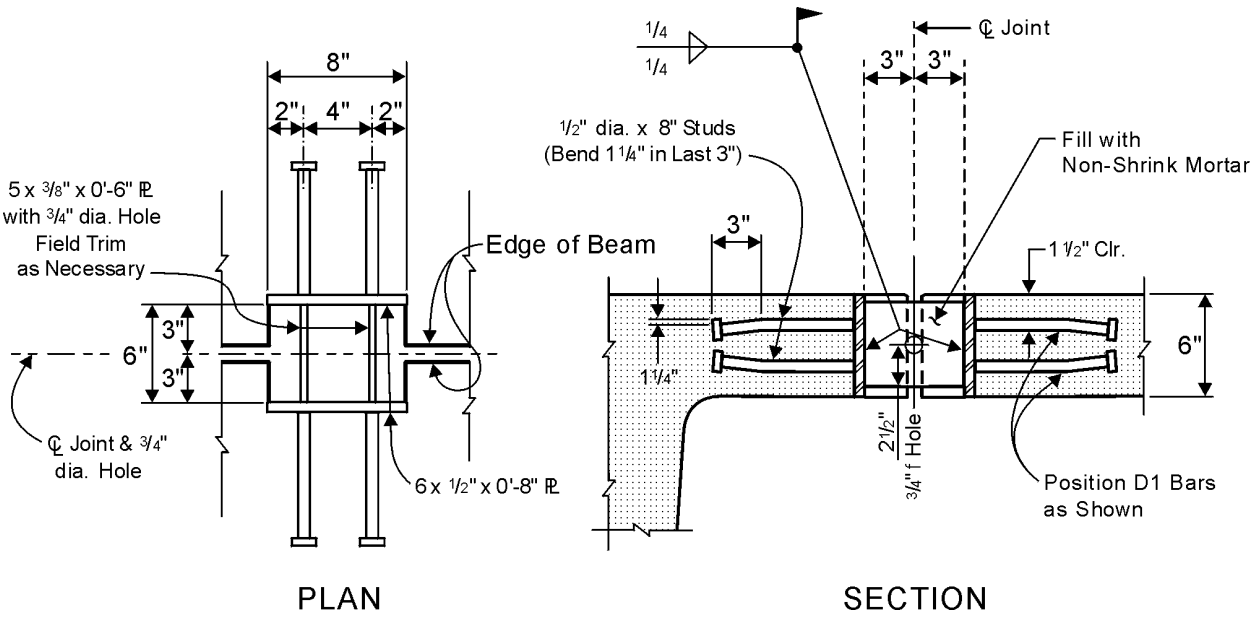

Figure 1. Original TxDOT Lateral Connection.

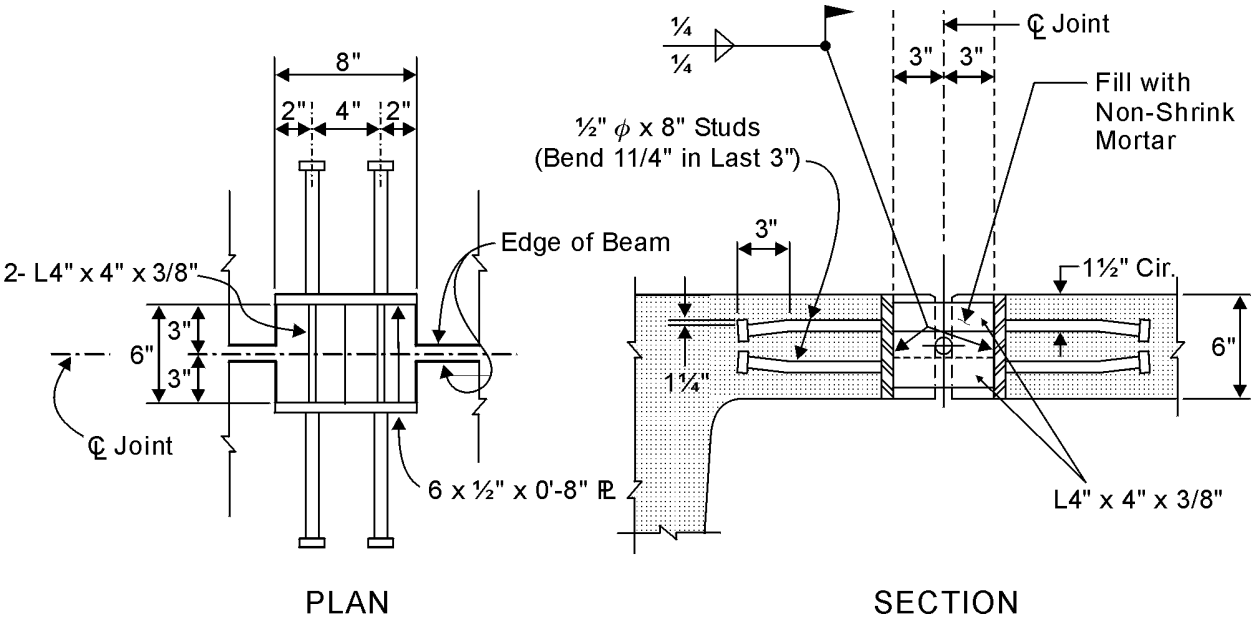

Figure 2. Modified TxDOT Lateral Connection.

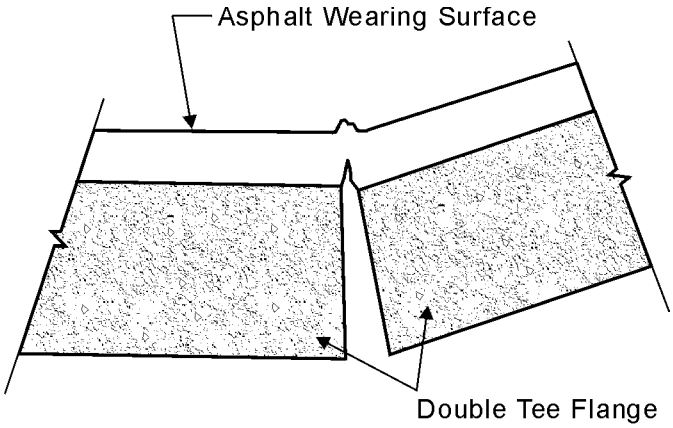

Figure 3. Differential Rotation of Tee Flanges.

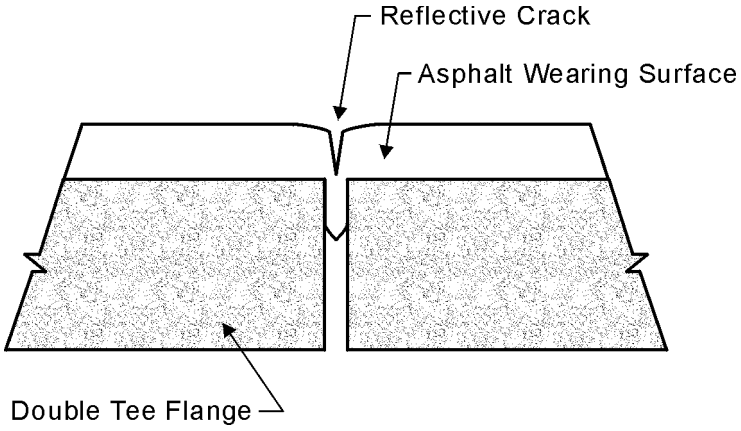

Figure 4. "Pumping" of Asphalt into Gap.

With composite concrete decks, the deck offers substantial resistance to differential rotation at the joint and as a result, wheel loads on the bridge lead to transverse bending moment in the slab over the abutting edges of the flange, which can produce stresses large enough to cause longitudinal cracking in the deck. This same mechanism is at work in prestressed concrete box beam structures with composite deck, and the effect is documented in the work of Jones [1999]. Lateral connections like those in Figs. 1 and 2 have negligible effect on transverse moment, which develops in the deck and hence on the propensity for longitudinal cracks to form.

Whether concrete deck or asphalt wearing surface, the occurrence of differential rotation shown in Fig. 3 between adjacent tee flanges drives the cracking process. As will be shown later, a discrete connection scheme along the lines of those considered practical can not significantly reduce the differential rotation and hence the tendency for cracking. The connection can, however, temper the effects of asphalt pumping by preventing or at least reducing the separation of adjacent flange edges under load. The addition of a shear key further improves the situation. The case of composite concrete deck is a difficult one. The box beam experience cited above found no suitable means of controlling and reducing the transverse bending moment to a level that precludes the formation of cracks, nor could one be found for double tees without resorting to either transverse post-tensioning or substantial cast-in-place elements, both deemed impractical for double tee use.

LATERAL LOAD DISTRIBUTION

Flanges of adjacent tees in bridges with asphalt wearing surface connect laterally to tie the superstructure together and for the purpose of transmitting wheel loads applied on one tee to adjoining tees. In this way, the maximum traffic-induced bending moment a single double tee beam must resist is reduced, leading to more efficient and economical structures. Presumably, as the lateral connections are made more substantial, greater load sharing would occur. There is obviously a trade-off between improved load sharing (reflected in a smaller live load lateral distribution factor to use in designing the tee) and the expense of more/larger lateral connections.

Bridges with composite concrete deck slab are more problematic. Our analysis indicates the discrete connection has negligible effect on lateral distribution of wheel loads in the presence of a deck slab. Thus, their use with deck slab would have to be justified on some other basis.

CONNECTION COST

Lateral connections between flanges are not an insignificant cost. The use of skilled tradesmen such as certified welders is a principal contributor to the cost, but the speed with which a connection can be installed is also important, though more difficult to quantify. The search for an improved lateral connection was influenced to some degree by a desire to reduce the cost relative to the current connection while at the same time having sufficient strength to resist the forces generated in it by vehicular loads.

EXPERIENCE WITH THE CURRENT TxDOT CONNECTION

In 1997, TxDOT personnel inspected 15 double tee bridges located in south Texas on SH and FM roadways [Cotham, 1997]. Some were situated on the coast where saltwater exposure was present. Studies considered both asphalt surface and composite concrete deck structures. Inspections included examination of longitudinal cracking and checking for signs of corrosion or failure in the connections. Table 1 contains information on the construction and inspection results for each bridge. Figs. 5 through 12 are photographs of the longitudinal cracking encountered on some of the bridges.

The inspections revealed no serious structural defects. Longitudinal cracking was characterized as slight, moderate, and large. All but two of the bridges had full span length cracks. The two without visible cracks were of the asphalt overlay type. Five had “slight” cracking, with three of those being asphalt overlay. An additional five had cracking characterized as “moderate” of which one was asphalt. “Large” cracks were found on three bridges of which two had asphalt surfaces. In four cases, severity of cracking had already triggered maintenance activities on the bridge riding surface.

IN SEARCH OF A BETTER CONNECTION

The above discussion suggests that the ideal lateral connection would possess the following characteristics:

- inexpensive and quick to install,
- provide good lateral distribution of wheel loads, and
- eliminate longitudinal cracking.

As one might suspect, and subsequent chapters of this report document, no single connection can do all of these things well. In addition, the case of composite concrete deck slab presents a

Table 1. Construction and Inspection Results for Bridges.

Item No.	Year Built	Structure Name	County	Near City	Highway	O.A. Length ft.	Span Lengths ft.	O.A. Width ft.	Beam Widths ft.	Stem Depth in.	Flange Thick in.	Asph or Concr	O'lay Thick in.
1	1988	Cayamon Creek	Nueces	San Patricio	FM 666	280	7 @ 40'	46	8-8-7-7-8-8	22	3	Conc	5.5
2	1988	Cayamon Creek Trib	Nueces	San Patricio	FM 666	600	12 @ 50'	46	8-8-7-7-8-8	30	3	Conc	5.5
3	1988	Draw	Nueces	San Patricio	FM 666	120	3 @ 40'	46	8-8-7-7-8-8	22	3	Conc	5.5
4	1988	Draw	Nueces	San Patricio	FM 666	80	2 @ 40'	46	8-8-7-7-8-8	22	3	Conc	5.5
5	1988	Quinta Creek	Nueces	Orange Grove	FM 624	90	2 @ 45	46	8-8-7-7-8-8	30	6	Asph	2.0
6	1995	Pintas Creek	Nueces	Banquete	FM 666	120	3 @40	36	6-6-6-6-6-6	22	6	Asph	2.0
7	1988	Radicha Creek	Kleberg	Kingsville	FM 772	120	3 @ 40	36	6-6-6-6-6-6	22	6	Asph	2.0
8	1986	Salado Creek	Kleberg	Riviera	SH 285	160	4 @ 40	46	8-8-7-7-8-8	22	6	Asph	3.5
9	1990	Oso Creek	Nueces	Robstown	SH 44	150	3 @ 50	40	8-8-8-8-8	22?	3	Conc	5.5
						(130)							
10	1988	Oso Creek	Nueces	Corpus Christi	SH 286	360	9 @ 40	46	8-8-7-7-8-8	22	6	Asph	2.0
						(340)							
11	1990	Peters Swale	San Patricio	Sinton	FM 1945	100	2 @ 50	32	8-8-8-8	30	6	Asph	2.5
12	1992	Mullens Bayou	Refugio	Bayside	FM 136	100	1 @ 45, 1 @ 55	46	8-8-7-7-8-8	30	6	Asph	2.0
13	1993	McCampbell Slough	San Patricio	Ingleside	FM 3512	220	4 @ 55	46	8-8-7-7-8-8	30	6	Asph	2.0
14	1994	Morris & Cum. Cut	Nueces	Aransas Pass	SH 361	440	8 @ 55	46	7-7-6-8*-6-6-7	30	3	Conc	5.5
						(415)							
15	1995	Redfish Bay	Nueces	Aransas Pass	SH 361	2090	38 @ 55	46	7-7-6-8*-6-6-7	30	3	Conc	5.5
						(2020)							

Table 1. Construction and Inspection Results for Bridges (Continued).

Item No.	AADT	Observed Traffic	Structure Name	Deck Cracks ?	Cracks Patched?	Connectors			Over Perm Water ?	Other Comments:
						Used?	Cover Cond.	Rust?		
1	1350	Hvy,Trk	Cayamon Creek	mod @ flng jt	No	No	n/a	n/a	No	lots of movement under truck loads
2	1350	Hvy,Trk	Cayamon Creek Trib	mod @ flng jt	No	No	n/a	n/a	No	lots of movement under truck loads
3	1350	Hvy,Trk	Draw	mod @ flng jt	No	No	n/a	n/a	No	lots of movement under truck loads
4	1350	Hvy,Trk	Draw	mod @ flng jt	No	No	n/a	n/a	No	lots of movement under truck loads
5	3400	mod	Quinta Creek	small @ flng	Yes	Yes	some uncov	surface	Fresh	less movement
6	660	mod	Pintas Creek	very small	No	Yes	some uncov	surface	No	less movement
7	400	low	Radicha Creek	not visible	No	Yes	Good	no	Salt	no joints in rail or deck
8	3300	high	Salado Creek	slight @ 3 jts	No	Yes	some uncov	surface	No	not a lot of bounce at shoulder during loading
9	9300?	light	Oso Creek	slight	No	No	n/a	n/a	fresh	SEJ full of debris
10	3300	mod	Oso Creek	large	Yes	Yes	some uncov	surface	brack	#5 hold downs, rusty stains on bot of stems, flngs
11	1100	mod	Peters Swale	not visible	No	Yes	Good	no	fresh	leakage at joints, white staining
12	2200	hvy	Mullens Bayou	large	Yes	Yes	Thin, hnycomb	surface	brack	honeycomb stem open, honeycomb conn patch - can see transv plts
13	700	light	McCampbell Slough	mod	Yes	Yes	non-uniform	pitted	fresh	locked up at abut, inter joints
14	5500	hvy	Morris & Cum. Cut	large	No	No	n/a	n/a	Salt	cracks in deck at flng jts and over stems, pads hanging over cap
15	5500	hvy	Redfish Bay	slight	No	No	n/a	n/a	Salt	mixed pad sizes at same bt

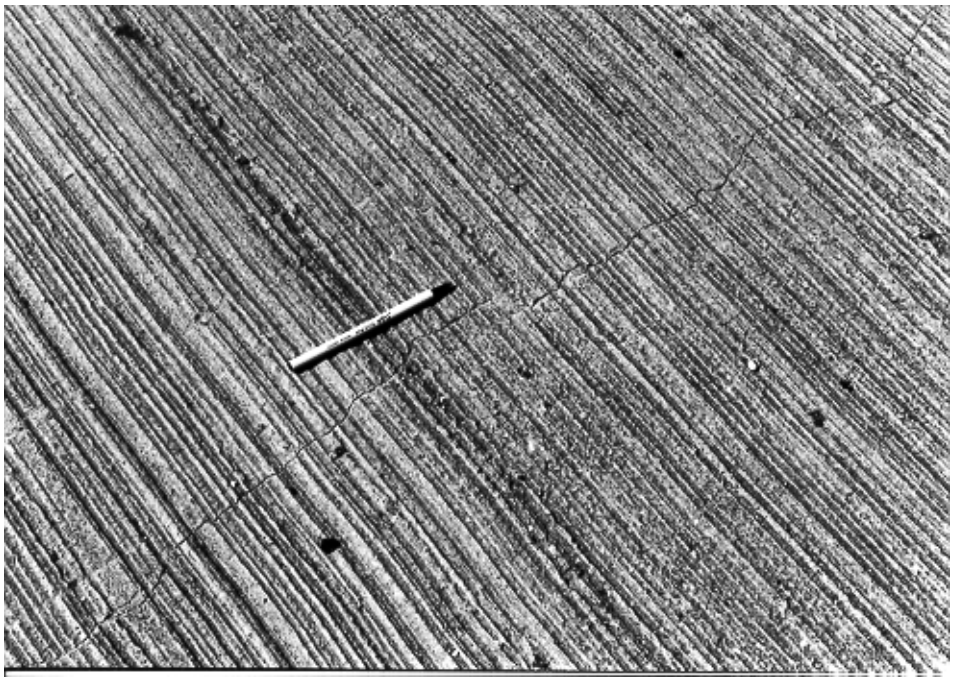

Figure 5. Deck Cracking – Draw Bridge.

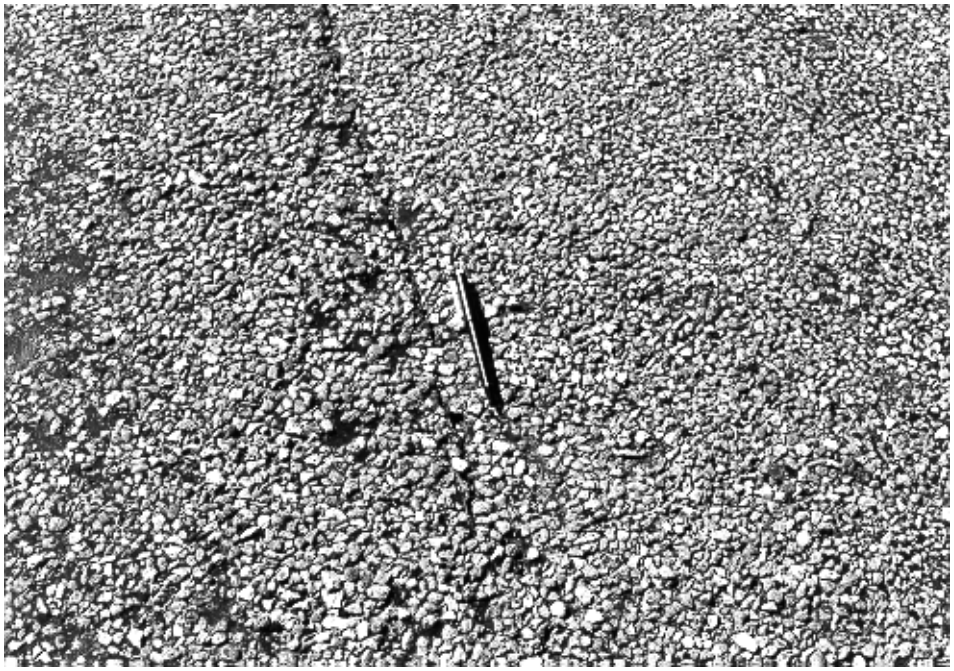

Figure 6. Asphalt Surface Cracking – Quinta Creek Bridge.

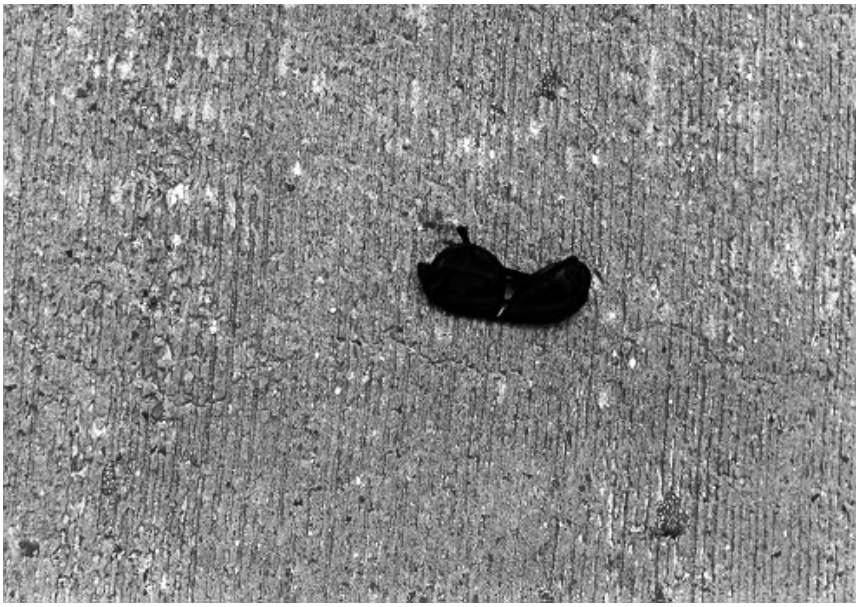

Figure 7. Deck Cracking – Oso Creek/SH 44 Bridge.

Figure 8. Asphalt Surface Cracking – Oso Creek/SH 286 Bridge (Overall View).

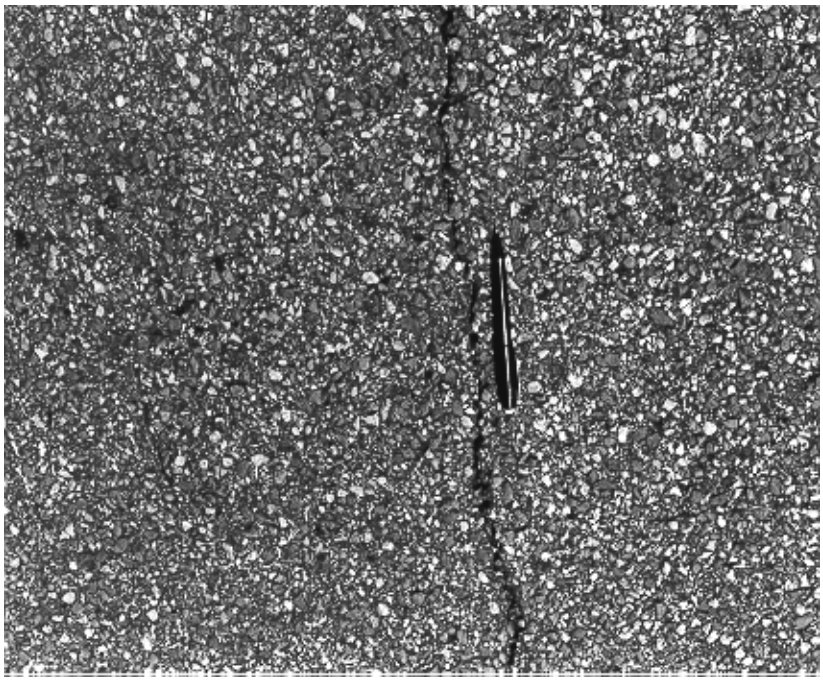

Figure 9. Asphalt Surface Cracking – Oso Creek/SH 286 Bridge (Zoomed View).

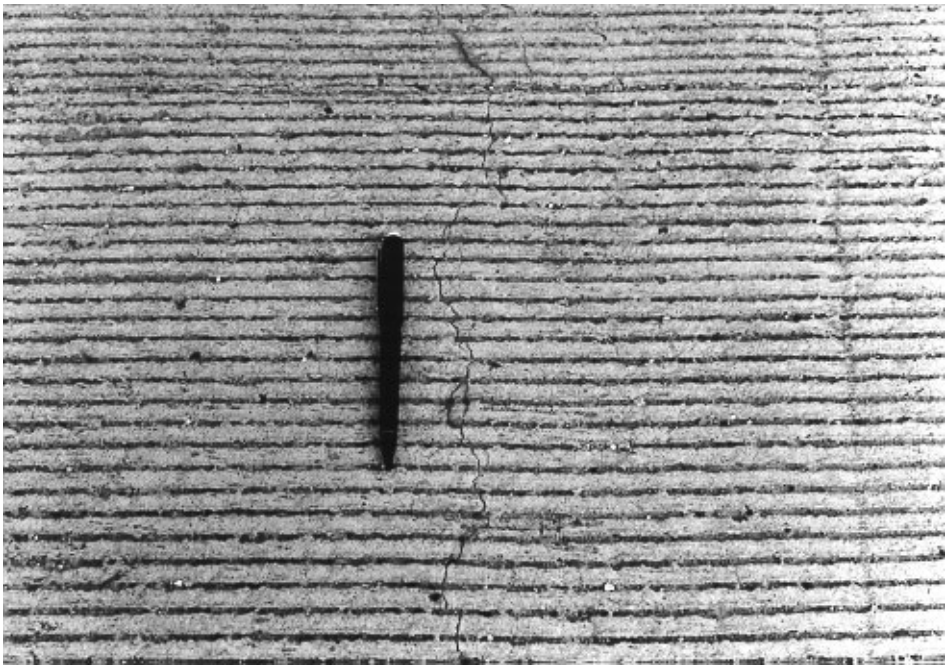

Figure 10. Deck Cracking – Morris and Cummings Cut Bridge (Zoomed View).

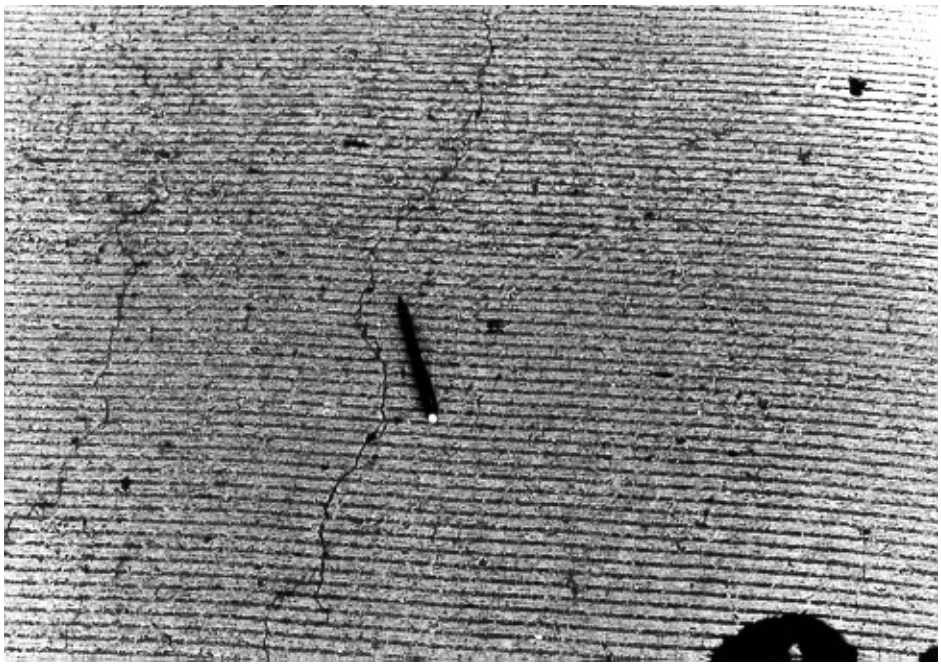

Figure 11. Deck Cracking – Morris and Cummings Cut Bridge (Overall View).

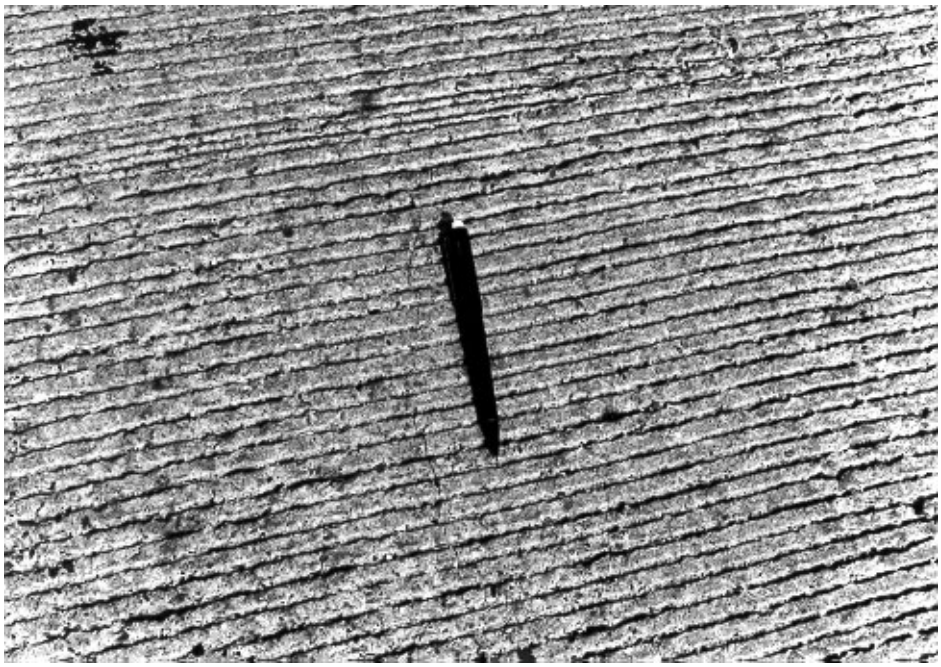

Figure 12. Deck Cracking – Redfish Bay Bridge.

different set of conditions than found in bridges equipped with discrete connections like those of Fig. 1 or 2 and an asphalt wearing surface. Chapter 2 addresses lateral connection in these two different types of construction, and recommendations for each type are offered.

REPORT ORGANIZATION

Briefly, this report is organized into six chapters. Chapter 2 reviews details for lateral connection of double tees found in the literature and recommends one for further evaluation on bridges with asphalt wearing surfaces. A connection detail for use with composite concrete deck is also presented, but no development or testing was performed on this connection. Chapter 3 describes a series of pilot tests. A short span, full-scale bridge model constructed with the current TxDOT connection detail was subjected to a series of loads and data collected on the forces in the connections. These data were used in an effort to validate an analytical model for predicting connection forces as well as other aspects of behavior of the double tee bridge. Also described in this chapter are the results of tests conducted on beams joined with the discrete connection recommended for use in double tee bridges with asphalt wearing surface. Chapter 4 introduces the analytical model used to predict the behavior of double tee bridges and their connections. Chapter 5 presents the results of extensive load tests on a new full-scale bridge whose tees were joined by the new discrete connection recommended in Chapter 2. Finally, Chapter 6 presents recommendations on the forces to be used in designing the discrete connections and on the live load distribution factors appropriate for this type of bridge.

CHAPTER 2. METHODS FOR LATERAL CONNECTION OF DOUBLE TEES

This chapter presents a summary of information developed on methods of connecting the edges of flanges in prestressed concrete double tee bridges to ensure that adequate lateral transfer of wheel loads takes place. The data presented come primarily from a survey of literature on connections for precast concrete elements and transportation structures, along with information gathered through telephone conversations with transportation officials in various states concerning their experiences with double tee bridges. After discussion of the merits of various connection types, recommendations are presented for connections that should be investigated further for possible use in TxDOT bridges.

SURVEY OF CONNECTION DETAILS

Parking Structures

Prestressed concrete double tees are most widely used in building structures. Among these, parking garages have conditions which loosely approximate those found in bridges in that vehicular wheel loads are to be transferred between adjacent units. In order to accomplish this, and also in some cases for seismic considerations, various schemes have been developed for tying adjacent flanges together. Figs. 13 and 14 show two details cited by Martin et al. [1983]. Each of these is typically spaced at 4–6 ft. centers along the common edge between adjacent tee units and involves no grouting. While relatively inexpensive to fabricate and install, there are little or no data on their performance under long-term HS-20 truck traffic. Fig. 15 shows another detail, developed by the Prestressed Concrete Institute (PCI) and described in PCI [1998], which offers a calculation procedure for sizing the 12 in. anchor bars and determining the spacing of connections along the edge. The spacing calculation is somewhat dubious in that it is based on the shear strength of the flange concrete and is not related to the vertical wheel force which must be transmitted across the joint. All three connections cited in this section are used without grouting of the joint and may involve the use of an asphalt wearing surface placed on the tees.

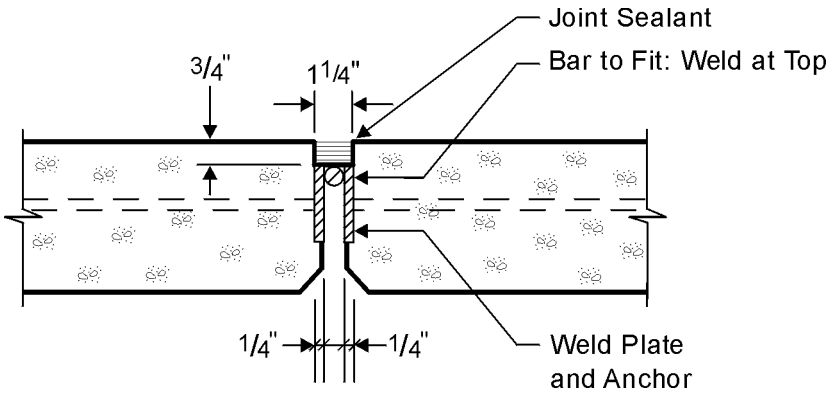

Figure 13. Connection Detail Developed by Martin et al. (First of Two Versions).

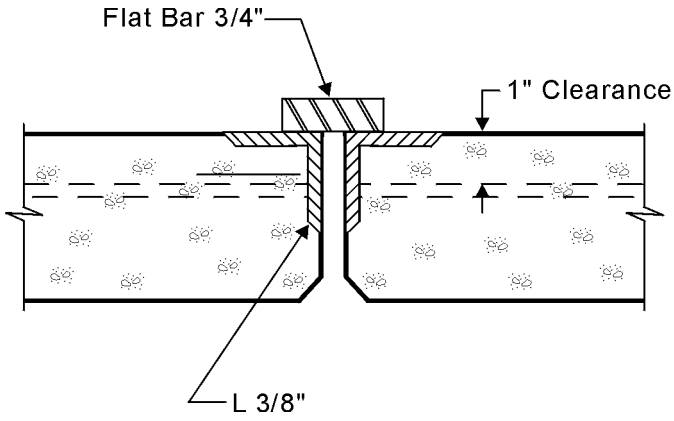

Figure 14. Connection Detail Developed by Martin et al. (Second of Two Versions).

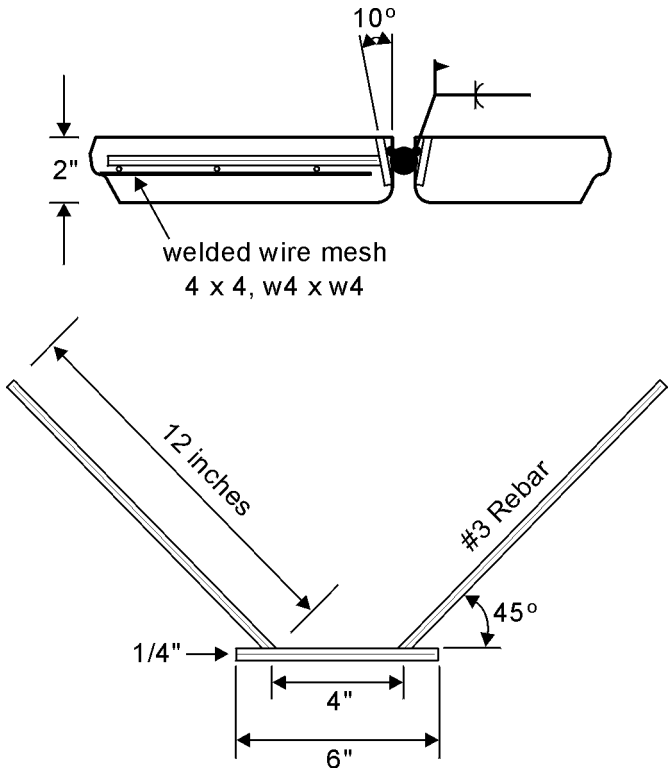

Figure 15. Connection Detail Developed by PCI.

State DOT Bridges

Martin et al. [1983] reports the experience of the Nebraska DOT with the connection shown in Fig. 16 on 27 in. tees having a 5 in. flange thickness and no composite deck slab. These structures were built as replacement bridges on relatively low-volume roads and at the time of the report, had served with no reported problems. Conventional grout was used in the shear keys and the plate/bar lateral connections were spaced at 4–6 ft. centers. At the time of the study, no difficulties were reported after approximately five years of service on a low-volume road with an unknown proportion of truck traffic.

El Shahawy [1990] describes a double tee design developed by Florida DOT for state and interstate class highways with spans up to 80 ft. The lateral connection detail is seen in Fig. 17 and consists of a continuous grouted shear key (“V-joint”) and heavy transverse post-tensioning. A half-scale bridge model was constructed and tested to determine the performance of this type of lateral connection. The model had 3.25 in. thick flanges, and non-shrink portland cement grout with minimum strength of 6,500 psi was used to form the shear key. Post-tensioning was applied

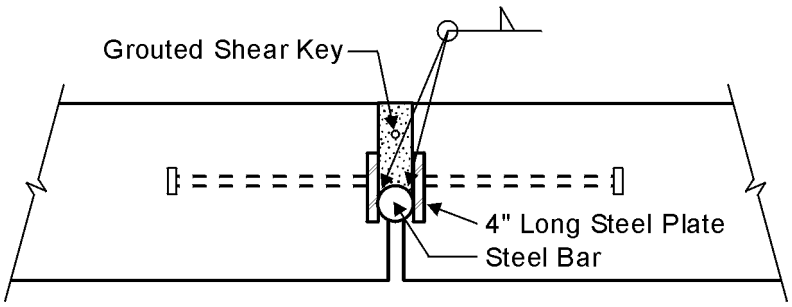

Figure 16. Connection Detail Used by Nebraska DOT.

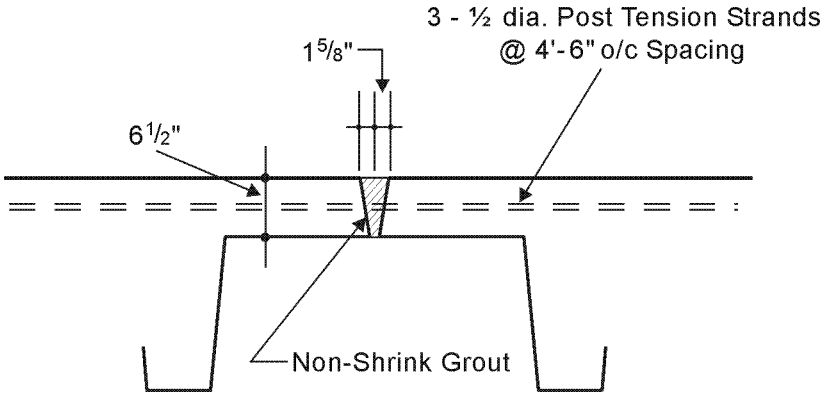

Figure 17. Connection Detail Developed by Florida DOT.

to produce a transverse normal stress across the joint of 150 psi in the central region and 300 psi in the end regions. Various forces were applied to the bridge to cause load transfer across the joint. Deflection measurements taken during tests were used to argue the absence of slip across the joint at this level of prestress. Crack width (joint opening) was also monitored during testing and was found to be small (less than 0.005 in.) at loads equivalent to an HS-20 truck.

El Shahway and Issa [1992] describe load tests on a full-scale bridge similar in detail to that described above. The structure spanned 60 ft., had an overall width of 30 ft., and was

constructed from six 34 in. deep tees with 6.5 in. thick flanges and no wearing surface or composite deck. The V-joint in Fig. 17 joined the edges of adjacent flanges and a transverse post-tensioning level of 200 psi was achieved by placing three 0.5-inch diameter grade 270K strands in 1.25 in. by 3.25 in. galvanized metal ducts. The bridge was loaded with two five-axle trucks, each weighing 204,000 lb, and deflection measurements were taken at ends, quarter points, and mid-span of each beam stem. After comparing measured deflections with theoretical values, the authors conclude "the results strongly suggest practically perfect moment and shear transfer between the double tee beams." In addition, they recommend a minimum of 150 psi transverse post-tensioning for satisfactory performance of their joint. Arockiasamy et al. [1991] reported the results of cyclic loading of the Florida V-joint in a 1:3.5 scale model. While cracking in the longitudinal joints was reported, it appears as if it is related to the magnitude of loads and not the result of degrading performance under the application of two million cycles of load.

Martin et al. [1983] reported the use of the welded plate detail shown in Fig. 18 by a state DOT, but does not identify which state. The spacing of the horizontal steel plates was not given, but likely is in the range of 4–6 ft. as cited earlier in their report. A non-shrink grout was used to fill the key. The same report presents several schemes for forming a lateral connection between precast deck panels. Fig. 19 shows one of those connection details which might have application to joining of flanges in double tees. It also cites the use of epoxy grout for shear keys by railroads on box beam bridges. These railroads report good results with this material. They form shear keys by prefilling the keyway with aggregate and then pouring the liquid epoxy directly into the key, making the installation much faster. They report using aggregate ratios up to 70 percent.

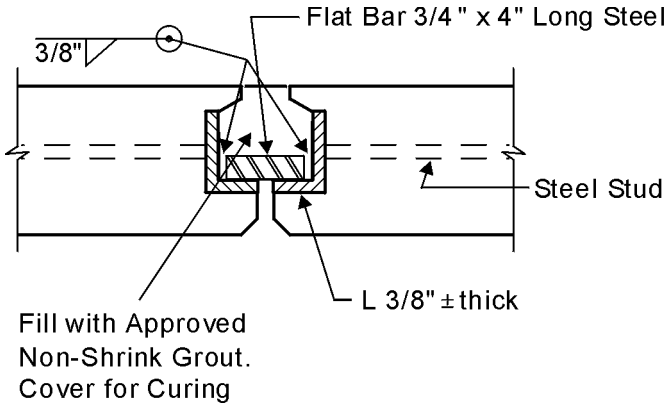

Figure 18. Welded Plate Detail by Martin.

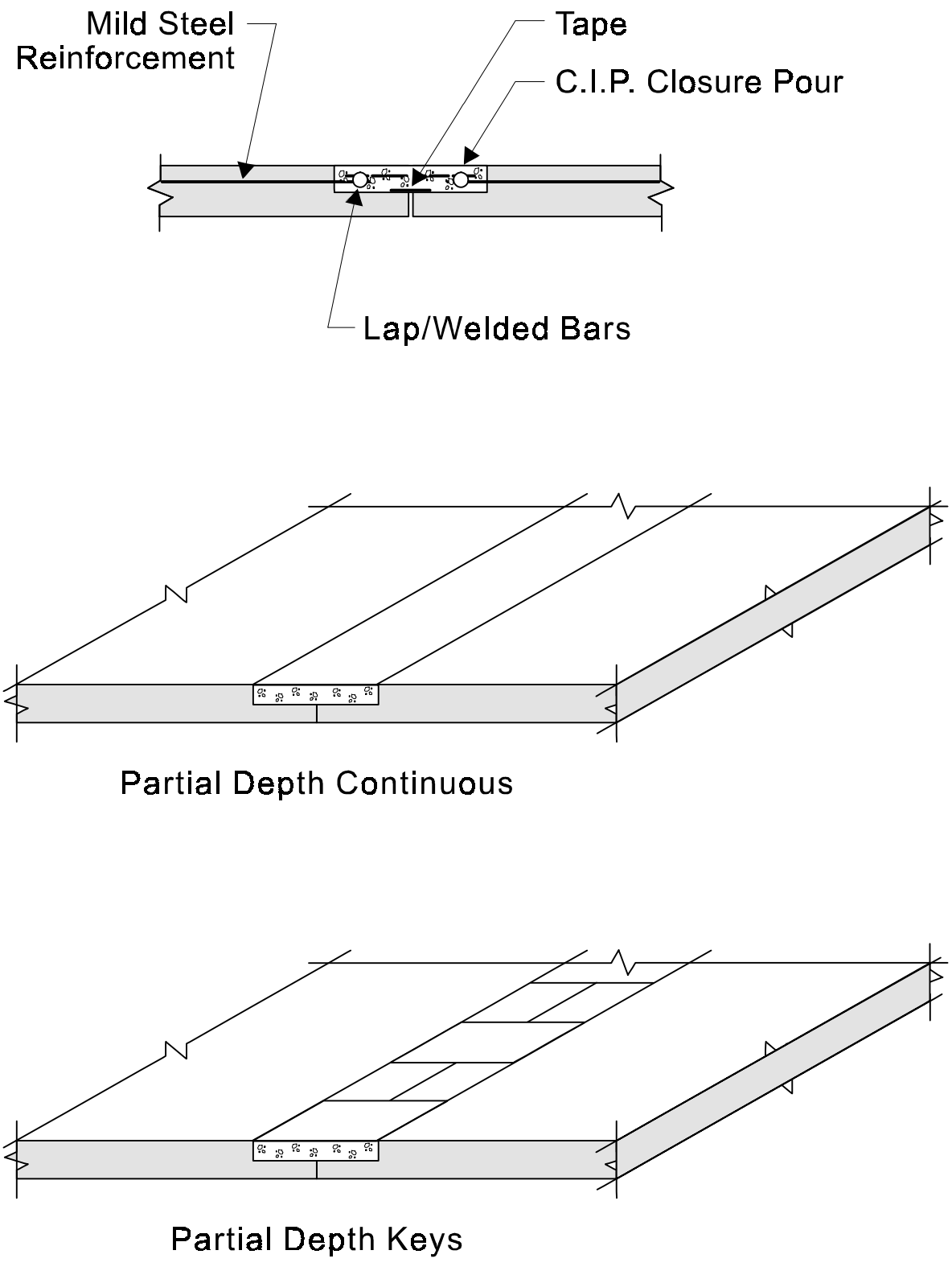

Figure 19. Connection Details for Joining of Flanges in Double Tees.

Stanton and Mattock [1986] reviewed methodologies for connecting multi-stemmed precast members. They point out that the American Association of State Highway and Transportation Officials (AASHTO) presently [1986] provides no guidelines for the design of joints between multi-stemmed members and in practice, grout key size and shapes and connector requirements are determined by using rule-of-thumb methods and historical performance, rather than rational analysis. They collected details which had been proposed or used by transportation agencies and which are shown in Figs. 20 through 23. All are a combination of grouted shear key and steel connectors, which were described as being spaced at 4–8 ft. centers. Stanton and Mattock, as well as others, suggest that the role of the steel connectors is to prevent the joint from separating under the action of loads and temperature change, while the grouted key transfers vertical shear across the joint. A survey of county transportation officials in the state of Washington where these details had been used suggested "a combination of a grout key and welded connectors function very well." No indication of the volume of truck traffic each structure carried was given, although being county roads, it is unlikely that it is comparable to that on interstate highways.

Stanton and Mattock made a significant effort to characterize the strength of the studs used to anchor typical welded connectors (see Figs. 16 and 21). They reviewed available design procedures for estimating the shear and tension resistance of these elements. In addition, they conducted a series of six load tests on the connection details shown in Figs. 24 through 26 to access the effects of the following variables on the response of the connection: (i) location of hardware within the thickness of the slab, (ii) weight of the connector hardware, and (iii) the size and shape of the grouted shear keys. Each test specimen contained a single welded connection between two 5 ft. long by 6 in. thick concrete panels. In some tests there was a grouted shear key and in others no key was poured. All specimens were loaded by a pair of concentrated forces acting on 6×6×1 in. steel plates, both situated on one side of the panel joint. The total shear force acting across the joint was recorded at failure. Table 2 presents those results.

From the results in Table 2 it is obvious the total shear transmitted across a joint is greatly enhanced by the shear key. (Compare 1A, 2A, and 3A with the remaining specimens which had a grouted key.) The welded connections alone sustained between 4,700 and 6,700 lb of shear before failure.

Keyway Detail

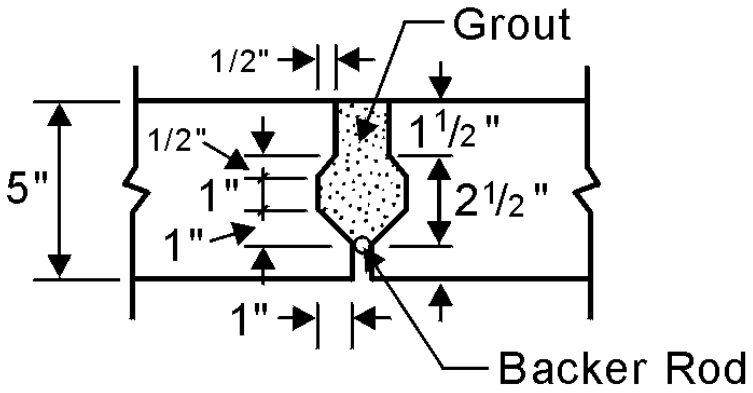

Welded Connections at 48 in. centers

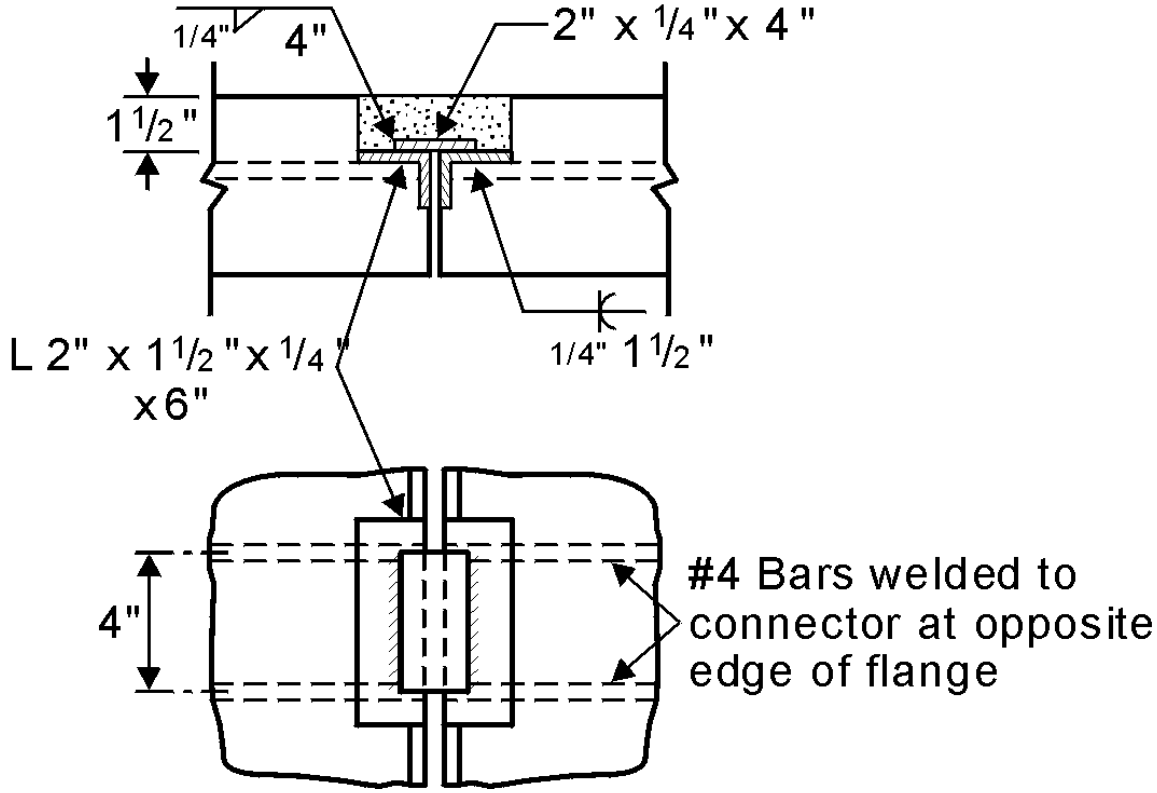

Figure 20. Methodologies for Connecting Multi-Stemmed Precast Members (48 in. Centers).

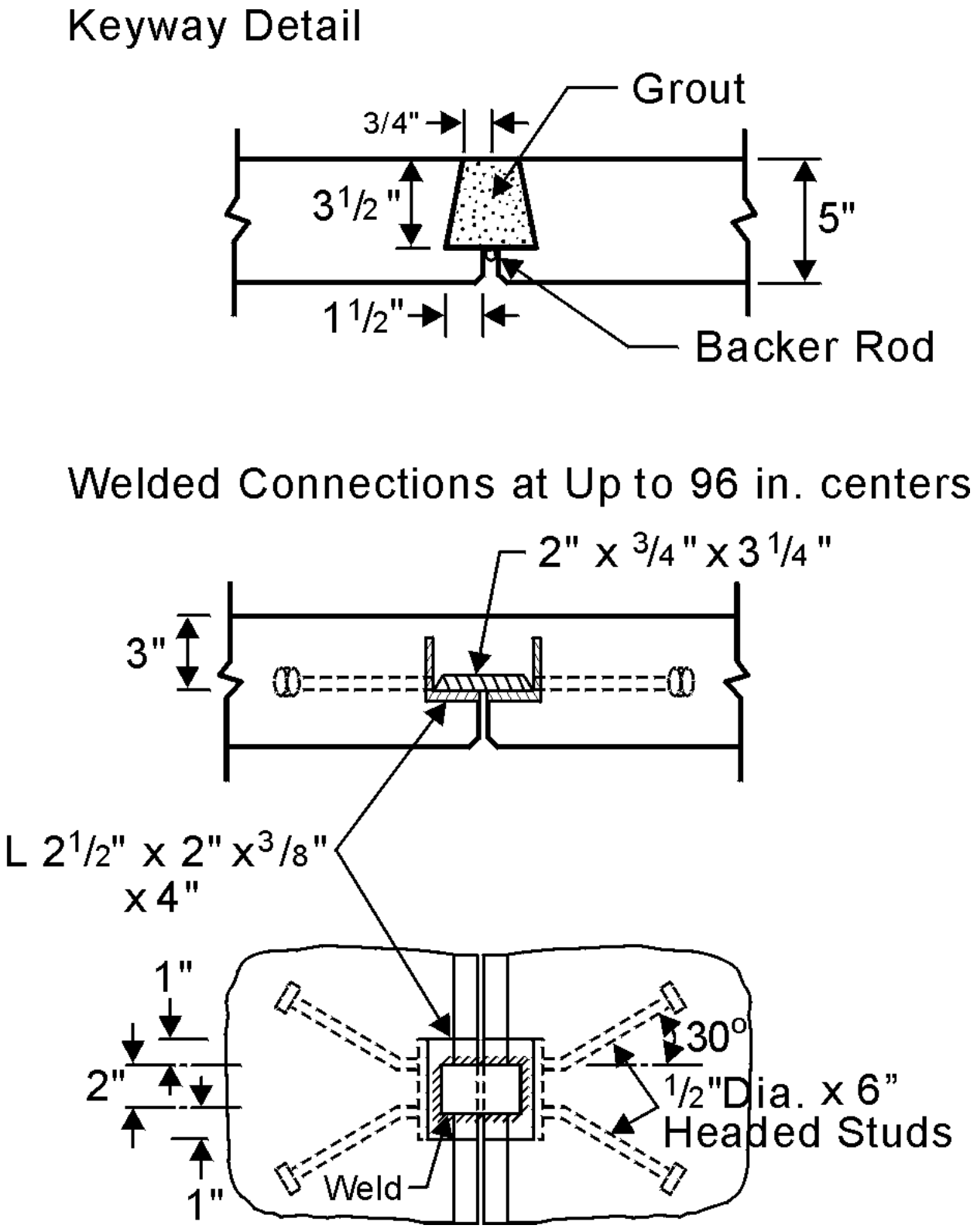

Figure 21. Methodologies for Connecting Multi-Stemmed Precast Members (96 in. Centers).

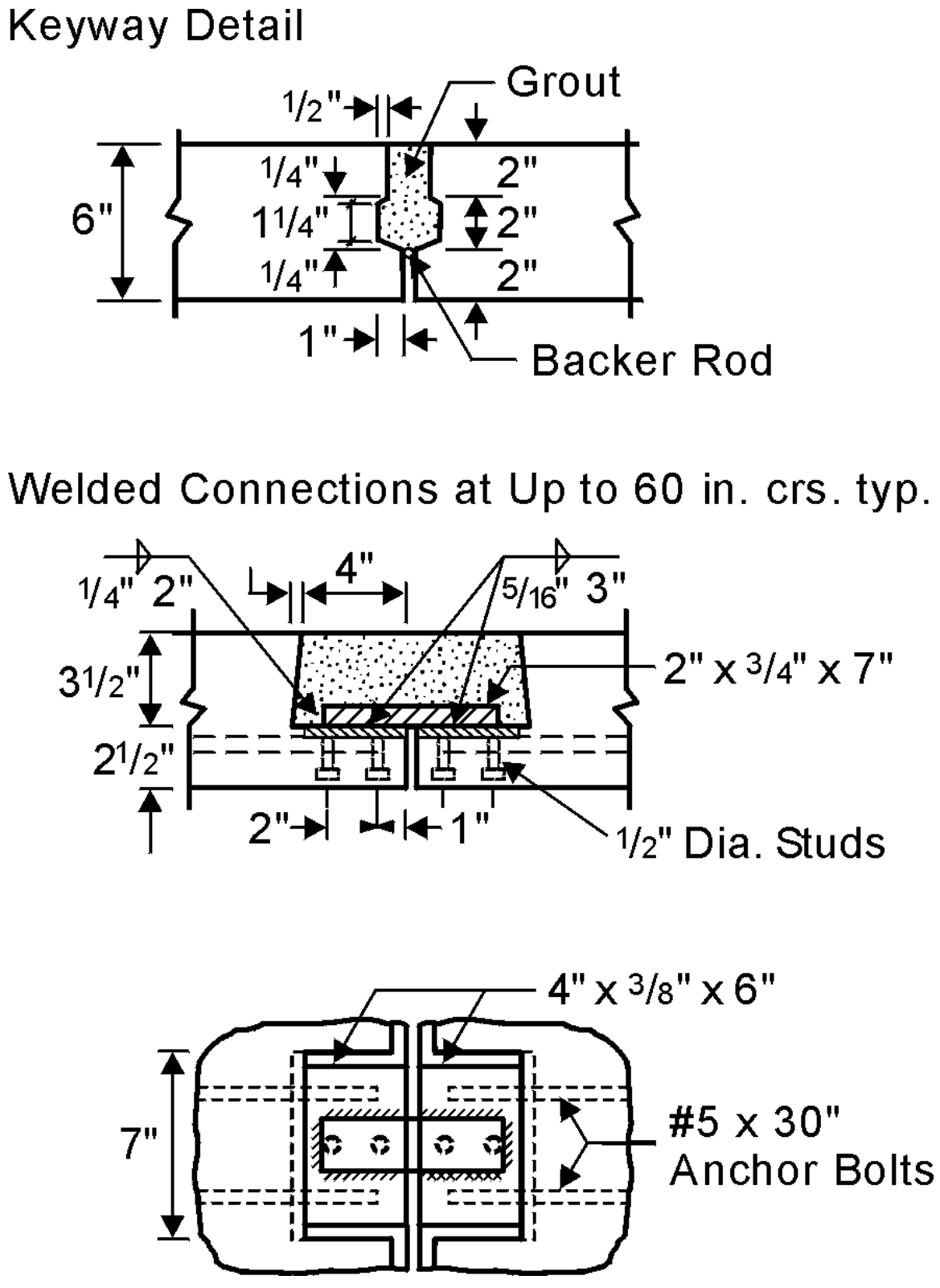

Figure 22. Methodologies for Connecting Multi-Stemmed Precast Members (60 in. Centers).

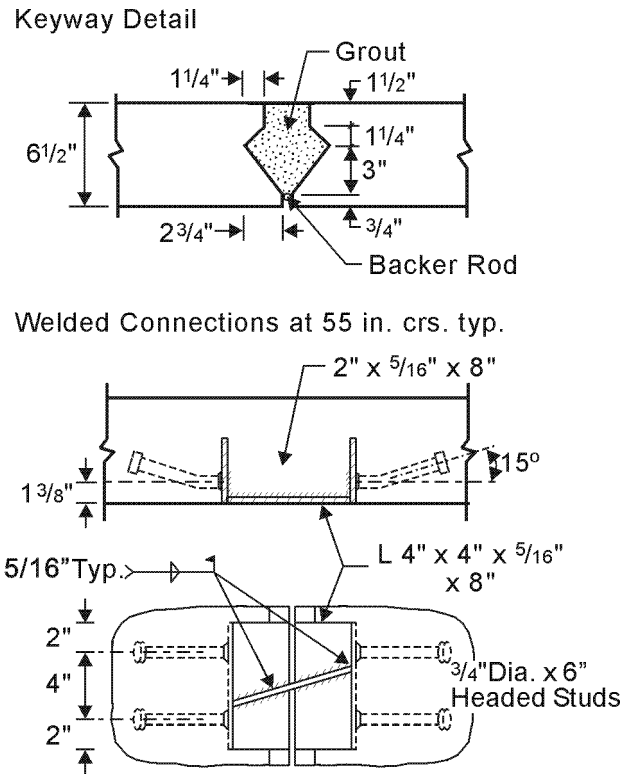

Figure 23. Methodologies for Connecting Multi-Stemmed Precast Members (55 in. Centers).

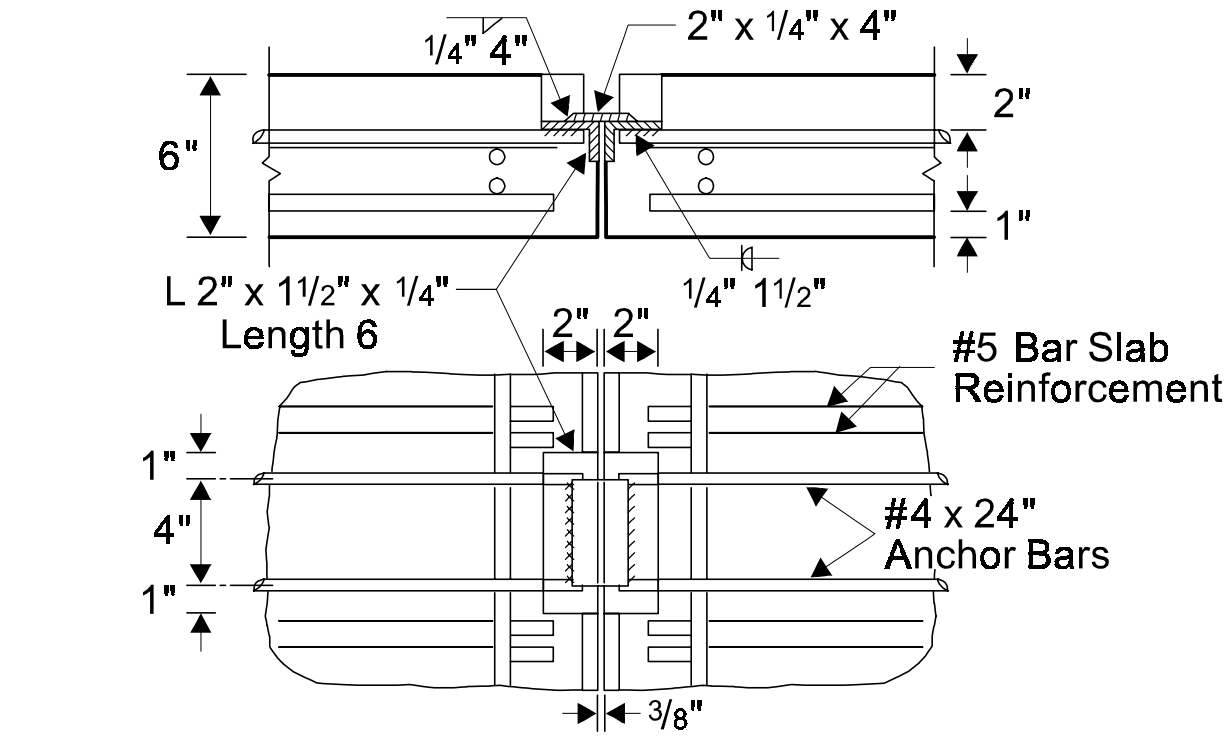

(a) Connector details, specimens 1A, 1B, & 1C

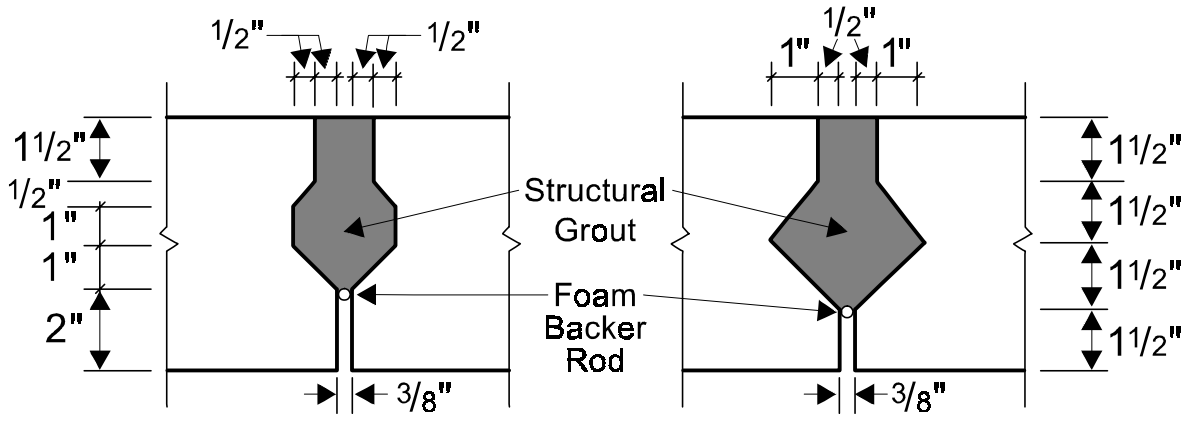

(b) Keyway details

Figure 24. Connector Details of Specimens 1A, 1B, and 1C.

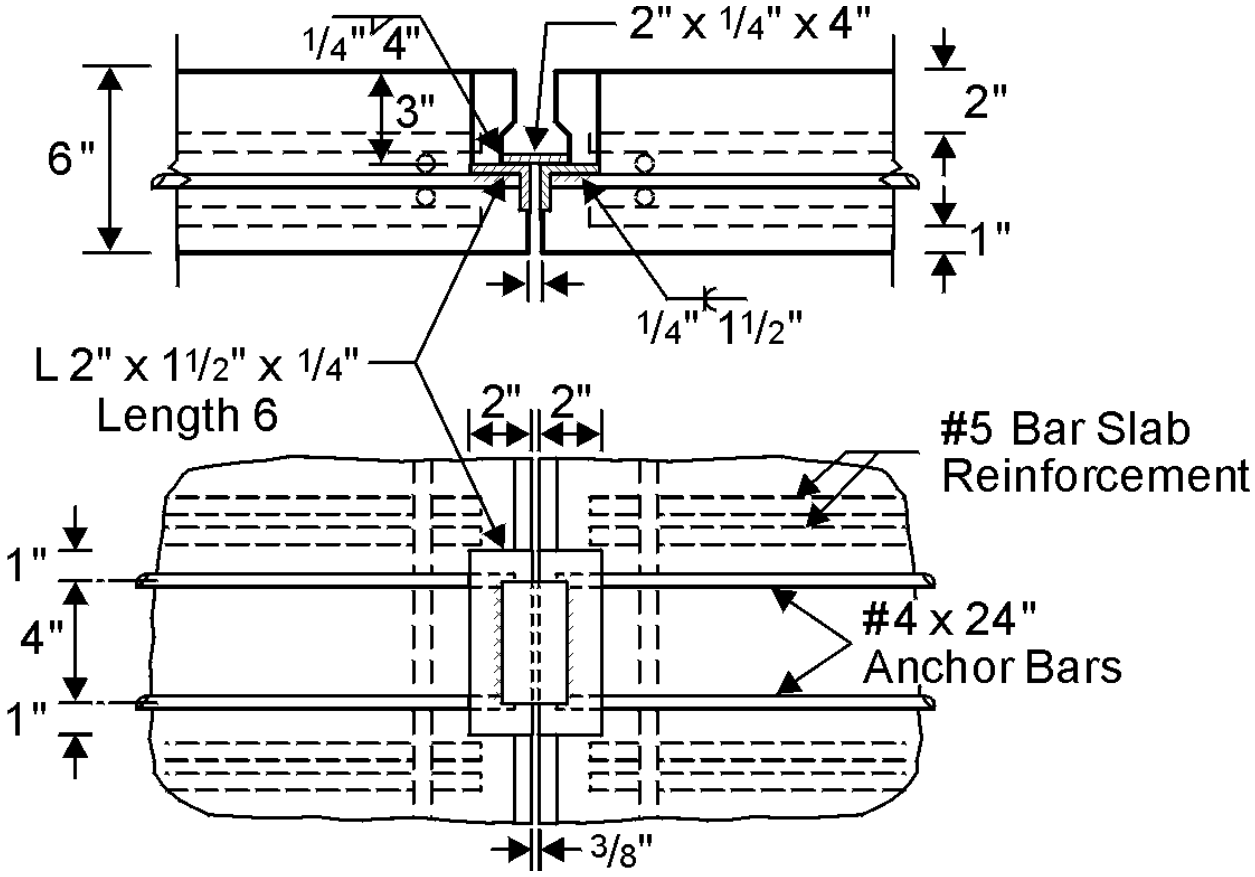

Figure 25. Connector Details of Specimen 2A.

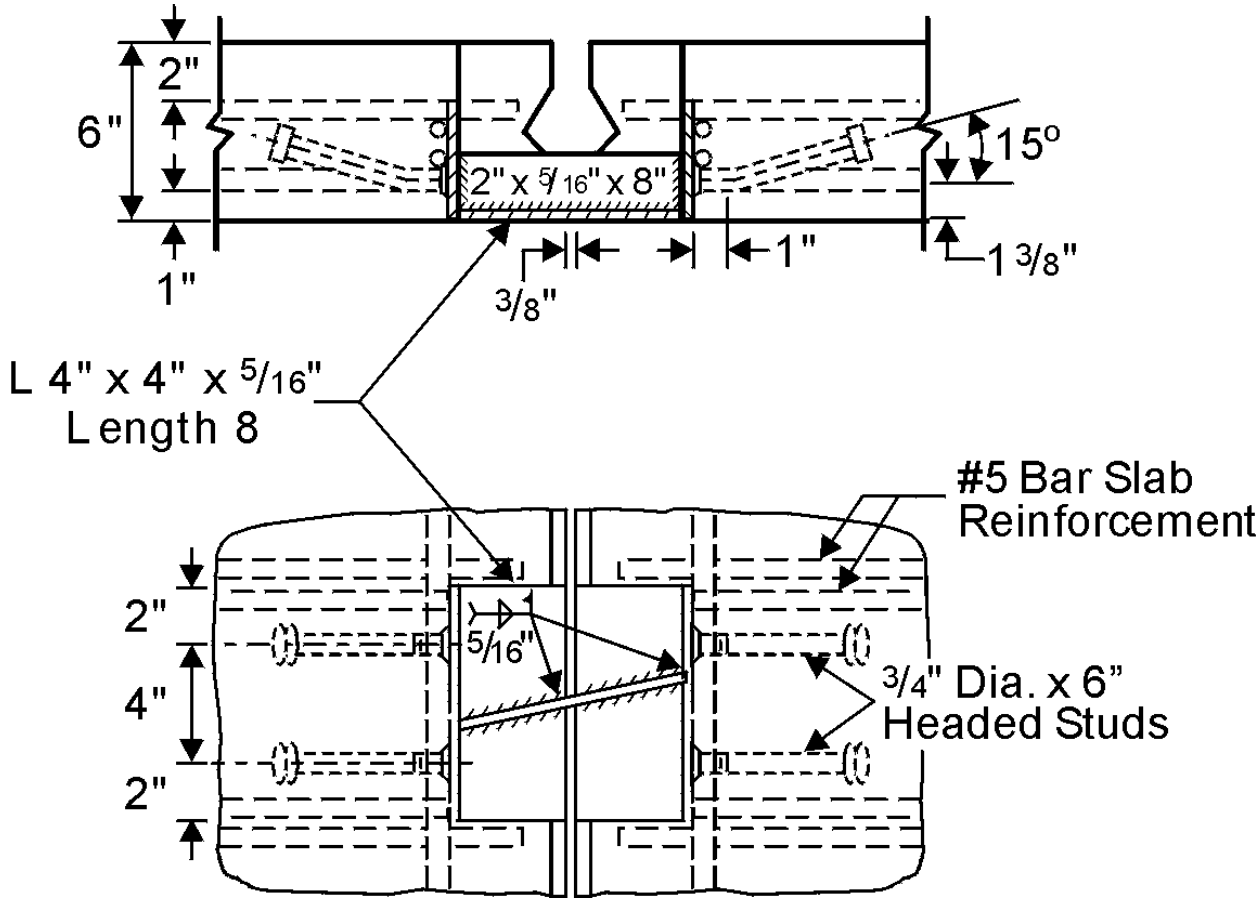

Figure 26. Connector Details of Specimens 3A and 3B.

Table 2. Total Shear Strength.

Specimen No.	Concrete Strength (psi)	Grout Strength (psi)	Shear in Connection at Failure (kips)
1A	5,470	*	4.78
1B	5,895	3,280	11.60
1C	5,775	3,615	17.35
2A	5,680	*	4.95
3A	5,600	*	6.70
3B	4,400	4,175	20.38

NEW CONNECTION METHOD RECOMMENDATIONS

The findings just described in this chapter were reviewed with representatives of TxDOT's design, construction, and maintenance functions in a series of two meetings. The following guidelines and conclusions emerged from those discussions:

- a connection with sufficient strength and stiffness to dramatically reduce longitudinal cracking is potentially too slow and expensive to install,
- a connection whose most attractive attribute is ease of installation and low cost is unlikely to significantly improve the structural conditions leading to longitudinal cracking, and
- given the mutually exclusive nature of the previous two conclusions, focus primary attention on developing a fast, low-cost connection targeted for double tee bridges with asphalt riding surface.

With the assistance of the TxDOT personnel cited above, two different connection prototypes were developed and are described below.

RECOMMENDED "SIMPLE" CONNECTION DETAIL

This detail is proposed to meet the need for ease of installation and low cost and is intended for bridges with asphalt wearing surface. As seen in Fig. 27, it consists of a pair of 0.5 in. thick steel plates embedded in the flange concrete and anchored with steel headed studs or welded rebar. Chapter 3 presents test results that show a tendency for the headed stud anchorage to cause spalling of concrete. Consequently, #4 rebar at least 18 in. long is recommended for anchoring the plates. The 10 degree slope on the plates offers a recess which receives the 1 in. diameter steel bar. It is believed this arrangement will accommodate variation in the 0.25 in. nominal spacing between adjacent tees resulting from sweep in the members. One of the connection's functions is to transmit vertical shear force between the flanges of adjacent tees by means of the weld connection between bar and embedded plates.

In reviewing the connection details used by others it is clear that most incorporate some sort of continuous grouted shear key. The results of inspections of Texas bridges described earlier suggests that a shear key will eliminate the problem of asphalt in the wearing surface being pushed down into the space between the edges of adjacent flanges, thus reducing (but likely not eliminating) maintenance problems associated with longitudinal reflective cracking. Several writers describe discrete connections as simply devices whose function is to keep the beams from separating, presumably to ensure the integrity of the key. The limited test data cited in Table 1 certainly suggest that in such connections, the shear key transfers substantial load with the connectors playing a secondary role. Test results from this study described in Chapters 3 and 5 further support this observation. Thus, the second function of the connection is to prevent lateral separation of adjacent tee flanges to help preserve the structural integrity of the grouted shear key.

The connection was developed with the idea that it would be spaced at approximately 5 ft. intervals along the flange. The sloping steel face plates allow for some variation in the 0.25 in. spacing between adjacent flanges while still accommodating the round steel bar. Outside the confines of the 12 in. long connection, a 1 in. backer rod dropped onto the sloping concrete faces will form the bottom of the shear key.

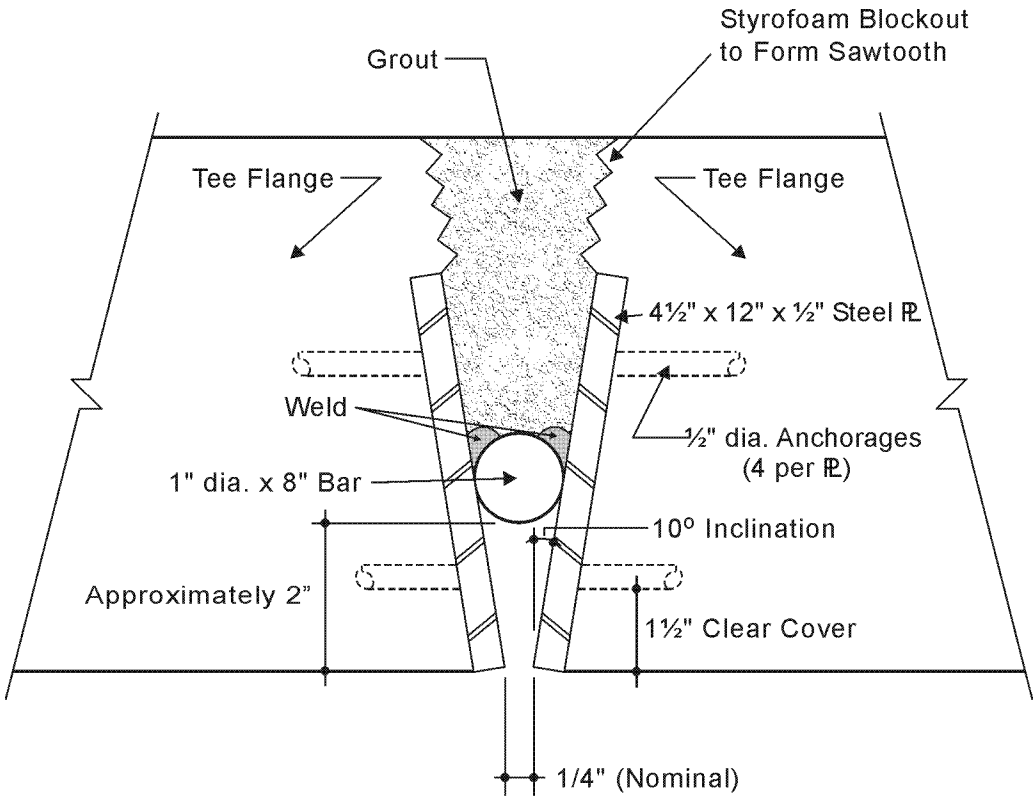

(a) Section Through Bar/Plate

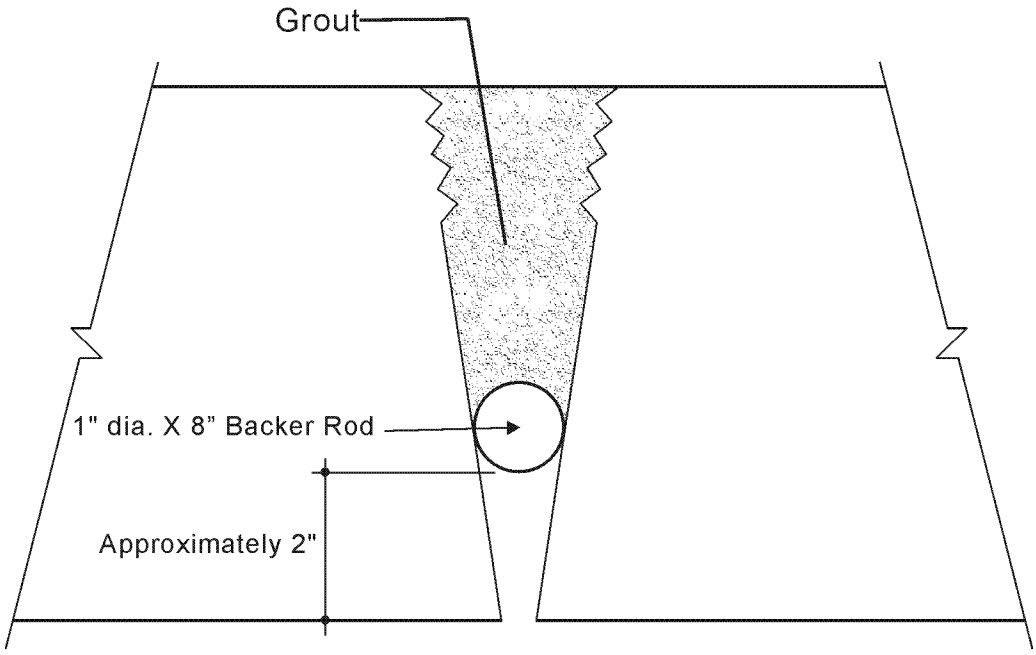

(b) Section at Other Locations

Figure 27. Proposed "Simple" Connection Detail.

RECOMMENDED "CONTINUOUS" CONNECTION DETAIL

This connection detail is proposed for use in bridges with composite concrete deck and is believed to offer much greater resistance to the formation of longitudinal cracks in the deck. As seen in Fig. 28, it involves blocking out a portion of the current flange, leaving the reinforcing present in the flange protruding beyond the new flange edge. Discussions with prestressed concrete manufacturers indicated this block out could be accomplished using pieces of Styrofoam placed against the rail of the standard 8 ft. tee form. The modified prestressed concrete double tee would then be placed on bridge bent caps in the usual way, but spaced laterally to allow for the casting of a segment of flange which joins adjacent tees and bonds to the rebar extending from each, as seen in Fig. 29. The figure suggests that this closure pour would be formed from the top side of the bridge using wire to hold a piece of form material against the underside of the existing flanges and tied off against a transverse support laying on the top of the tee flanges. Once this closure has been poured and cured, the cast-in-place portion of the deck slab would be poured in the usual way.

The important advantage this detail offers over discrete connections like those in Fig. 1 or 2 is the elimination of a section between flanges of adjacent tees where only the cast-in-place deck is available to resist transverse bending moment. The proposed detail offers a section to resist transverse moment equal to the combined depth of tee flange and overlying deck slab. The "simple" connection of Fig. 27 fills the void between flanges with a grouted shear key giving the appearance of a full thickness slab, but the effectiveness of that key acting in conjunction with a deck slab above it is unexplored and unproven. Only bond stress between grout and flange edge concrete make the shear key effective in resisting transverse moment, while the "continuous" detail has #4 rebar.

For these reasons, the "continuous" connection is recommended as the best means for minimizing or eliminating longitudinal cracks in concrete decks like those in the photographs of Figs. 5, 7, 10, 11, and 12.

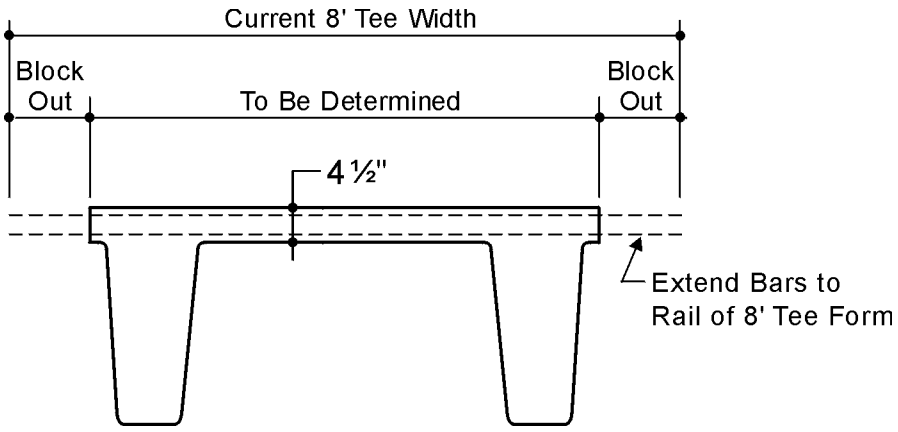

Figure 28. Proposed "Continuous" Connection Detail.

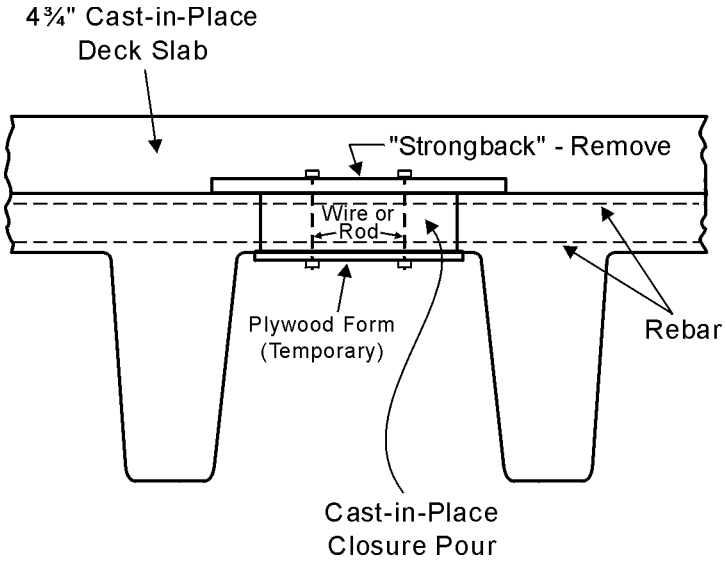

Figure 29. Closure Pour in "Continuous" Connection.

CHAPTER 3. PILOT TESTS

Researchers conducted a series of load tests on a short span (18 ft.), full-scale bridge constructed in the laboratory with two 28 in. deep by 8 ft. wide TxDOT double tees with 6 in. thick flanges. At each beam support point a 4 in. wide by 5 in. long by 0.5 in. thick rubber pad was placed between the underside of the beam stem and the steel beam support simulating the bent cap support. The two members were connected laterally using the TxDOT connection method shown in Fig. 1. In addition, a continuous shear key was added to this detail. These load tests served several functions. First, baseline strength data were obtained for this type of connection, along with some measures of the effectiveness of a shear key used in conjunction with the standard connection. The second purpose for the tests was to generate experimental data that could be used to validate an analytical model developed for this type of bridge. Finally, researchers performed tests to characterize the behavior of the overhanging flange at the end of the bridge in the absence of an end diaphragm.

The previous chapter (Fig. 27) describes another set of tests conducted on concrete beams that contained the recommended "simple" connection detail. These tests provided estimates of ultimate carrying capacity and likely modes of failure. This chapter describes the details of these various tests and tabulates the experimental results.

DOUBLE TEE BRIDGE TESTS

Fig. 30 shows a plan view and dimensions of the structure tested, and Fig. 31 is a photograph of the completed bridge in the laboratory. In this series of tests, strain measurements were taken on the two vertical steel plates in each of the four connections to provide data for later comparison with analytical predictions. The connection detail used is that discussed in Chapter 1 and shown schematically in Fig. 1. Fig. 32 contains photographs of a typical connection. The connections are labeled I through IV on the plan seen in Fig. 30. Typically four strain gages were attached to each of the two steel plates in a connection with the exception of connection III (see Fig.32b), which had six per plate. Fig. 33 shows gage location and the notation used to label each gage. Fig. 34 gives the dimensions of the shear key which was formed by the fabricator using a block out and which is absent in the current TxDOT standard tee design.

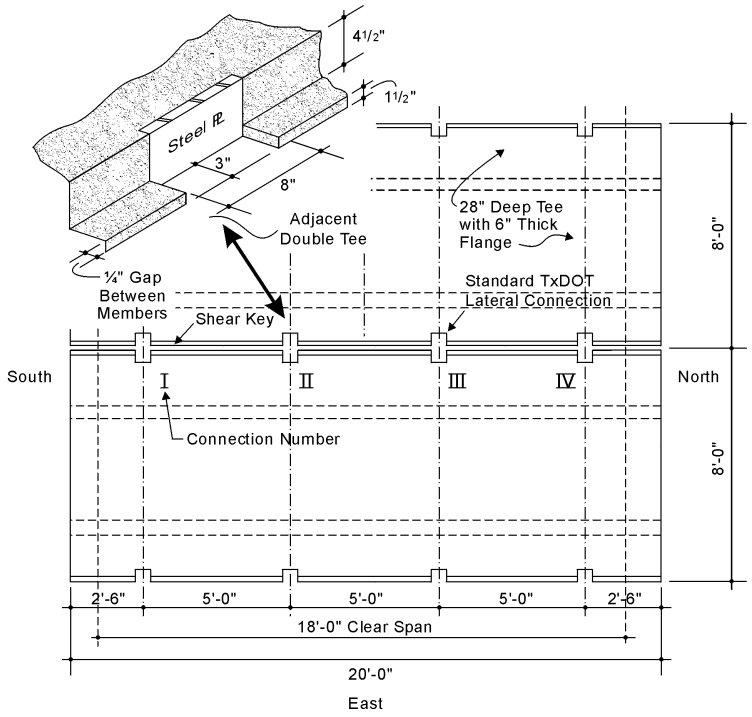

Figure 30. Plan View of Double Tee Laboratory Bridge.

Figure 31. Double Tee Laboratory Bridge.

(a)

Figure 32 (b). Strain Gages on Connection Plates.

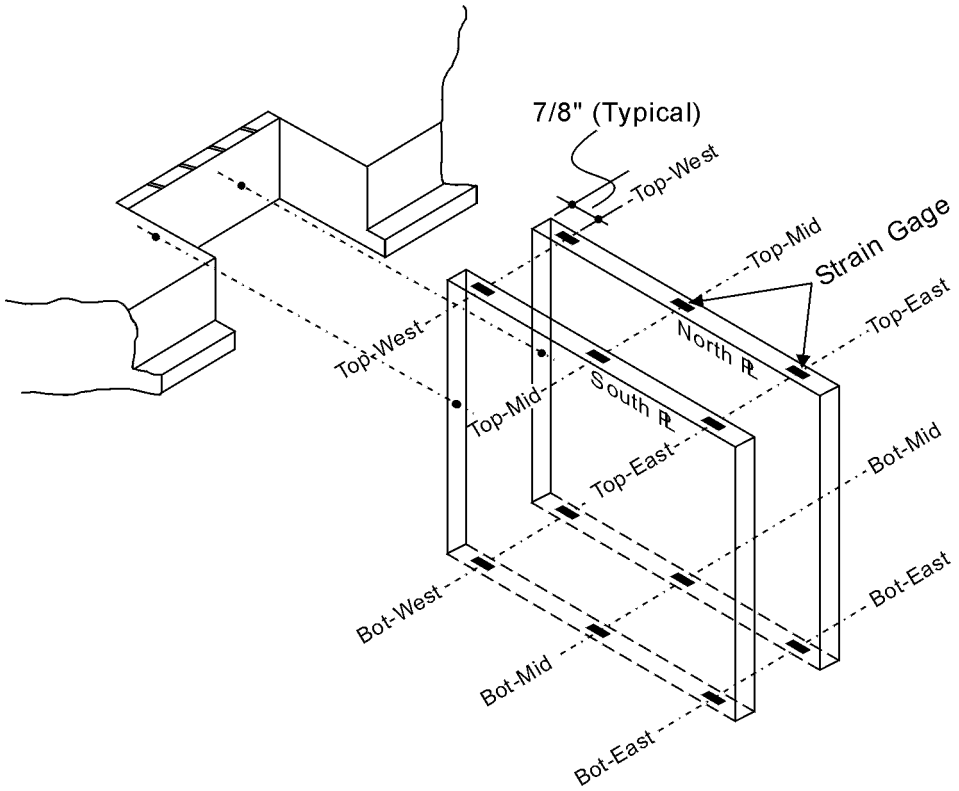

Figure 33. Location of Strain Gages on Connection Plates.

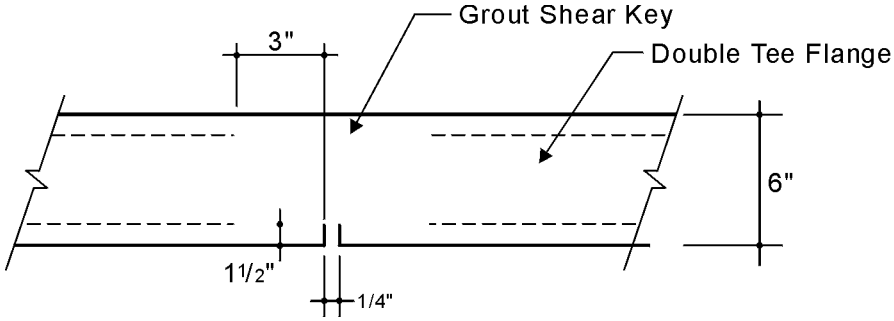

Figure 34. Shear Key.

The structure was loaded with a single 20 kip load generated by hydraulic ram reacting against the steel load frame visible in Fig. 31. The ram was positioned at the four different locations marked A, B, C, and D in Fig. 35, then activated to a load of 20 kips and strain readings from the gages on the steel connection plates recorded. In each test, the structure was actually loaded to the full load, then unloaded and reloaded to verify the reproducibility of the strain readings.

The first loading series was conducted without grout in the shear key. The results are reported in Tables 3 through 6 in the form of stresses, computed by taking the measured strains and multiplying them by the modulus of elasticity of steel (30,000,000 psi). The stresses in the various plates were generally low, never exceeding 10,000 psi and averaging less than half that level. Upon completion of these tests, a shear key was cast using Masterflow 928 high-strength grout. After 19 days, three standard 2 in. mortar cubes from the key pour were tested and found to have strengths of 9,490, 9,980, and 11,480 psi. The following day the sequence of four load positions applied prior to the shear key installation were repeated, strains recorded, and the measured strains converted to the stresses listed in Tables 7 through 10. Cursory comparison of the two sets of tables clearly shows the shear key assuming the predominant role in transfe rring forces between adjacent tees, as reflected in the dramatic reduction in stresses in the steel connecting plates, which never exceed 2,000 psi. Further analysis of the connections and shear key are undertaken in Chapter 4, which introduces the analytical model used in this study and draws comparisons between the measured and predicted stresses in the connection plates.

Table 3. Stresses in Connection Plates for Load Position A.

Connection I

South Plate		North Plate	
	Measured		Measured
Location	Stress (ksi)	Location	Stress (ksi)
Top-West	-1.526	Top-West	-7.298
Bot-West	3.316	Bot-West	9.797
Top-East	-0.405	Top-East	-1.208
Bot-East	-0.274	Bot-East	-0.199

Connection II

South Plate		North Plate	
	Measured		Measured
Location	Stress (ksi)	Location	Stress (ksi)
Top-West	-1.458	Top-West	-7.543
Bot-West	2.474	Bot-West	3.241
Top-East	-0.507	Top-East	-1.848
Bot-East	0.699	Bot-East	0.939

Connection III

South Plate		North Plate	
	Measured		Measured
Location	Stress (ksi)	Location	Stress (ksi)
Top-West	-1.678	Top-West	-5.940
Bot-West	1.477	Bot-West	3.844
Top-Mid	-1.725	Top-Mid	-5.200
Bot-Mid	1.754	Bot-Mid	5.668
Top-East	-1.433	Top-East	-4.790
Bot-East	1.310	Bot-East	5.479

Connection IV

South Plate		North Plate	
	Measured		Measured
Location	Stress (ksi)	Location	Stress (ksi)
Top-West	-0.825	Top-West	-0.199
Bot-West	0.927	Bot-West	0.093
Top-East	-1.492	Top-East	-2.976
Bot-East	1.729	Bot-East	0.239

The 20 kip force used in the tests cited resulted in stresses well below the capacity of either concrete or steel elements in the bridge. Consequently, a final series of tests was conducted on the double tee bridge in which load was applied in close proximity to connections I and II as seen in Fig. 35 load positions E and F, and Fig. 36. The test used a load distributed over an area 8 in. by 12 in., the approximate size of a truck tire print. Both tests took the loading to the capacity of the hydraulic ram, approximately 96 kips, and neither test induced significant damage. Inspection of the structure after each of the two loadings revealed only minor cracking on the underside of the flange adjacent to the connection. No cracking was visible in the shear key although hairline cracks at the grout/concrete flange interface were beginning to form. It would be accurate to characterize the lateral connection system's resistance to a wheel load applied to the deck as substantially greater than the 96 kip wheel load applied.

Table 4. Stresses in Connection Plates for Load Position B.

Connection I

South Plate

Location	Measured Stress (ksi)
Top-West	-1.253
Bot-West	2.088
Top-East	-1.029
Bot-East	0.849

North Plate

Location	Measured Stress (ksi)
Top-West	-4.839
Bot-West	8.690
Top-East	-2.632
Bot-East	3.847

Connection II

South Plate

Location	Measured Stress (ksi)
Top-West	-1.623
Bot-West	2.649
Top-East	-0.560
Bot-East	0.601

North Plate

Location	Measured Stress (ksi)
Top-West	-9.260
Bot-West	3.640
Top-East	-1.664
Bot-East	0.635

Connection III

South Plate

Location	Measured Stress (ksi)
Top-West	-2.285
Bot-West	2.034
Top-Mid	-1.987
Bot-Mid	2.010
Top-East	-1.694
Bot-East	1.134

North Plate

Location	Measured Stress (ksi)
Top-West	-7.766
Bot-West	4.523
Top-Mid	-5.518
Bot-Mid	6.034
Top-East	-3.807
Bot-East	4.197

Connection IV

South Plate

Location	Measured Stress (ksi)
Top-West	-1.239
Bot-West	1.436
Top-East	-1.368
Bot-East	1.406

North Plate

Location	Measured Stress (ksi)
Top-West	-0.428
Bot-West	0.154
Top-East	-3.090
Bot-East	0.231

Table 5. Stresses in Connection Plates for Load Position C.

Connection I

South Plate

Location	Measured Stress (ksi)
Top-West	-1.016
Bot-West	1.347
Top-East	-1.124
Bot-East	1.468

North Plate

Location	Measured Stress (ksi)
Top-West	-3.150
Bot-West	6.976
Top-East	-3.880
Bot-East	5.993

Connection II

South Plate

Location	Measured Stress (ksi)
Top-West	-1.315
Bot-West	2.143
Top-East	-0.769
Bot-East	0.974

North Plate

Location	Measured Stress (ksi)
Top-West	-7.182
Bot-West	3.101
Top-East	-2.151
Bot-East	1.064

Connection III

South Plate

Location	Measured Stress (ksi)
Top-West	-3.166
Bot-West	2.649
Top-Mid	-2.387
Bot-Mid	2.357
Top-East	-3.432
Bot-East	0.931

North Plate

Location	Measured Stress (ksi)
Top-West	-9.388
Bot-West	4.763
Top-Mid	-5.884
Bot-Mid	6.116
Top-East	-3.281
Bot-East	3.158

Connection IV

South Plate

Location	Measured Stress (ksi)
Top-West	-1.602
Bot-West	-6.405
Top-East	-0.886
Bot-East	71.195

North Plate

Location	Measured Stress (ksi)
Top-West	-0.822
Bot-West	0.252
Top-East	-2.659
Bot-East	0.176

Table 6. Stresses in Connection Plates for Load Position D.

Connection I

South Plate

Location	Measured Stress (ksi)
Top-West	-1.031
Bot-West	1.330
Top-East	-1.210
Bot-East	1.522

North Plate

Location	Measured Stress (ksi)
Top-West	-3.101
Bot-West	6.975
Top-East	-3.754
Bot-East	6.103

Connection II

South Plate

Location	Measured Stress (ksi)
Top-West	-1.396
Bot-West	2.274
Top-East	-0.755
Bot-East	1.052

North Plate

Location	Measured Stress (ksi)
Top-West	-7.422
Bot-West	3.209
Top-East	-2.154
Bot-East	1.124

Connection III

South Plate

Location	Measured Stress (ksi)
Top-West	-3.275
Bot-West	2.676
Top-Mid	-2.448
Bot-Mid	2.475
Top-East	-1.025
Bot-East	-0.593

North Plate

Location	Measured Stress (ksi)
Top-West	-9.543
Bot-West	4.797
Top-Mid	-5.936
Bot-Mid	6.130
Top-East	-3.287
Bot-East	3.113

Connection IV

South Plate

Location	Measured Stress (ksi)
Top-West	-1.636
Bot-West	2.316
Top-East	-0.839
Bot-East	0.722

North Plate

Location	Measured Stress (ksi)
Top-West	-0.831
Bot-West	0.257
Top-East	-2.664
Bot-East	0.178

Table 7. Stresses in Connection Plates with Shear Key for Load Position A.

Connection I

South Plate

Location	Measured Stress (ksi)
Top-West	-0.256
Bot-West	0.306
Top-East	-0.208
Bot-East	0.258

North Plate

Location	Measured Stress (ksi)
Top-West	-1.215
Bot-West	2.206
Top-East	-1.042
Bot-East	1.292

Connection II

South Plate

Location	Measured Stress (ksi)
Top-West	-0.320
Bot-West	0.327
Top-East	-0.239
Bot-East	0.323

North Plate

Location	Measured Stress (ksi)
Top-West	-1.323
Bot-West	0.483
Top-East	-0.843
Bot-East	0.275

Connection III

South Plate

Location	Measured Stress (ksi)
Top-West	-0.247
Bot-West	0.284
Top-Mid	-0.256
Bot-Mid	0.332
Top-East	-0.111
Bot-East	0.367

North Plate

Location	Measured Stress (ksi)
Top-West	-0.994
Bot-West	0.894
Top-Mid	-0.908
Bot-Mid	1.034
Top-East	-0.945
Bot-East	1.020

Connection IV

South Plate

Location	Measured Stress (ksi)
Top-West	-0.127
Bot-West	0.082
Top-East	-0.247
Bot-East	0.116

North Plate

Location	Measured Stress (ksi)
Top-West	-0.039
Bot-West	0.015
Top-East	-0.343
Bot-East	0.022

Table 8. Stresses in Connection Plates with Shear Key for Load Position B.

Connection I

South Plate

Location	Measured Stress (ksi)
Top-West	-0.360
Bot-West	0.175
Top-East	-0.369
Bot-East	0.199

North Plate

Location	Measured Stress (ksi)
Top-West	-1.046
Bot-West	1.525
Top-East	-1.173
Bot-East	1.269

Connection II

South Plate

Location	Measured Stress (ksi)
Top-West	-0.552
Bot-West	0.191
Top-East	-0.320
Bot-East	0.280

North Plate

Location	Measured Stress (ksi)
Top-West	-1.687
Bot-West	0.473
Top-East	-0.855
Bot-East	0.148

Connection III

South Plate

Location	Measured Stress (ksi)
Top-West	-0.439
Bot-West	0.208
Top-Mid	-0.466
Bot-Mid	0.506
Top-East	-1.420
Bot-East	0.084

North Plate

Location	Measured Stress (ksi)
Top-West	-1.509
Bot-West	1.245
Top-Mid	-1.385
Bot-Mid	1.415
Top-East	-1.312
Bot-East	1.129

Connection IV

South Plate

Location	Measured Stress (ksi)
Top-West	-0.291
Bot-West	0.204
Top-East	-0.404
Bot-East	0.185

North Plate

Location	Measured Stress (ksi)
Top-West	-0.092
Bot-West	0.026
Top-East	-0.634
Bot-East	0.032

Table 9. Stresses in Connection Plates with Shear Key for Load Position C.

Connection I

South Plate

Location	Measured Stress (ksi)
Top-West	-0.232
Bot-West	0.206
Top-East	-0.194
Bot-East	0.155

North Plate

Location	Measured Stress (ksi)
Top-West	-0.794
Bot-West	1.252
Top-East	-0.980
Bot-East	1.228

Connection II

South Plate

Location	Measured Stress (ksi)
Top-West	-0.462
Bot-West	0.320
Top-East	-0.405
Bot-East	0.255

North Plate

Location	Measured Stress (ksi)
Top-West	-1.422
Bot-West	0.509
Top-East	-0.756
Bot-East	0.251

Connection III

South Plate

Location	Measured Stress (ksi)
Top-West	-0.469
Bot-West	0.369
Top-Mid	-0.391
Bot-Mid	0.468
Top-East	-1.086
Bot-East	-0.252

North Plate

Location	Measured Stress (ksi)
Top-West	-1.611
Bot-West	1.425
Top-Mid	-1.448
Bot-Mid	1.568
Top-East	-1.311
Bot-East	1.324

Connection IV

South Plate

Location	Measured Stress (ksi)
Top-West	-0.290
Bot-West	0.135
Top-East	-0.464
Bot-East	0.198

North Plate

Location	Measured Stress (ksi)
Top-West	-0.114
Bot-West	0.033
Top-East	-0.722
Bot-East	0.040

Table 10. Stresses in Connection Plates with Shear Key for Load Position D.

Connection I

South Plate

	Measured
Location	Stress (ksi)
Top-West	-0.220
Bot-West	0.050
Top-East	-0.393
Bot-East	0.132

North Plate

	Measured
Location	Stress (ksi)
Top-West	-0.704
Bot-West	0.952
Top-East	-0.876
Bot-East	1.070

Connection II

South Plate

	Measured
Location	Stress (ksi)
Top-West	-0.536
Bot-West	0.217
Top-East	-0.428
Bot-East	0.240

North Plate

	Measured
Location	Stress (ksi)
Top-West	-1.421
Bot-West	0.358
Top-East	-0.839
Bot-East	1.035

Connection III

South Plate

	Measured
Location	Stress (ksi)
Top-West	-0.637
Bot-West	0.269
Top-Mid	-0.525
Bot-Mid	0.441
Top-East	-2.097
Bot-East	0.512

North Plate

	Measured
Location	Stress (ksi)
Top-West	-1.854
Bot-West	1.500
Top-Mid	-1.517
Bot-Mid	1.575
Top-East	-1.356
Bot-East	1.141

Connection IV

South Plate

	Measured
Location	Stress (ksi)
Top-West	-0.299
Bot-West	0.315
Top-East	-0.519
Bot-East	0.180

North Plate

	Measured
Location	Stress (ksi)
Top-West	-0.145
Bot-West	0.038
Top-East	-0.968
Bot-East	0.050

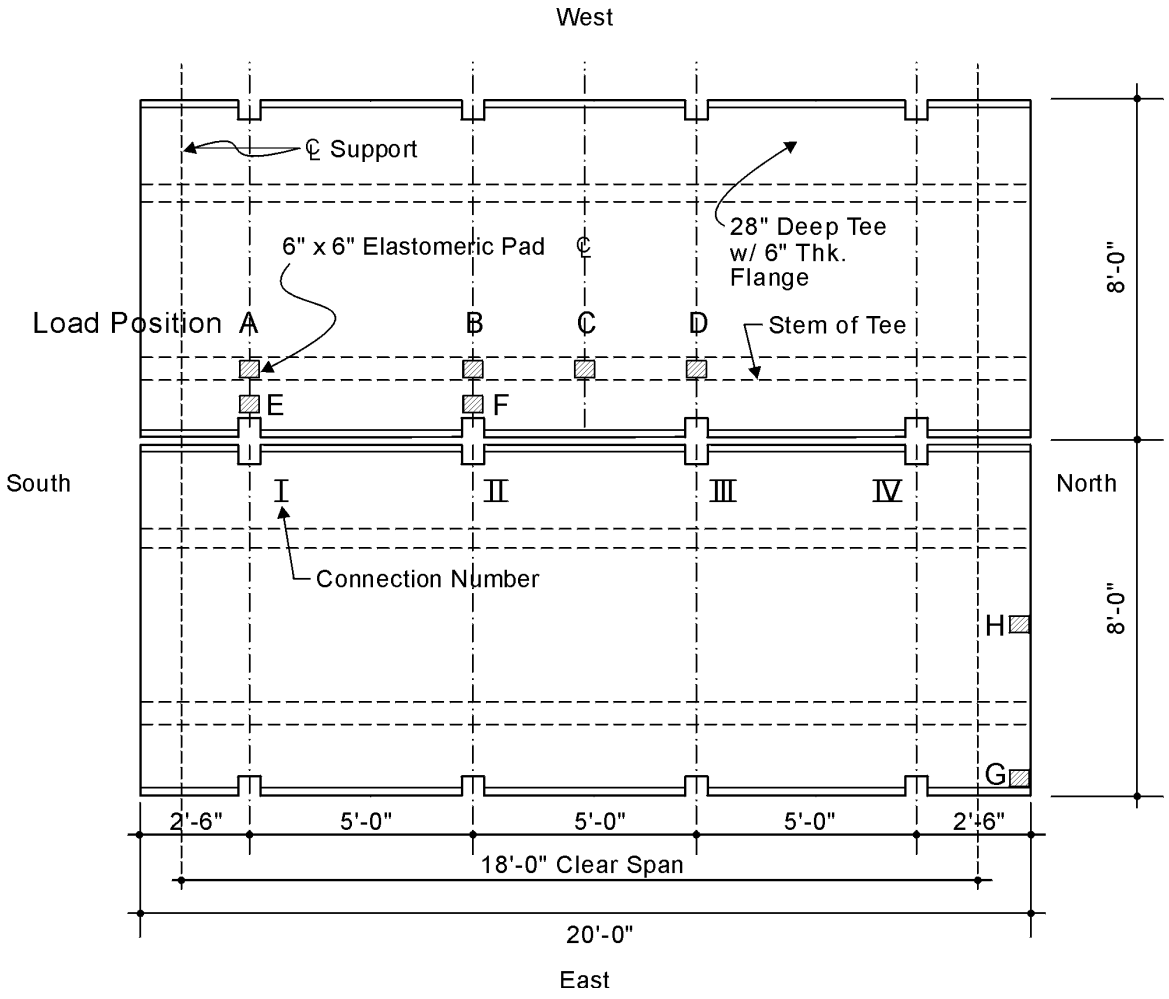

Figure 35. Loading Points for Tests.

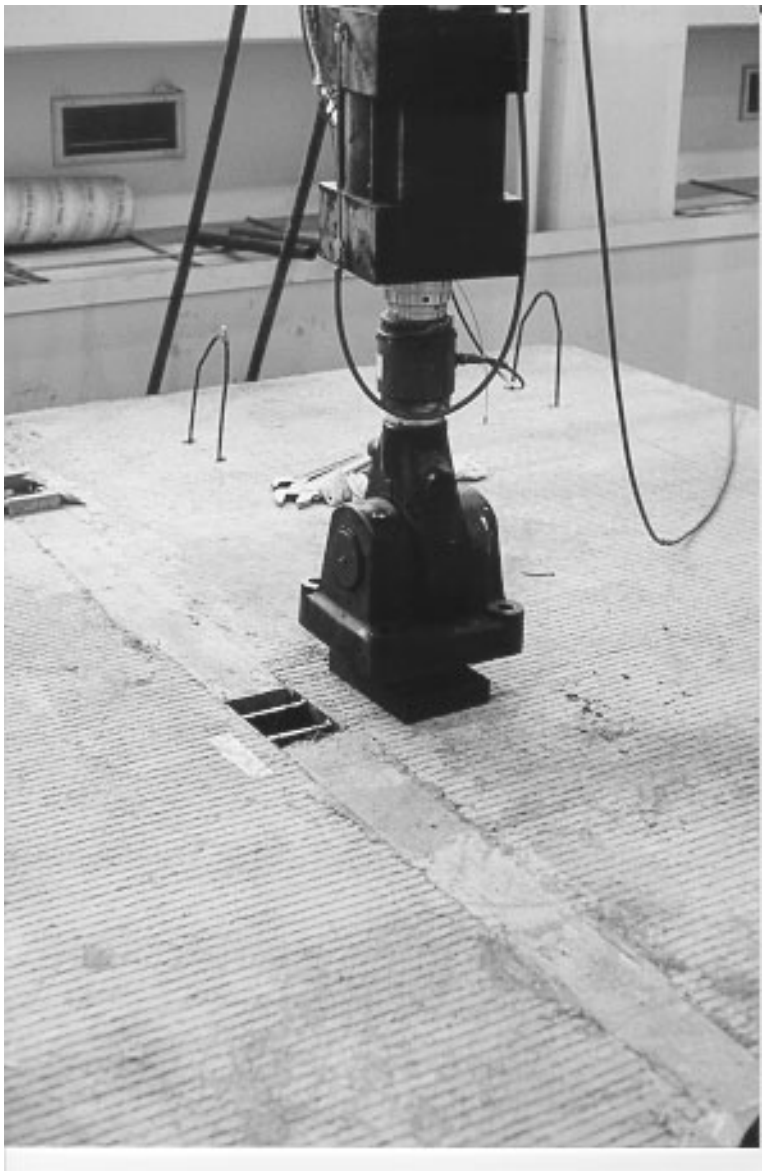

Figure 36. Simulated Wheel Load Applied at Connection II.

The final loadings applied to the bridge were chosen to test the strength and stiffness of the tee flange at the end of the bridge. TxDOT standards currently call for a diaphragm to be cast at the ends of beams. The diaphragm serves several purposes, including support and stiffening of the slab (the flange). However, whether such support is actually needed with a 6 in. thick flange is a matter of some conjecture. In the first test, the load was applied to the overhanging flange at the end of the bridge, as seen in Fig. 37 and shown as load position G in Fig. 35. The load was increased at a constant rate until failure occurred at 51.9 kips. The failure mode was flexural cracking, which extended diagonally (in plan view) across the corner of the flange, as seen in Fig. 38.

After failing the flange at the corner, the ram was moved laterally to the center of the east tee (load position H in Fig. 35) so that the force was applied midway between the two stems and at the end of the bridge, as seen in the photograph of Fig. 39. Constant rate loading continued until failure occurred at 85.7 kips. The failure had the appearance of punching shear and is shown in Fig. 40.

CONNECTION BEAM TESTS

Before undertaking a full-scale bridge test program incorporating the “simple” connection detail recommended in Chapter 2, a series of six load tests was performed on the connection using a beam specimen shown in Fig. 41. Each beam was intended to simulate the connection and an accompanying 12 in. width of tee flange. Details of the beam specimens are shown in Figs. 42 and 43, and a photograph of a test in progress is seen in Fig. 44. By varying the position “a” of the left support in Fig. 42 relative to the connection, the amount of bending moment accompanying the shear force transferred across the joint was varied. This condition is of interest in an actual bridge where it is controlled by the transverse rotational stiffness of the connection. The tests used three different V/M ratios. In each test, the load was applied with hydraulic ram and increased until the connection failed. During the course of each test, linear variable displacement tranducers (LVDTs) stationed on each side of the joint monitored vertical displacement of the beam. The average compressive strength (2 cylinders) of beam concrete at testing was 7,400 psi. and cube strength (average of 3 cubes) of the grout was 9,700 psi. Table 11 summarizes the results from each of the six tests performed. Fig. 42 lists the applied load and corresponding shear force and bending moment at the connection when failure occurred. The

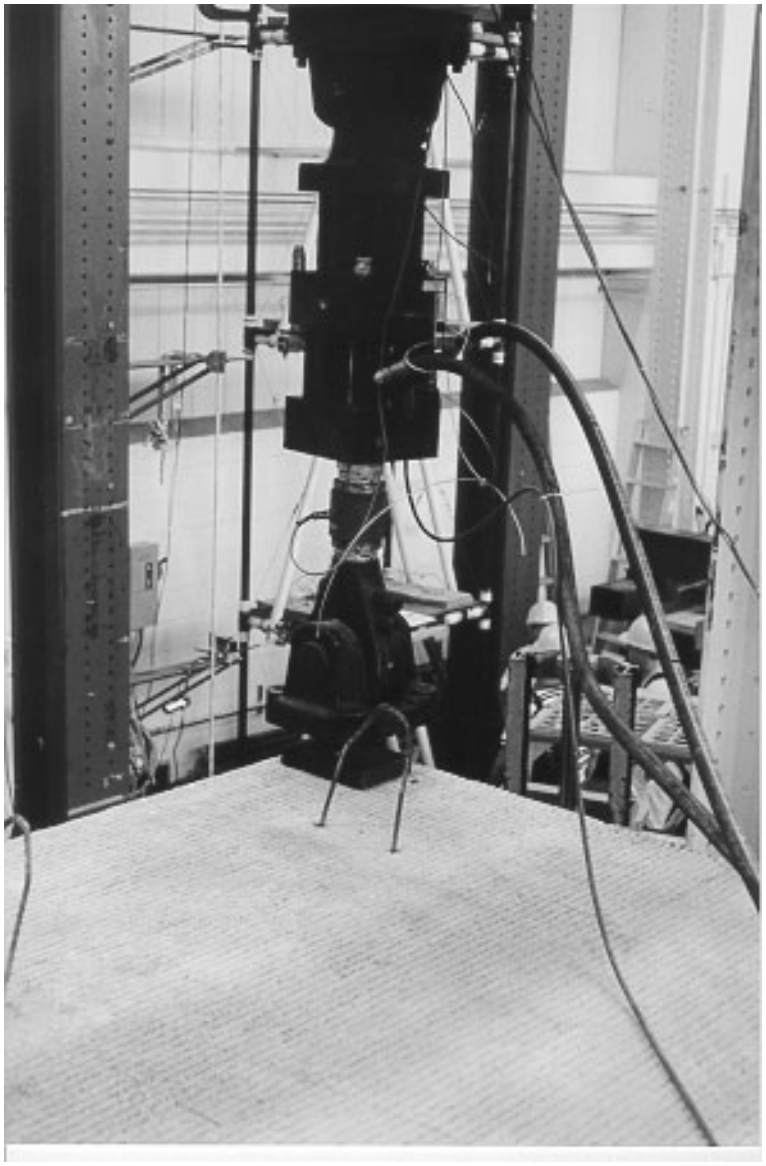

Figure 37. Loading at Outside Edge of Tee.

Figure 38. Failed Flange from Loading Outside Flange Edge.

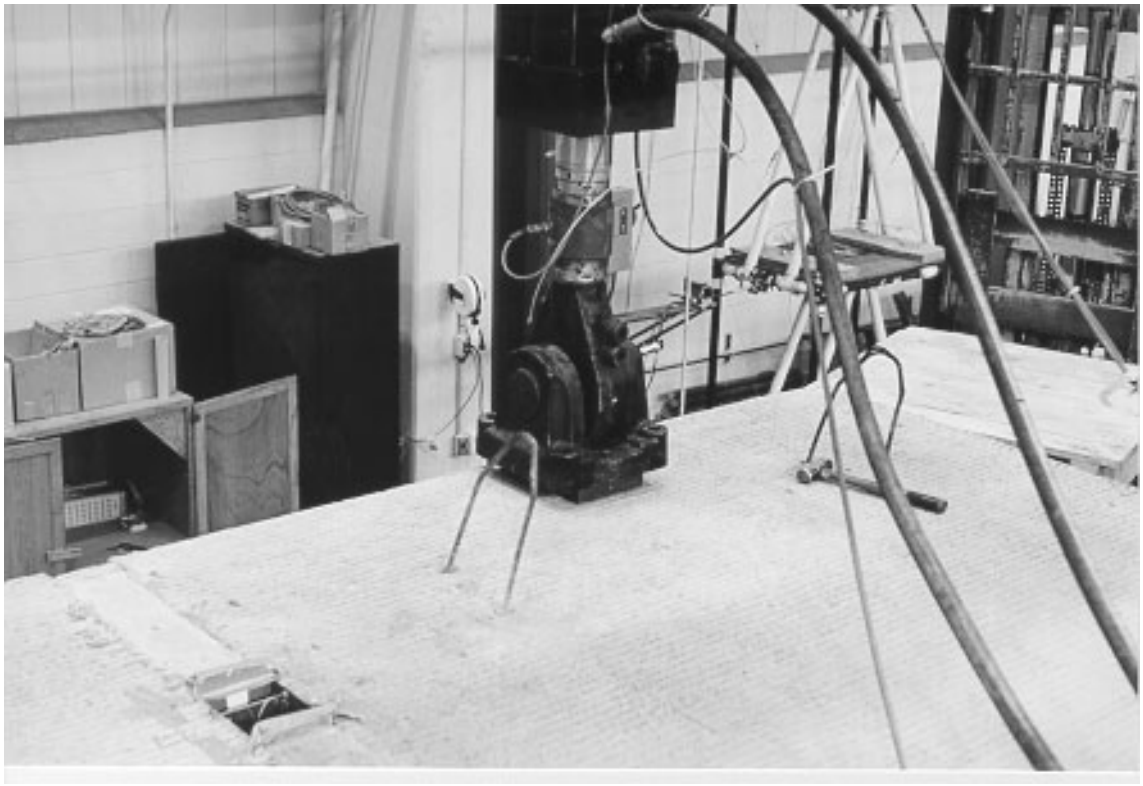

Figure 39. Loading at Center Edge of Tee.

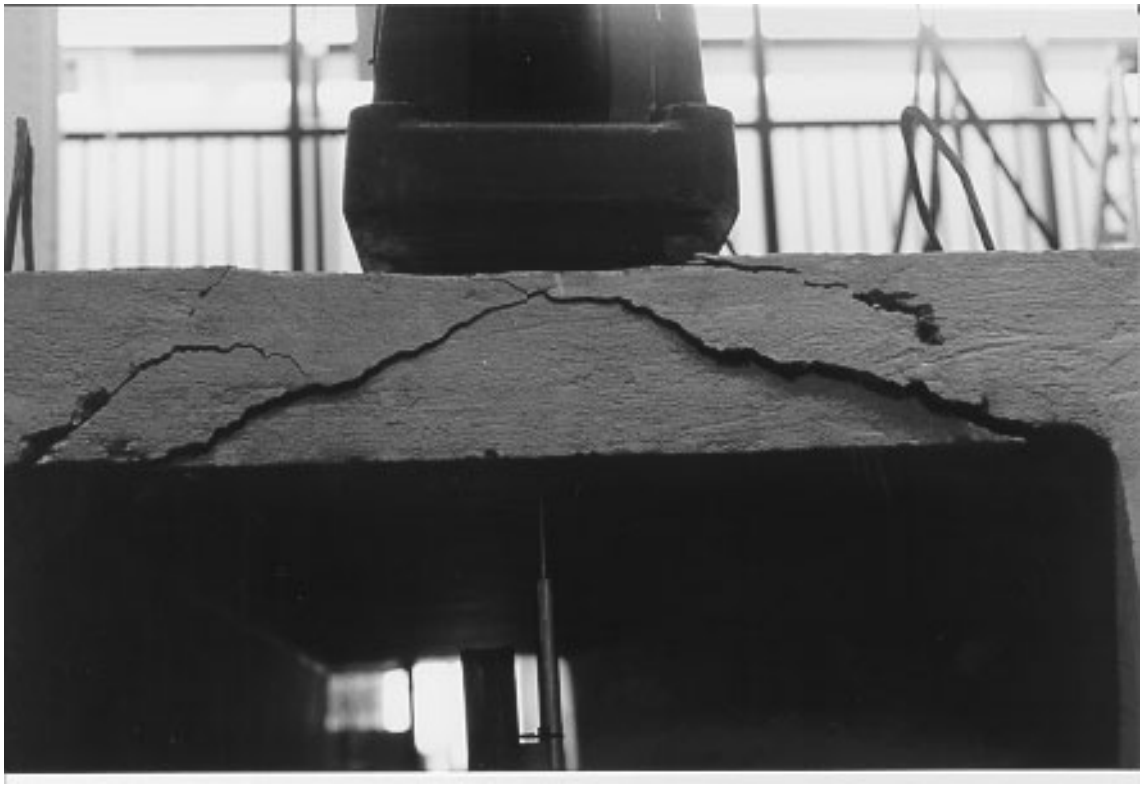

Figure 40. Failed Flange from Center Edge Loading.

Figure 41. "Simple" Connection Test Specimens.

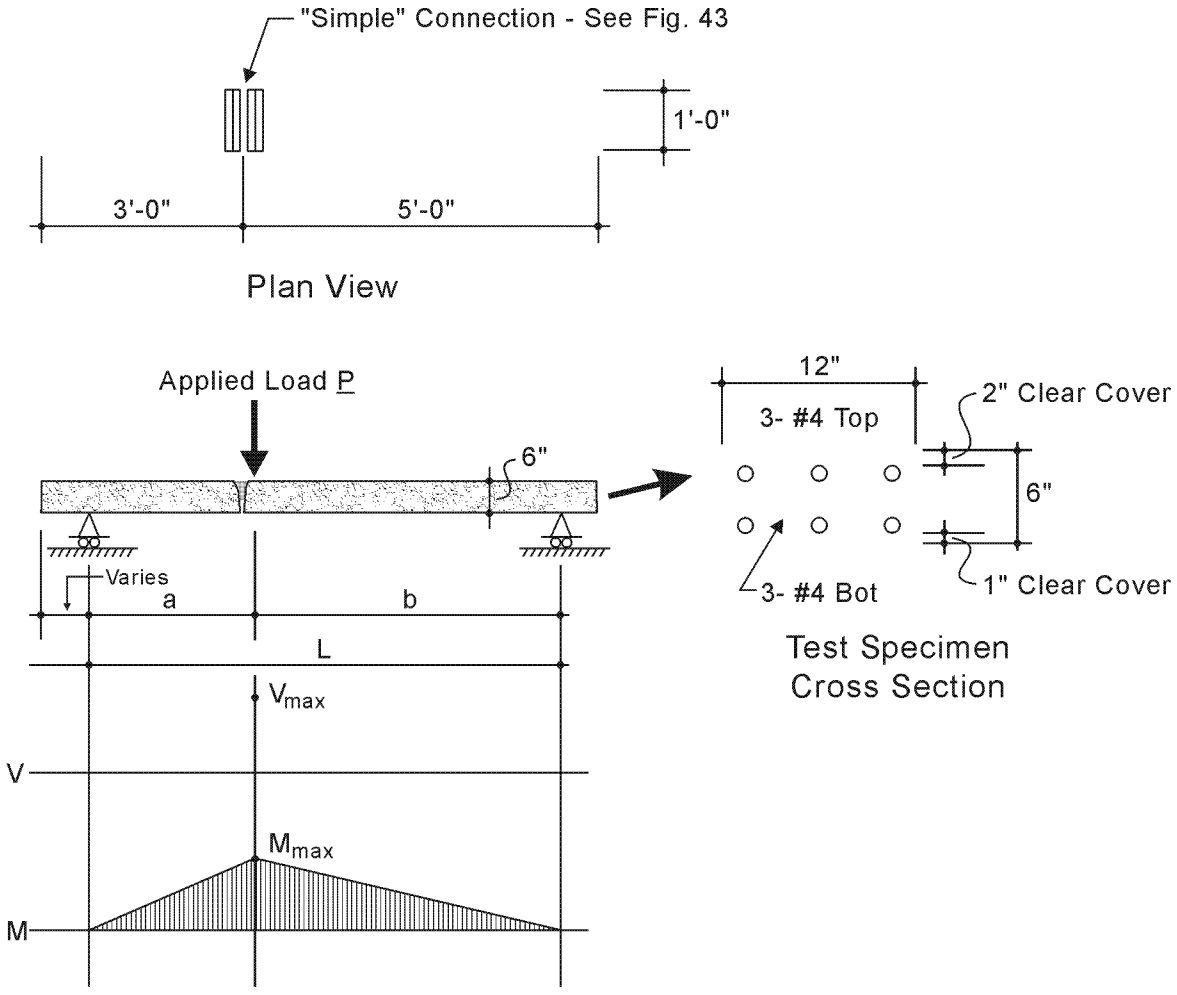

Figure 42. Details of Beam Test Specimens.

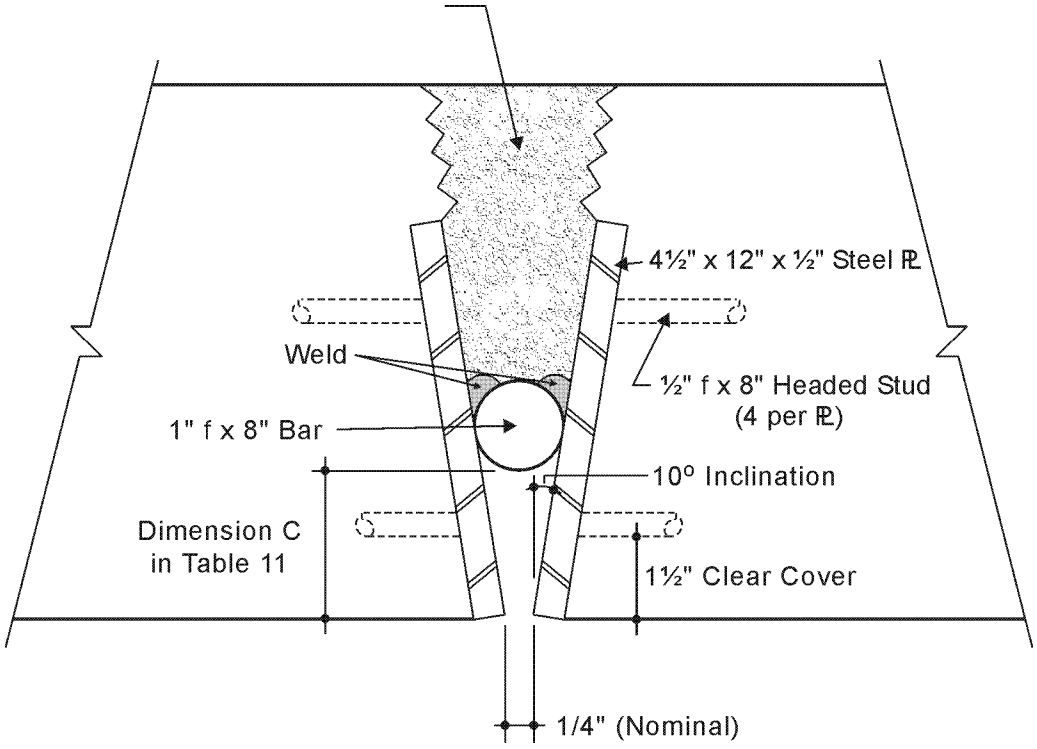

Figure 43. Details of "Simple" Connection Used in Beams.

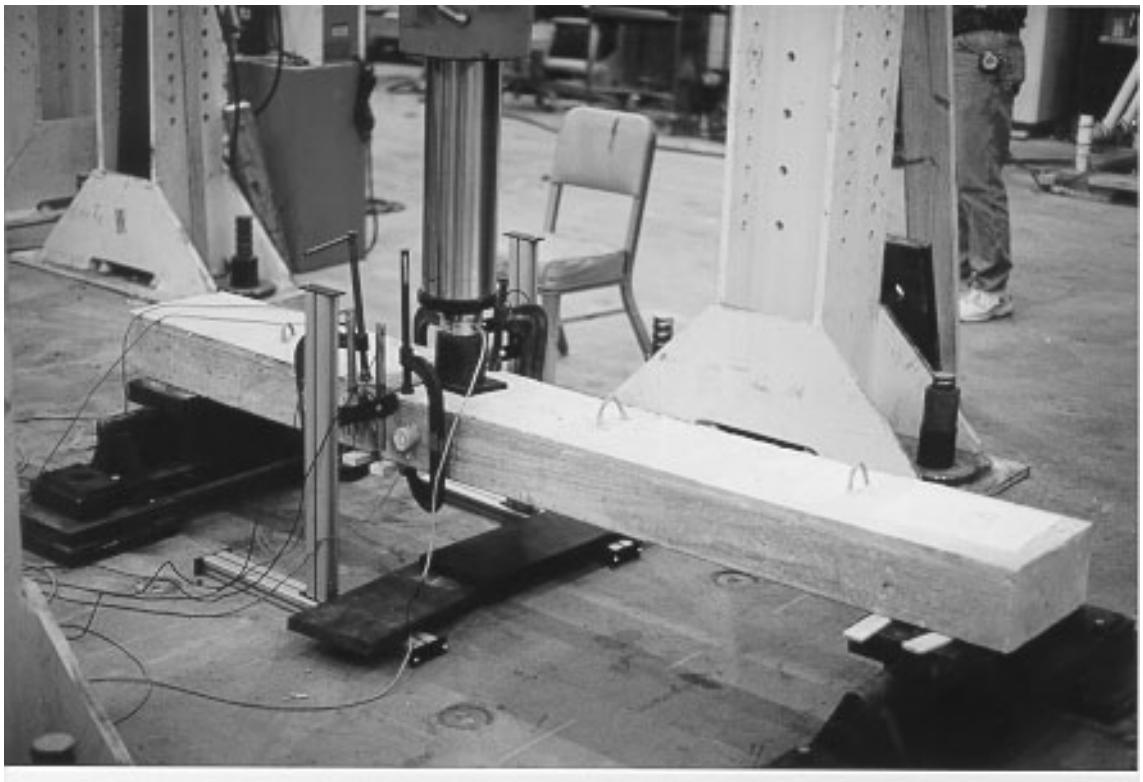

Figure 44. Beam Connection Test in Progress.

Table 11. Summary of Test Results.

	Dimensions			Ultimate	Ultimate	Ultimate
Test	a	L	c	P	V	M
Designation	(in.)	(in.)	(in.)	(lb)	(lb)	(in.-lb)
28B-1	28	52	1.875	7,100	7,100	91,754
28B-2	28	52	2.25	5,300	5,300	68,492
17B-1	17	52	1.625	9,070	9,070	103,782
6B-1	6	52	1.875	17,700	17,700	93,946
6B-2	6	52	2	16,400	16,400	87,046
6B-3	6	29	2.5	25,600	25,600	121,821

mode of failure in all six tests was the same – pullout of the headed studs anchoring the weld plate to the concrete (Fig. 45) with general spalling of the concrete cover on the underside of the beam (Fig. 46).

The failure of the connection was clearly premature in the sense that with better anchorage, it would have sustained greater loads. Conditions in a tee flange are somewhat better in that there can be no edge effects. However, spalling of the under flange concrete surface would be unimpeded as was the case in the beams. Longer anchorage length and use of deformed bars rather than headed studs was implemented in subsequent double tee tests in an attempt to prevent the pull-out failures which controlled the beam failures.

Figure 45. Pull-Out of Weld Plate in Beam Connection Test.

Figure 46. Spalling of Cover Concrete in Beam Connection Test.

CHAPTER 4. NUMERICAL SIMULATION

A suitable analytical model is essential to understanding the transfer of forces through the connections between adjacent tees in a multi-beam bridge as well as for assessing the effectiveness of live load transfer. Additionally, the model is needed to develop appropriate live load lateral distribution factors for use in design of the prestressed double tees. In this study, a model originally proposed by Duberg et al. [1960], generalized by Powell et al. [1969], and modified for discrete lateral connections by Jones and Boaz [1986] was used. Jones developed software implementing the multi-beam bridge model and it was used in a study of multi-box beam bridges (Jones [1999]).

This chapter summarizes the basics of the model and makes comparisons between its predicted connection forces and those observed in the pilot bridge described in Chapter 3. The model is then used in conjunction with a laboratory testing program on a new full-scale bridge to assess performance of the recommended "simple" connection type recommended in Chapter 2, Fig. 27.

MULTI-BEAM BRIDGE MODEL

The analytical model used treats each double tee beam as a single structural element using elementary beam theory and the flange connections (either discrete connections, or a shear key, or both) are modeled with linear springs. Fig. 47 shows the notation and coordinate system needed to identify the individual beams. Beam properties required for each double tee are area, torsional stiffness, moment of inertia about the y- and z-axes shown in Fig. 47, as well as the modulus of elasticity and shear modulus. The moments of inertia and area compiled by TxDOT for various standard tees with 6 in. thick flanges are shown in Table 12. The TxDOT J values for torsional stiffness listed are approximations, computed using simple, approximate formulae. A more exact torsional stiffness for a complicated cross section like the double tee can be obtained using a FEM model of the double tee built with 3D solid "brick" elements. A unit torque is applied to a rod-like member having the beam cross section and recording the angle of

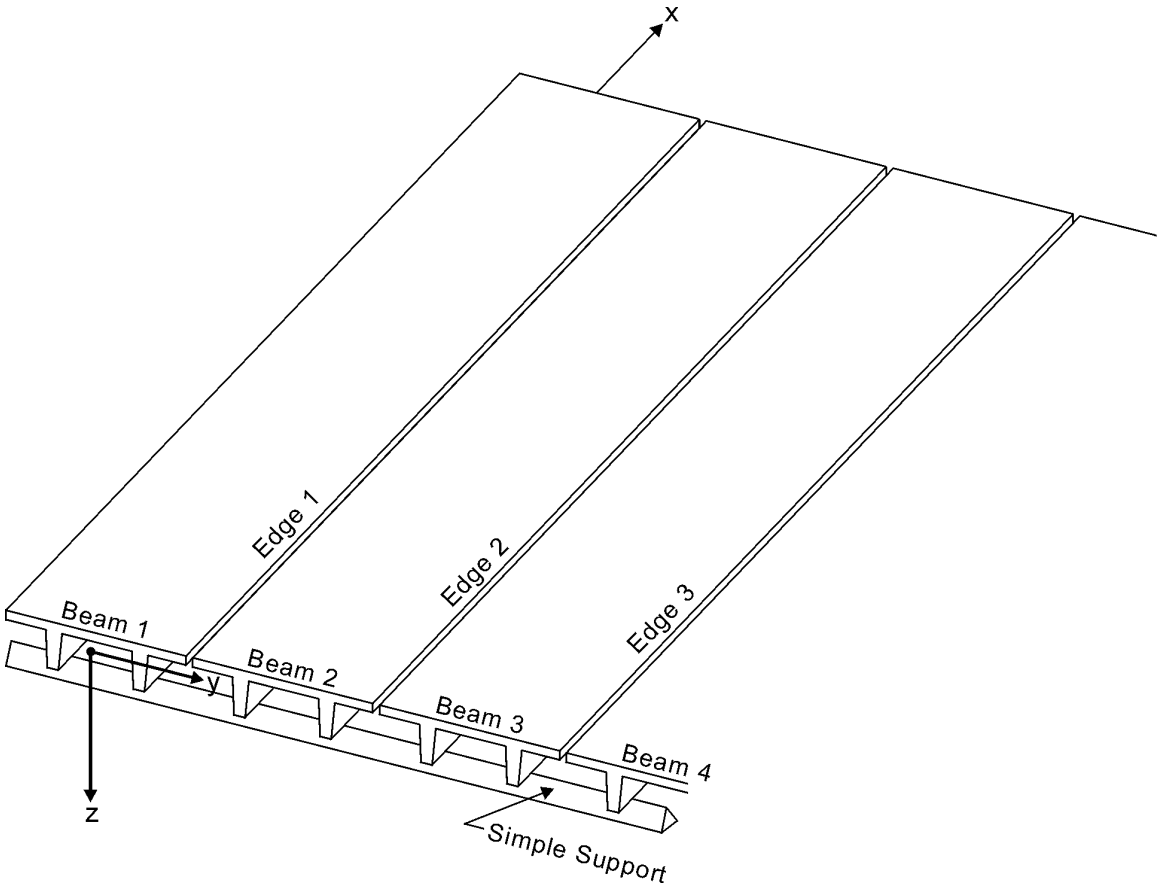

Figure 47. Typical Multi-Beam Double Tee Bridge.

Table 12. Section Properties of TxDOT Standard Double Tees with 6 in. Thick Flange.

Beam Designation	Nominal Depth (in.)	Area ($in.^2$)	Inertia about z-axis ($in.^4$)	Inertia about y-axis ($in.^4$)	TxDOT J ($in.^4$)	FEM Computed J ($in.^4$)
6T22	22	715	352,000	26,570	8,375	20,770
7T22	22	787	461,730	27,940	9,235	22,400
8T22	22	859	607,740	29,110	10,100	23,880
6T28	28	804	403,380	51,580	8,970	26,440
7T28	28	876	513,110	54,290	9,835	28,430
8T28	28	948	659,120	56,620	10,700	30,120
6T36	36	908	463,650	99,650	8,815	34,020
7T36	36	980	573,380	104,970	9,680	36,690
8T36	36	1052	719,39	109,580	10,545	38,990

twist of the section. The J value is then computed using a simple formula involving the angle of twist, beam length, and shear modulus. The method is described in Jones [1999] and was used to compute the torsional stiffnesses listed in the last column of Table 12. These latter values, which are significantly larger than the more approximate values, were used in all calculations of this study.

Each double tee has four points of support where it rests on bent caps. The bridge model uses linear springs to simulate the effect of the bearing pad which rests between the underside of the tee stems and the bent cap, as depicted in Fig. 48. The spring stiffnesses k_{py}, k_{pz} and k_{px} (latter spring not shown) represent stiffness of the entire pad and can be computed from known properties and dimensions.

Each point of connection between flanges of adjacent tees is modeled with a series of four linear springs which give rise to the set of four forces F_x, F_y, F_z, M_c shown in Fig. 49. Fig. 50 depicts the orientation of each of these springs which generates a force proportional to the relative displacement between points positioned opposite each other on adjoining flange edges. The stiffnesses k_x, k_y, k_z, k_Φ must be defined for each connection simulated, and the determination of these constants is described in subsequent sections of this report. In addition to the discrete connections installed on TxDOT bridges, a continuous shear key can be modeled through the addition of closely spaced spring sets along the entire length of the span and defining the stiffnesses appropriately.

The computer program implementing the multi-beam bridge model can treat a series of concentrated forces applied to the bridge in any pattern desired, allowing the placement of AASHTO truck loads either singly or in combinations. For any loading, the program also reports reaction forces at supports, the four force components in each lateral connection and shear, moments, and torque at selected locations along each beam in the structure. In addition, the program has the capability for placing one truck in each traffic lane and then adjusting the lateral position of each vehicle within its lane to produce the maximum bending moment in any beam of the bridge. This feature allows the computation of lateral distribution factors needed for beam design.

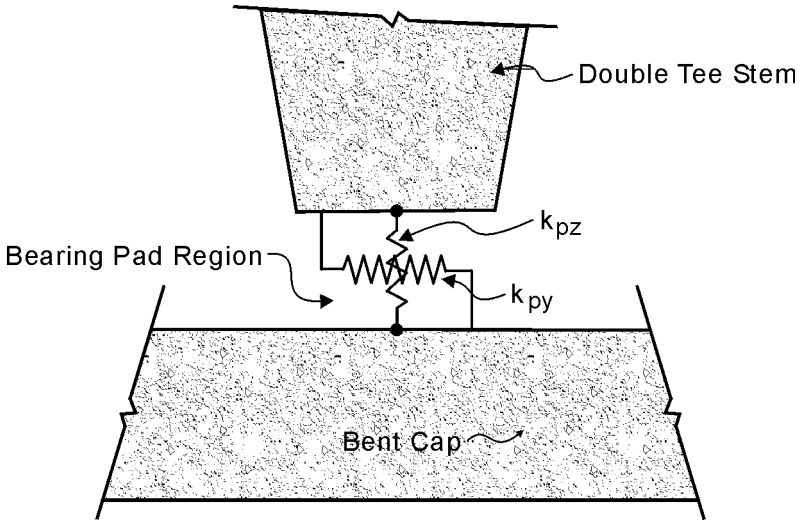

Figure 48. Modeling of Double Tee Supports.

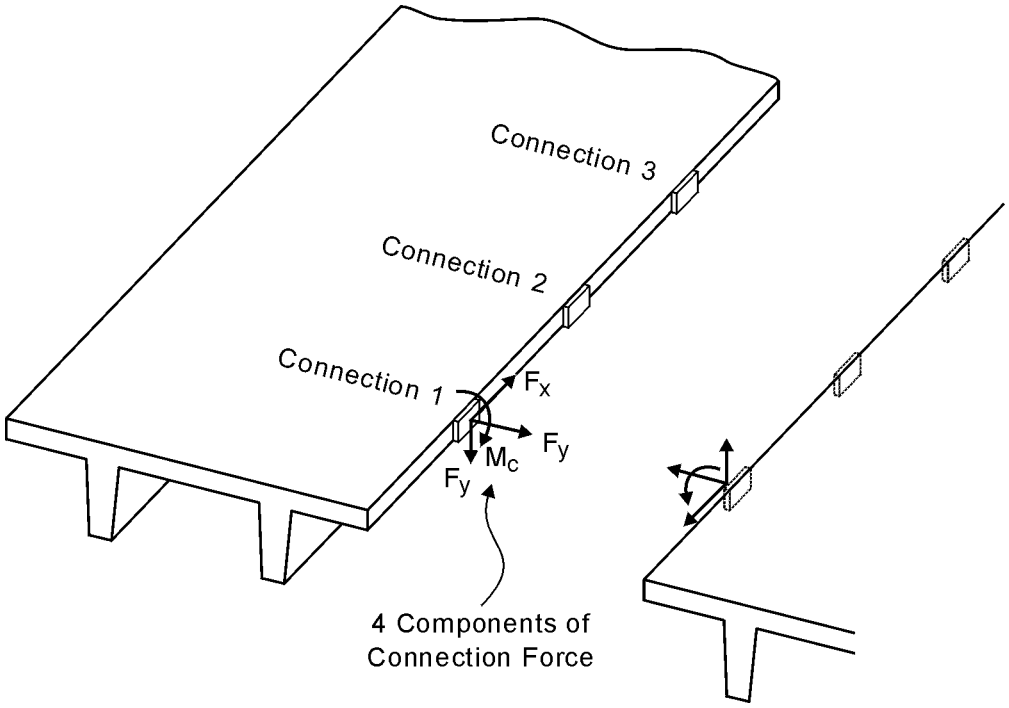

Figure 49. Force Components Developed is Discrete Connection.

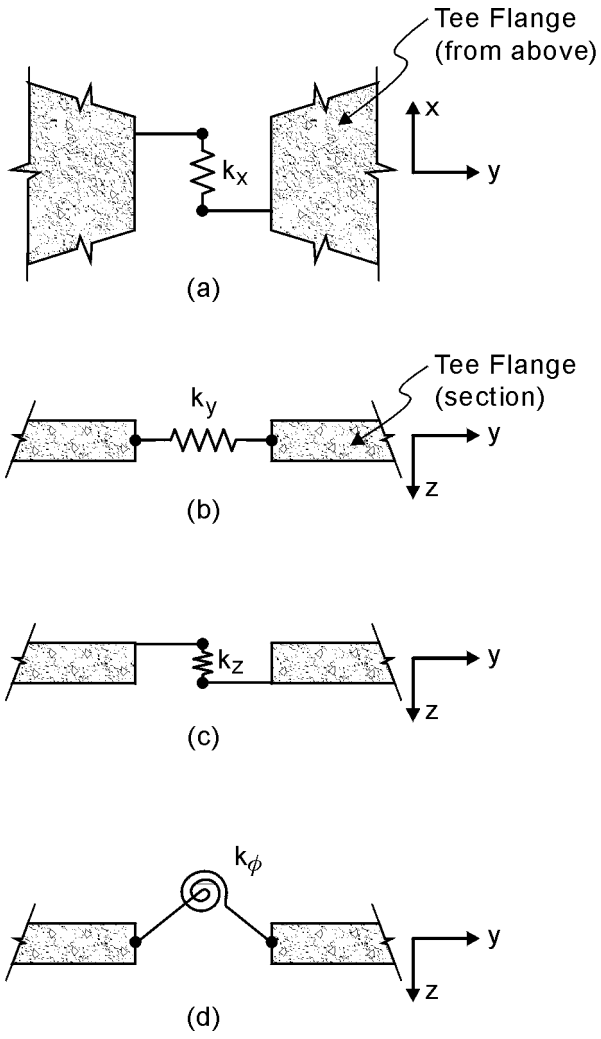

Figure 50. Spring Stiffnesses Used in Modeling Discrete Connection.

DOUBLE TEE BRIDGE TESTS ON THE PILOT BRIDGE

The pilot bridge described in Chapter 3 and shown in Figs. 30 through 34 was analyzed under the four loading conditions A through D given in Fig. 35. At each beam support point a 4 in. wide by 5 in. long by 0.5 in. thick rubber pad was present between the underside of the beam stem and the steel beam support simulating the bent cap support. A compression test was run on a typical pad to estimate the vertical stiffness k_{pz}. As seen in Fig. 51, response is somewhat nonlinear over the entire range. Fig. 52 is a re-plot of the region of the curve in the vicinity of 5 kips, the approximate dead load reaction of the beam. A regression run on the data points in Fig. 52 gave a k_{pz} of 135 kips/in. which was used in all analyses of the bridge.

The connection stiffnesses k_x, k_y, k_z, k_Φ discussed in the previous section can be estimated in a straightforward way for the vertical plate connection used in this structure from simple beam theory. Referring to Fig. 1, the two plates together constitute a "beam" with thickness of 0.75 in., depth of 5 in. and span of 6 in. The stiffnesses are taken from the corresponding components of a planer beam element (see, for example, Przemieniecki [1968]). Using a modulus of elasticity value of 30,000 ksi for steel gives the following stiffnesses: $k_x = 293$ kips/in., $k_y = 18{,}750$ kips/in., $k_z = 13{,}000$ kips/in. and $k_\phi = 39{,}000$ k-in./rad.

Researchers performed an analysis for a 20 kip load applied at each of the four load positions of Fig. 35 using the values of connection stiffness given above and assuming no shear key. In order to form a basis for comparison between the measured and predicted response, it was necessary to combine the stresses from the two plates in a connection into equivalent connection force components. This was accomplished by adding the stresses at corresponding points in the east and west plates of each connection, and then computing from them the connection force components M_c and F_y (Fig. 49) using ordinary beam theory. This amounts to back-calculating the bending moment and axial force present at a point along a beam where the normal stress is known at the top and bottom of the section. Tables 13 through 16 present the results of these calculations and compare them with the values predicted by multi-beam bridge theory. Note that in

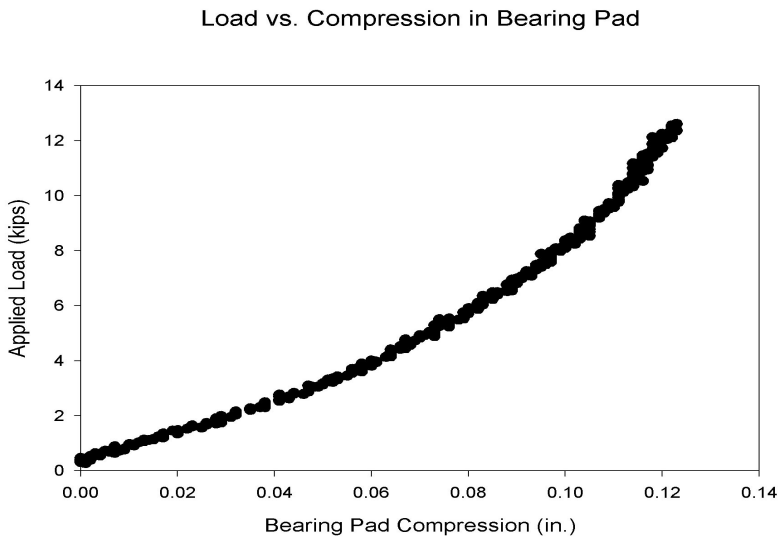

Figure 51. Compression Data for Bearing Pad Used in Lab Bridge.

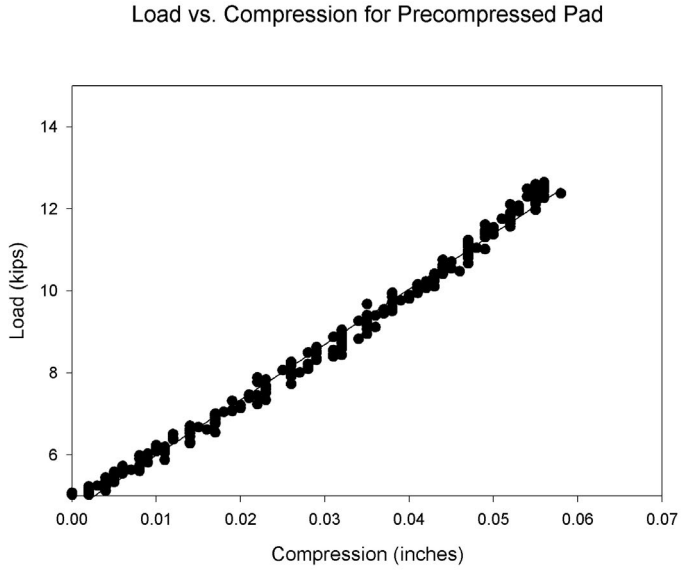

Figure 52. Best Fit Line for Bearing Pad Data.

Table 13. Comparison of Computed and Measured Plate Stress, Load Position A.

Connection I

	Computed From Measured Strains		Multi-Beam Bridge Theory	
Location	Fy (kips)	Mc (kip-in.)	Fy (kips)	Mc (kip-in.)
West End	4.00	-17.10		
East End	-1.99	-0.90	0.15	-14.80

Connection II

	Computed From Measured Strains		Multi-Beam Bridge Theory	
Location	Fy (kips)	Mc (kip-in.)	Fy (kips)	Mc (kip-in.)
West End	-3.01	-11.50		
East End	-0.70	-3.10	-0.44	-13.00

Connection III

	Computed From Measured Strains		Multi-Beam Bridge Theory	
Location	Fy (kips)	Mc (kip-in.)	Fy (kips)	Mc (kip-in.)
West End	-2.20	-10.10		
East End	0.50	-10.20	0.30	-10.90

Connection IV

	Computed From Measured Strains		Multi-Beam Bridge Theory	
Location	Fy (kips)	Mc (kip-in.)	Fy (kips)	Mc (kip-in.)
West End	0.00	-1.60		
East End	-2.30	-5.00	-0.73	-8.90

Table 14. Comparison of Computed and Measured Plate Stress, Load Position B.

Connection I

	Computed From Measured Strains		Multi-Beam Bridge Theory	
Location	Fy (kips)	Mc (kip-in.)	Fy (kips)	Mc (kip-in.)
West End	4.40	-13.20		
East End	1.00	-6.50	4.30	-12.70

Connection II

	Computed From Measured Strains		Multi-Beam Bridge Theory	
Location	Fy (kips)	Mc (kip-in.)	Fy (kips)	Mc (kip-in.)
West End	-4.30	-13.40		
East End	-0.90	-2.70	-6.60	-14.90

Connection III

	Computed From Measured Strains		Multi-Beam Bridge Theory	
Location	Fy (kips)	Mc (kip-in.)	Fy (kips)	Mc (kip-in.)
West End	-3.30	-13.00		
East End	-0.20	-8.50	0.14	-12.60

Connection IV

	Computed From Measured Strains		Multi-Beam Bridge Theory	
Location	Fy (kips)	Mc (kip-in.)	Fy (kips)	Mc (kip-in.)
West End	-0.10	-2.50		
East End	-2.60	-4.80	2.10	-10.60

Table 15. Comparison of Computed and Measured Plate Stress, Load Position C.

Connection I

	Computed From Measured Strains		Multi-Beam Bridge Theory	
Location	Fy (kips)	Mc (kip-in.)	Fy (kips)	Mc (kip-in.)
West End	4.20	-11.40		
East End	2.00	-8.70	3.20	-11.70

Connection II

	Computed From Measured Strains		Multi-Beam Bridge Theory	
Location	Fy (kips)	Mc (kip-in.)	Fy (kips)	Mc (kip-in.)
West End	-3.50	-12.90		
East End	-0.50	-3.70	-3.20	-13.90

Connection III

	Computed From Measured Strains		Multi-Beam Bridge Theory	
Location	Fy (kips)	Mc (kip-in.)	Fy (kips)	Mc (kip-in.)
West End	-4.20	-15.10		
East End	-0.20	-7.80	-3.20	-13.90

Connection IV

	Computed From Measured Strains		Multi-Beam Bridge Theory	
Location	Fy (kips)	Mc (kip-in.)	Fy (kips)	Mc (kip-in.)
West End	0.10	-3.10		
East End	-0.50	-3.30	3.20	-11.70

Table 16. Comparison of Computed and Measured Plate Stress, Load Position D.

Connection I

	Computed From Measured Strains		Multi-Beam Bridge Theory	
Location	Fy (kips)	Mc (kip-in.)	Fy (kips)	Mc (kip-in.)
West End	3.80	-9.70		
East End	2.10	-9.80	2.10	-10.70

Connection II

	Computed From Measured Strains		Multi-Beam Bridge Theory	
Location	Fy (kips)	Mc (kip-in.)	Fy (kips)	Mc (kip-in.)
West End	-3.20	-11.10		
East End	-0.80	-3.90	0.20	-12.70

Connection III

	Computed From Measured Strains		Multi-Beam Bridge Theory	
Location	Fy (kips)	Mc (kip-in.)	Fy (kips)	Mc (kip-in.)
West End	-5.40	-15.80		
East End	-1.40	-6.20	-6.60	-15.00

Connection IV

	Computed From Measured Strains		Multi-Beam Bridge Theory	
Location	Fy (kips)	Mc (kip-in.)	Fy (kips)	Mc (kip-in.)
West End	0.10	-4.00		
East End	-2.40	-3.40	4.30	-12.80

each connection an F_y and M_c value is computed from the measured strains at each end of the plate – a variation not represented in model.

ASSESSMENT OF ANALYTICAL MODEL PREDICTIONS

Comparison between measured and predicted stresses in the plates of the lateral connections in the bridge under loads in positions A through D in Fig. 35 are made in Tables 13 through 16. The predicted and measured values compare well in some cases, but in others are significantly different. Despite efforts to ensure consistent experimental results, it is apparent there are some inconsistencies. For example, loading case C is symmetric, indicating stresses in connections I and II should be the same as those in III and IV. However, as Table 15 shows, such was not the case. The cause for these discrepancies was never determined, although it is certain that non-uniformity of the welds on each plate resulting from tight and constraining clearances played a role. However, the four tables overall would suggest at least “ballpark” agreement between the connection forces measured and those predicted.

CHAPTER 5. ADDITIONAL BRIDGE MODEL TESTS

Chapter 2 of this report recommended a "simple" detail for connecting together the edges of adjacent tees. The performance of this connection, pictured in Fig. 27, was evaluated with beam tests described in Chapter 3, in which it was discovered that the use of headed stud anchors precipitated premature bond failure. As a result, the detail was changed and longer, 0.5 in. diameter reinforcing bars were substituted for the headed studs. The refined connection was then incorporated in a new, longer span two tee bridge model and tested in the laboratory.

The testing program served two functions. First, the performance of the new connection in a full-scale structure required validation, and second, the stiffnesses of the connection needed to be established in order to apply the multi-beam bridge analytical model introduced in Chapter 4 to typical TxDOT bridges. Unlike the vertical plate connection used in the bridge model tested in Chapter 3, there is no obvious rational procedure for estimating the four connection stiffnesses k_x, k_y, k_z, k_Φ nor any simple correlation between strains which could be measured in or around the connection and those stiffnesses. Consequently, an indirect approach was developed in which reaction forces in the bridge were measured under various loading conditions and the connection stiffnesses in the analytical model adjusted until reasonable agreement between predicted and measured reactions was obtained. Researchers performed additional load tests to study the response of the connection under cyclic loading, and finally much larger loads were applied in an attempt to cause failure in the connections. This chapter describes and documents these tests.

DOUBLE TEE BRIDGE MODEL DESCRIPTION

A new bridge with a 27 ft. span was constructed in the laboratory with two TxDOT standard 8 ft. wide by 22 in. deep double tees with 6 in. flange thickness (TxDOT designation 8T22). As seen in Fig. 53, the two tees were connected at 5 ft. intervals with the lateral connection in Fig. 27, except that the "sawtooth" indentation in the concrete above the embedded plate had to be omitted (see Fig. 54) because of time constraints with the fabricator. The headed studs in Fig. 27 were replaced with 0.5 in. diameter by 18 in. long deformed steel bars. For reference purposes, the connections are numbered I through VI in the figure. The

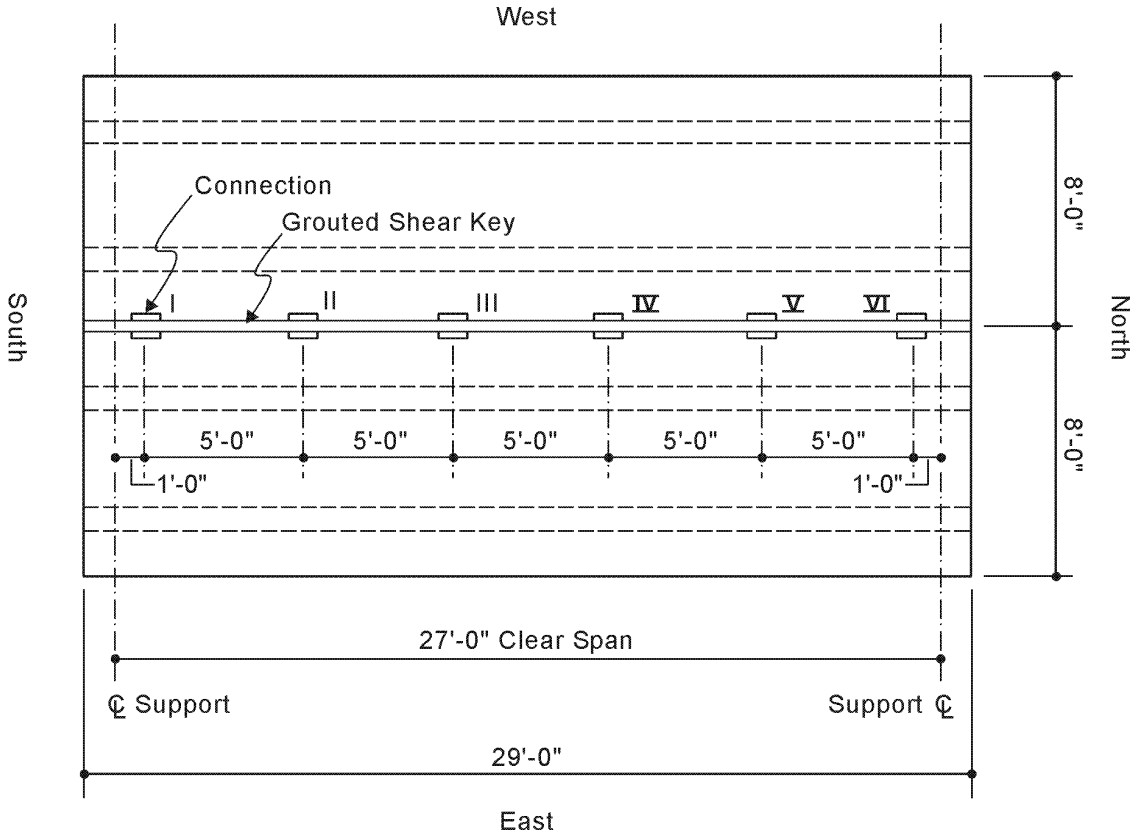

Figure 53. Plan View of Lab Bridge Model.

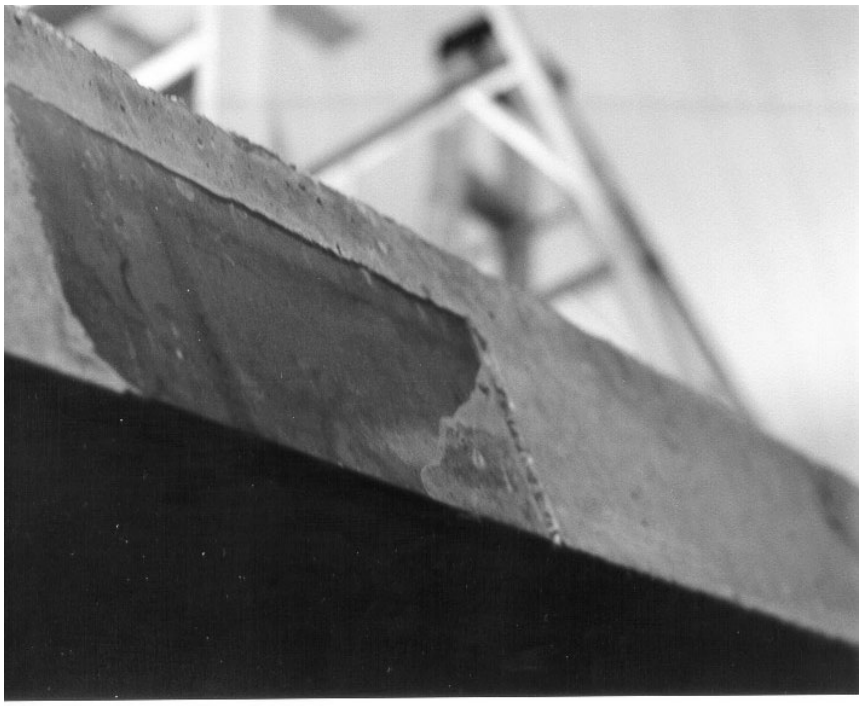

Figure 54. Embedded Plate before Connection Made.

bridge ends were supported on the steel frames shown in Fig. 55. Each beam contained TxDOT standard conventional reinforcing and standard prestressing strand pattern for the span (eight strands in each joist stem). The double tees were positioned on the supporting frames with a target separation of 0.25 in. between adjacent beam flanges. Actual separation along the 29 ft. of joint varied between 0.25 in. and 0.5 in. Fig. 56 shows a typical 8 in. long steel bar after welding to the embedded plates in accordance with the detail of Fig. 27. One inch diameter PVC pipe was used for backer rod and laid in the joint between the connections. The face of each tee flange was cleaned with a rotary steel brush and then washed with water prior to placing the MasterFlow 928 grout to form the shear key. The average compressive strength of the grout in the shear key was 8,120 psi, based on tests of three standard cubes performed 11 days after casting. Average strength after 92 days was 8,230 psi.

INSTRUMENTATION

The primary instrumentation used in these tests were load cells. A load cell was inserted beneath the underside of each tee stem and the steel support framework, providing a direct measurement of the reaction forces in the bridge. Fig. 57 shows a schematic of the load cell installation, and Fig. 58 is a photograph of an installed load cell. In addition, 12 displacement transducers were positioned to measure vertical displacements in the structure. Three displacement measurements per stem were necessary to filter out the effect of compression in the elastomeric bearing pads shown in Fig. 57 on the overall vertical displacement at mid-span of the bridge. Fig. 59 shows the locations of both types of transducers and the numbering scheme used to identify them. After the grouted shear key was installed and cured, electrical resistance strain gages were installed on the upper face of the key at the locations shown in Fig. 60 to measure transverse strain induced in the top surface of the key by loads on the bridge.

PROOF TESTS

The purpose of this series of tests was to load the individual double tees before they were connected together in order to check the reasonableness of the measured responses. For example, loading at mid-span and along the centerline of the member should produce four equal reaction forces for comparison with the values measured with the load cells. Loading at the

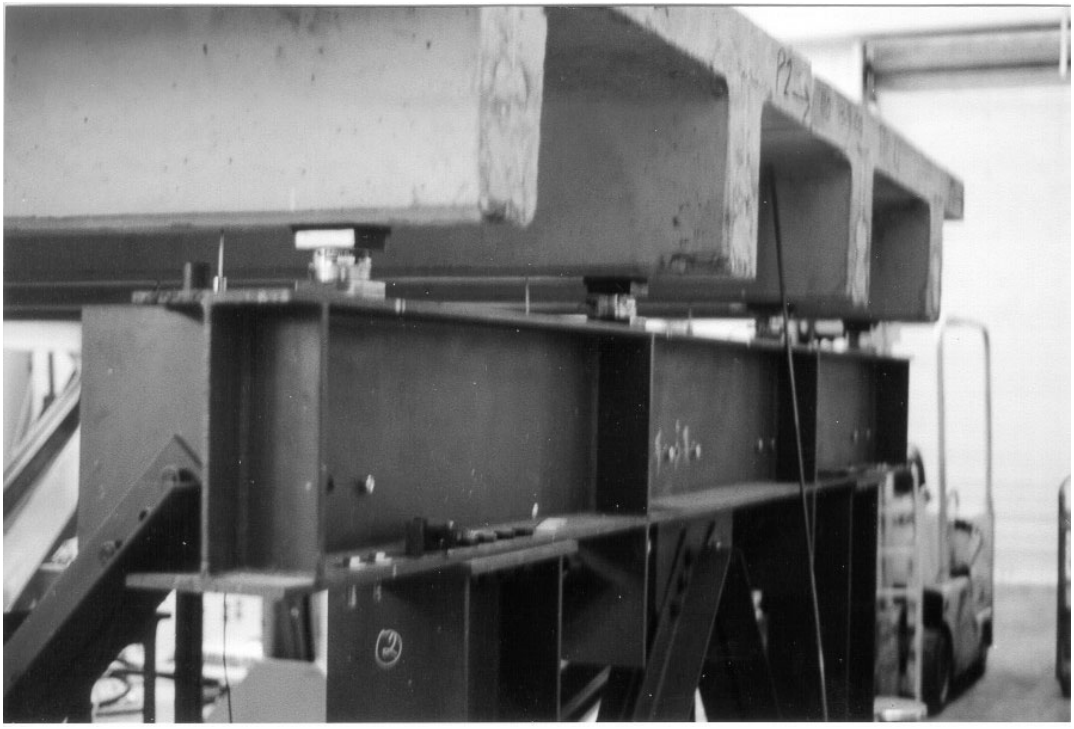

Figure 55. Steel Frame Supporting Bridge Model.

Figure 56. Steel Bar Welded into Connection.

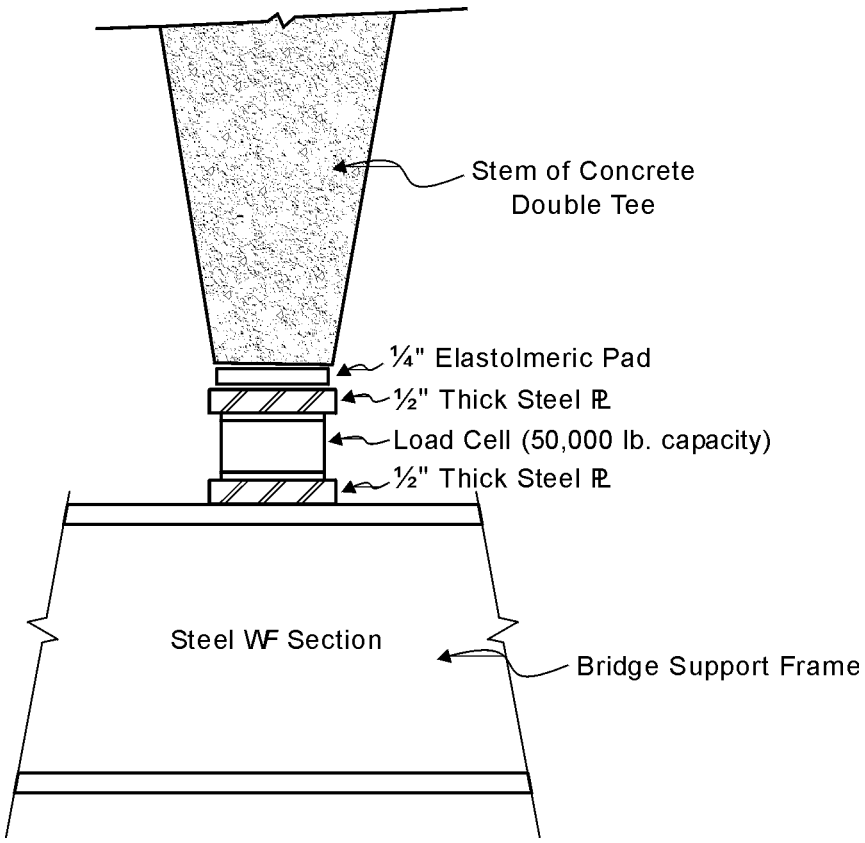

Figure 57. Schematic of Load Cell Support System.

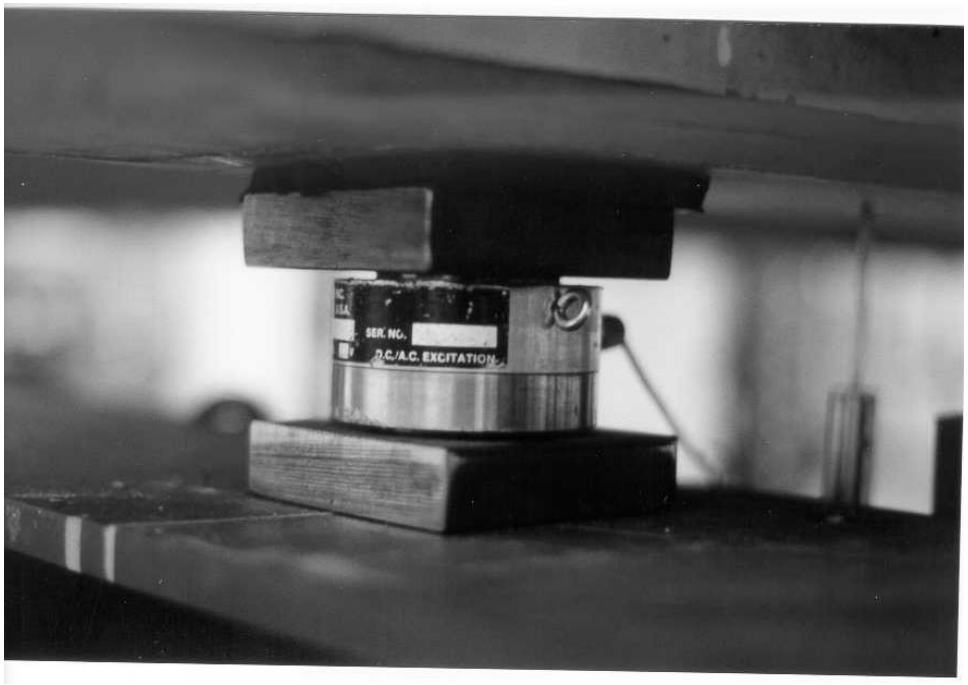

Figure 58. Photograph of Load Cell.

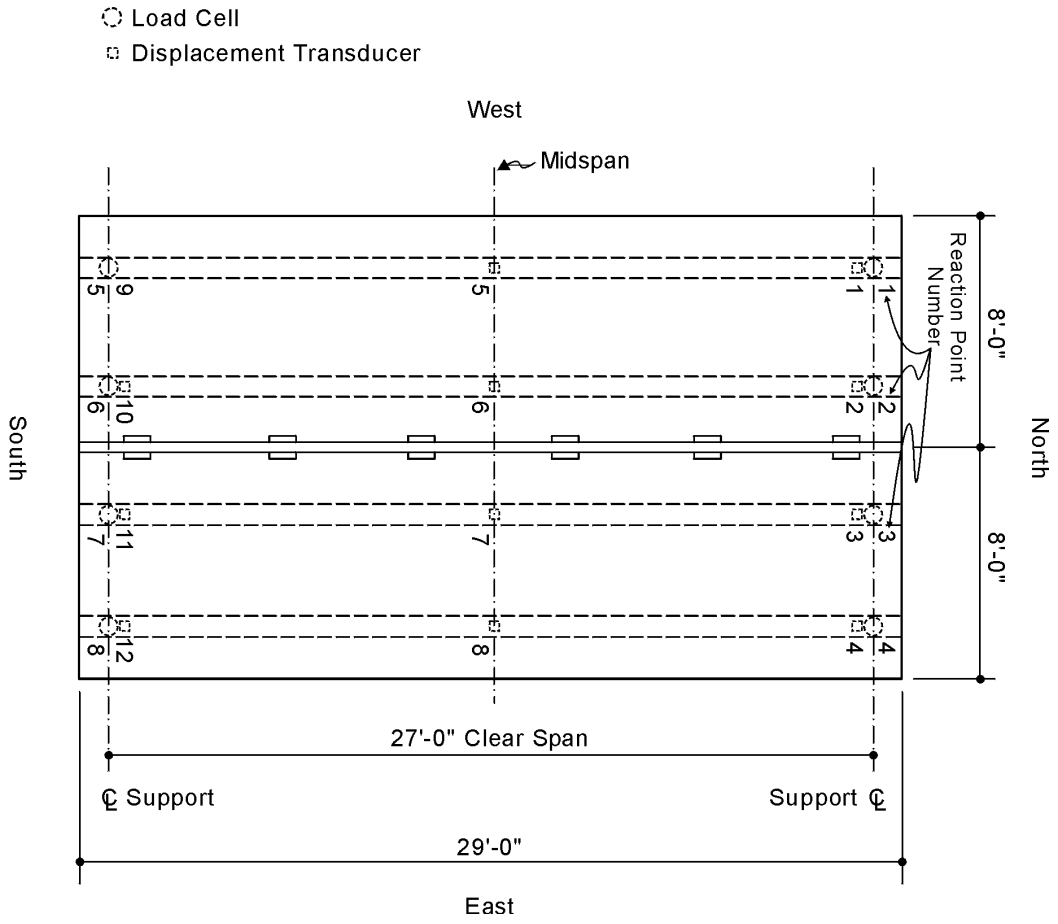

Figure 59. Location of Load Cells and Displacement Transducers.

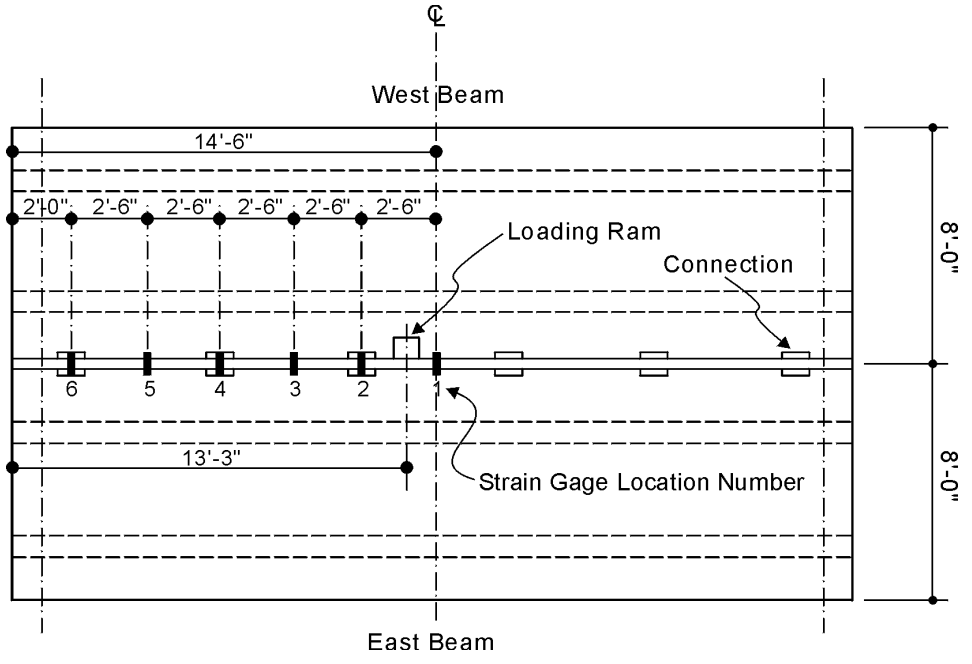

Figure 60. Position of Strain Gages on Shear Key.

centerline but away from mid-span (e.g., the quarter point) should lead to equality of the two reaction components at the same end of the beam, and the sum of those two reactions at each end can be calculated from simple statics. Other, more unsymmetrical loadings could be checked against the analytical model (in which the connection stiffnesses were set to zero), as could the measured mid-span displacement, although the latter was so small as to be of questionable accuracy. The proof tests were carried out through the following steps.

The load cells were first calibrated in a compression testing machine and then positioned on the supports with steel bearing plates and an elastomeric pad shown in Fig. 57 and initial readings taken. The two double tees were lifted into place one at a time and seated on the bearing plates and pad. Initial readings were then taken from each of the load cells and are listed in Table 17, where the reaction point numbers refer to those shown in Fig. 59.

By summing the readings from the four load cells supporting a single tee, the weight of the tee was measured and this weight divided by 4 to get the predicted reactions shown in the line of the table labeled “Dead Load.” Comparison of these two lines indicates the measured reactions were not all precisely equal, although the differences between them are relatively small. This deviation from symmetry in the reactions is believed due to slight unsymmetric camber in the tees and possibly somewhat different seating of the tee stems on the load cells.

Next a single force of approximately 20 kips was applied at the load positions shown on each of the two double tees in Fig. 61, and the reaction forces recorded. An approximate ram force was read by monitoring the fluid pressure in the cylinder of the ram. A more accurate measure of the ram force applied was obtained by summing the eight reaction forces reported by the load cells. This value was used as the applied load in making predictions of reactions with the multi-beam bridge model. In each load position, the actuator force was slowly increased to the peak value of (approximately) 20 kips, held at that level for several minutes, then offloaded back to zero, reloaded and then brought back to zero again. Very good repeatability of measured reactions between successive loadings was found in every case, with maximum variations on the order of 0.1 to 0.2 kips between a reaction force on the first loading and the second loading. The reactions from the first application of load in each load position are listed in Table 17 as the measured values. In Table 17, as well as subsequent tables listing reaction forces, a positive value indicates an increase in the upward reaction force over its initial value (i.e., before application of the ram force), while a negative value results when the reaction force diminishes. In either case, however, the reaction force shown is that produced by the applied ram load. The

Table 17. Predicted and Measured Reaction Forces of Individual Tees.

		West Beam				East Beam			
		Reaction Point Number				Reaction Point Number			
Loading		1	2	5	6	3	4	7	8
Dead Load	Meas.	6.86	6.77	6.59	6.99	6.60	6.10	7.24	6.66
	Pred.	6.80	6.80	6.80	6.80	6.65	6.65	6.65	6.65
20 kips @	Meas.	-2.16	12.29	-2.34	12.22				
Position 1	Pred.	-2.50	12.50	-2.50	12.50				
20 kips @	Meas.	-2.25	6.61	-1.81	17.44				
Position 2	Pred.	-3.63	7.95	-1.37	17.05				
20 kips @	Meas.	4.66	5.44	5.05	4.85				
Position 3	Pred.	4.93	4.93	4.93	4.93				
20 kips @	Meas.	2.17	2.16	7.47	8.20				
Position 4	Pred.	2.16	2.16	7.84	7.84				
20 kips @	Meas.					4.82	4.46	4.63	5.11
Position 5	Pred.					4.76	4.76	4.76	4.76
20 kips @	Meas.					2.20	2.15	8.02	7.63
Position 6	Pred.					2.16	2.16	7.84	7.84
20 kips @	Meas.					11.68	-1.68	12.58	-2.59
Position 7	Pred.					12.50	-2.50	12.50	-2.50
20 kips @	Meas.					6.74	-2.42	17.52	-1.84
Position 8	Pred.					7.95	-3.63	17.05	-3.63

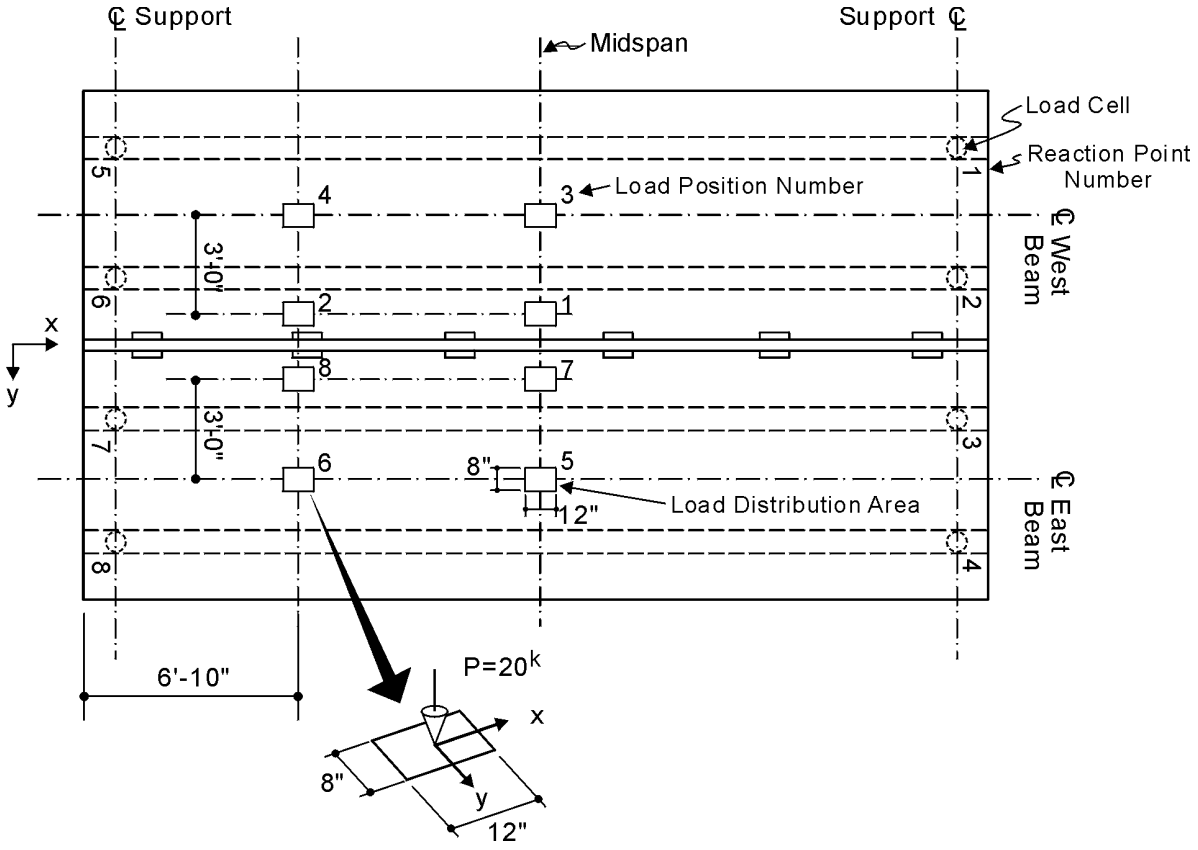

Figure 61. Loading Positions for Proof Tests.

table also lists predicted values, which were obtained with the multi-beam bridge model described in Chapter 4 or from symmetry arguments.

In general, agreement between measured and predicted reaction forces in Table 17 is good. Differences between measured and predicted values of reactions could be due in part to the actuator load not acting precisely through the center of the 8 in. by 12 in. steel plate (Fig. 36) used to distribute the force over the deck surface. To explore the sensitivity of the measured reactions to this effect, the multi-beam bridge model was run for a 20 kip force at load position 3 in Fig. 61. The force was then moved to various other positions within the confines of the 8 by 12 inch rectangle formed by the steel bearing plate and the model re-run. Table 18 presents those results. Positive reaction force is upward. Inspection of the data suggests that a maximum variation of about 0.5 kips (with a total load of 20) in a reaction force could be attributed to the applied load having a 6 in. eccentricity relative to the center of the loaded area beneath the steel plate on the bridge deck. Roughly speaking, this is about 0.1 kips per inch of

Table 18. Variation of Reactions with Load Position.

Concentrated Force Eccentricity (in.)	West Beam Reaction (kips)			
	Reaction Point Number			
	1	2	5	6
0" , 0"	-1.09	5.40	-3.92	19.60
-6" , 0"	-0.99	4.94	-4.01	20.06
6" , 0"	-1.17	5.86	-3.83	19.13
0" , -4"	-0.79	5.04	-2.61	18.30
0" , 4"	-1.44	5.76	-5.23	20.90

misplacement, suggesting that a realistic deviation of load position could account for 02.-0.3 kips of reaction deviation.

"SIMPLE" CONNECTION STIFFNESS DETERMINATION

The introduction to this chapter cited the need to establish values for the four connection stiffnesses k_x, k_y, k_z, k_Φ described in Chapter 4 and depicted in Fig. 50. This was accomplished through a series of load tests in which a (approximate) load of 20 kips was positioned on the laboratory bridge structure at one of the eight locations shown in Fig. 61 and the four reaction forces on each beam measured. For a particular load position, the multi-beam bridge model predicts the reaction forces. The predicted reactions in turn depend upon the value of each of the four connection stiffnesses. Roughly speaking, the connection stiffness values which give the best agreement between measured and predicted reactions forces provide good estimates of the true values. Additional credence is lent to this argument if at each of the several different load positions, the estimation process leads to the same values of stiffness.

Two sets of stiffnesses required estimation. The first were those associated with the embedded steel plate and welded bar located at discrete intervals along the bridge, and the second were those arising from the continuous shear key. A two-step process was followed in which the reaction forces from loadings applied after the discrete connections were installed but prior to installation of the key were used to establish the discrete connection stiffnesses. Data taken from load tests after pouring of the shear key were then used to obtain estimates of the spring stiffnesses appropriate for modeling the key.

Numerical experimentation established that k_x and k_y have very little influence on the reactions when only vertical loads are applied to the bridge, and consequently these values were set to 1.0 for convenience. It was discovered that the stiffness k_ϕ of the discrete connection was predicted by the multi-beam bridge model to have almost no effect on the reaction forces, leaving only k_z to be determined. Similarly, the analytical model predicted that with shear key in place, the reactions were extremely insensitive to the k_z of the key, and hence only k_ϕ for the shear key could be estimated from the test data.

Fig. 62 shows a typical plot of total reaction force error versus the stiffness k_z of the bar/plate connection for a 20 kip load applied at location 4 in Fig. 61. Total reaction force error E_T is defined as

$$E_T = \sum_{i=1}^{8} abs(R_i - \Re_i) \qquad \text{Eq. (5.1)}$$

where R_i is the ith reaction component predicted by the multi-beam bridge model, and $\Re_i$ is the corresponding measured reaction. Clearly the aggregate difference between measured and predicted reactions diminishes with increasing k_z in this case and reaches a minimum around k_z=400 kips/in. Table 19 lists the values of k_z computed in this way for the other seven load positions. The values there range between 50 and 1000, with the average being about 470 kips/in. This average value was adopted and used in all subsequent analyses for the k_z value of the embedded steel plate and welded bar component of the simple connection.

After the load tests described above were completed, the shear key (see Fig. 27) was grouted. The bridge was once again loaded at the eight positions indicated in Fig. 61, and the reaction forces were recorded for each load position. The multi-beam bridge model was then used to predict the reaction forces under each of the load positions, but with the following modifications to the analytical model used to characterize the steel plate and welded bar component of the connection. First, the k_z value for this component was set to the 470 kips/in. established earlier. Unlike the discretely positioned steel plate and bar components, the shear key is continuous along the length of the bridge. This condition was approximated in the multi-beam bridge model by placing spring sets at 1 ft. intervals along the span. Thus the stiffnesses determined represent the stiffness per lineal foot of shear key.

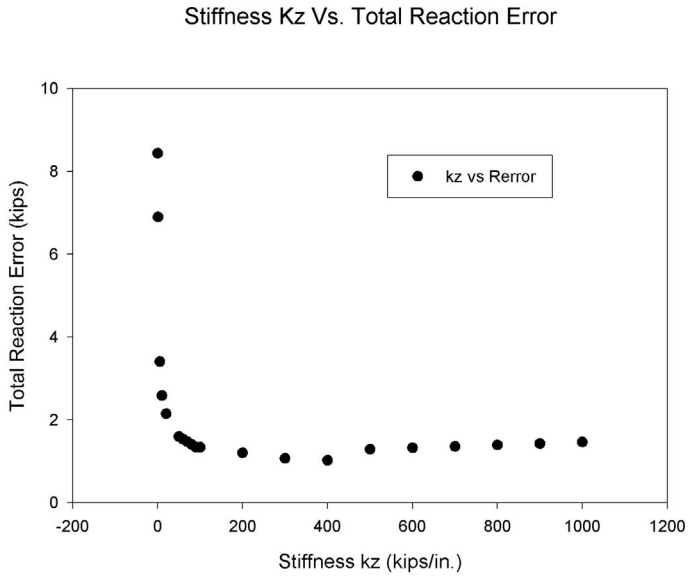

Figure 62. Reaction Error Versus Stiffness k_z, Load Position 1.

Table 19. Computed K_z of Discrete Connection by Load Case.

Load Position	Best K_z Value (kips/in.)	Total Reaction Force Error (kips)
1	500	3.767
2	1000	4.731
3	400	1.600
4	400	1.026
5	400	0.760
6	400	1.234
7	600	2.365
8	50	3.917

Analyses with the multi-beam bridge model revealed the interesting fact that the k_z stiffness of the shear key had negligible effect on the reaction forces, even when this parameter was varied over more than four orders of magnitude. The most plausible explanation for this behavior appears to be that the plate/bar components, when spaced at 5 ft. increments, provide sufficient vertical shear transfer between adjacent beams to render the additional transfer provided by the shear key ineffective. This is likely not a general condition but rather one peculiar to the short span (27 ft.) of the laboratory bridge tested. The analyses did indicate a significant dependence of the reaction forces upon the value of the rotational stiffness k_ϕ for the shear key. However, this dependence occurred only for load positions having an eccentricity relative to a longitudinal centerline of the beam (load positions 1, 2, 7, and 8). For positions 3, 4, 5, and 6, where the load was applied on the centerline, the reaction forces demonstrated almost complete independence of both the k_z and k_ϕ values used for the shear key. As a result, only the former four load positions could be used to estimate the value of the shear key k_ϕ value.

Fig. 63 plots the total reaction force error versus the value of k_ϕ used for the shear key in load position 1. Like Fig. 62, which demonstrated the effects of varying the k_z of the plate/bar component, the total reaction error variation takes on a minimum value for a specific value of stiffness. In addition, the region in which the minimum occurs is relatively flat, suggesting that a "ballpark" estimate of stiffness is sufficient for analysis purposes. Table 20 lists the value of k_ϕ established from the four load positions. The average of these values is 6,250 in.-kips/rad./ft., which was used for k_ϕ of the shear key.

CYCLIC LOAD TESTING

After completion of the test program to determine stiffnesses of the lateral connection, the bridge was subjected to cyclic loading to look for degradation effects in the structure caused by fatigue effects. The loading ram was positioned on the west double tee as shown in Fig. 60. This location placed the 12 in. by 8 in. load plate on the edge of the west beam, approximately a foot off of mid-span. Also shown in the figure are the locations of six strain gages that were bonded to the top of the grout in the shear key. Each gage was positioned at the center of the key and oriented to read strain in the transverse (east-west) direction. The gages used were

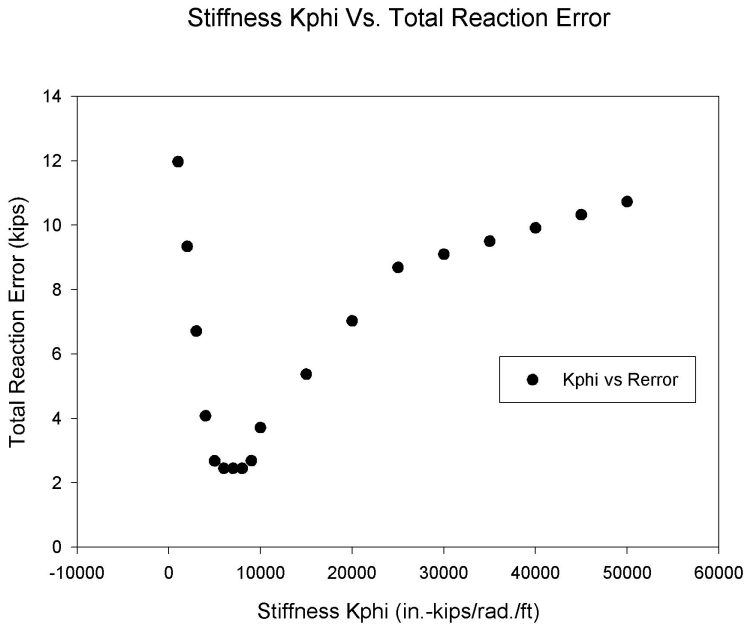

Figure 63. Reaction Error Versus Stiffness k_z, Load Position 1, with Shear Key.

Table 20. Computed Kphi of Shear Key by Load Case.

Load Position	Best Kphi Value (in.-kips/rad./ft.)	Total Reaction Force Error (kips)
1	6000	2.451
2	5000	3.794
7	6000	1.629
8	8000	4.534

conventional foil gages with a 0.25 in. gage length and 120 ohm resistance. At each gage site, the grout surface was ground smooth, cleaned, and then covered with an epoxy coating. After the epoxy had cured, it was sanded smooth and cleaned. The strain gage was then mounted on the epoxy patch using a commercial strain gage adhesive.

The measured strains were used in two ways. First, by a simple calculation introduced below, the transverse moment (M_c in Fig. 49) at a gage location could be computed. Secondly, the strain response to a statically applied load was recorded at intervals during the cyclic testing as a means of detecting damage such as delamination of the grout from the concrete face of the tee flange or substantial failure in the weld between bar and plate. Although the type or extent of damage can not be predicted from just the measured strains, it was felt that a significant change in the strain recorded at a particular location under the same static load applied before and then after the application of some number of cycles of variable load would suggest a significant change in the load transfer mechanism of the connection and shear key.

A total of 1.5 million cycles of loading was applied through the ram position shown in Fig. 60. The load was varied from zero to a peak and back to zero at a rate of three cycles per second in a sinusoidal variation. During the first 500,000 cycles, the peak load was 16 kips. The next half million cycles were applied with peak load at 24 kips, and then the final half million cycles were applied at a peak load of 32 kips. At intervals ranging from approximately 50,000 to 250,00 cycles, the test was momentarily shut down, the ram restored to static mode, and then a static load test was run. This test was identical to the regimen followed in earlier tests where the load was increased slowly to 20 kips (approximately), reduced to zero, and then raised to 20 kips once again to check for repeatability. Fig. 64 shows a graph of transverse stress in the top face of the shear key computed from strain at each of the six gage locations under a statically applied 20 kip load as a function of the number of cycles of load applied prior to static testing. These stresses were obtained by multiplying the measured strains by a modulus of elasticity value of 5,400,000 psi.

The stress at a gage point generally diminishes with distance from the point of loading, as expected. Although gages 1 and 2 were nearly equidistant from the load point, gage 2 was centered over a steel plate connection, causing it to see substantially lower stress than gage 1 where there was only the shear key. The computed stress at all six locations is relatively constant over the 1.5 million cycles of load, with the variations being more random than systematic. Analysis showed nothing in the patterns of stress suggesting a breakdown in the connection or

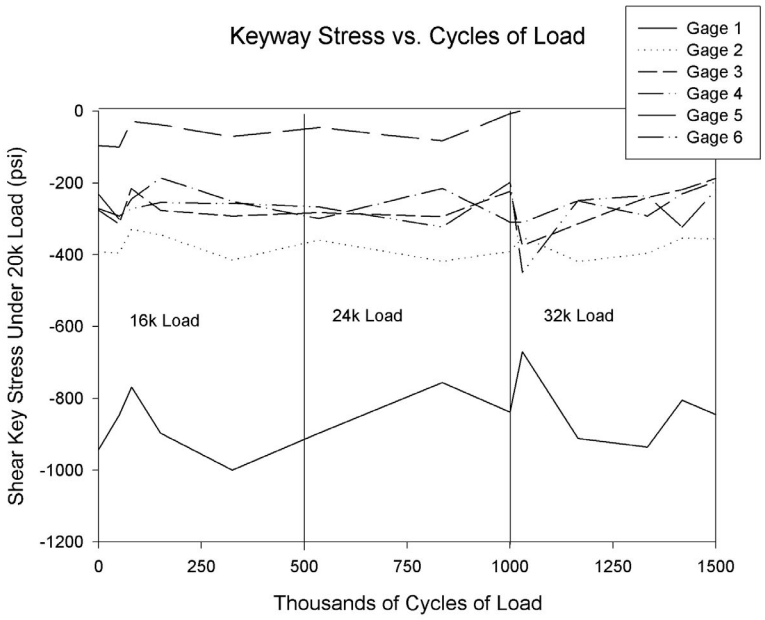

Figure 64. Shear Key Stress Versus Cycles of Load.

keyway. After cyclic loading, researchers chipped away the grout over each discrete connection to expose the steel bar and weld material joining the bar to the embedded steel plates. They found no visual evidence of weld failure. Fig. 65 shows connection III (see Fig. 53), which was closest to the load and therefore most highly stressed by the cyclic loading. Die penetration testing was also used in an attempt to make visible possible fatigue cracks in the upper surface of the weld. The darker areas in the photograph are pits in the surface created by the welding process and not cracks. The die penetrant revealed no evidence of fatigue cracking in the weldment material.

A hammer and chisel were used to break out sections of the shear key to expose the interface which had existed between grout and flange edge concrete. The edge of the flange is seen in Fig. 66 while the section of grout shear key is visible in Fig. 67. The separation between the two surfaces is relatively clean, suggesting very little interlocking, an impossibility

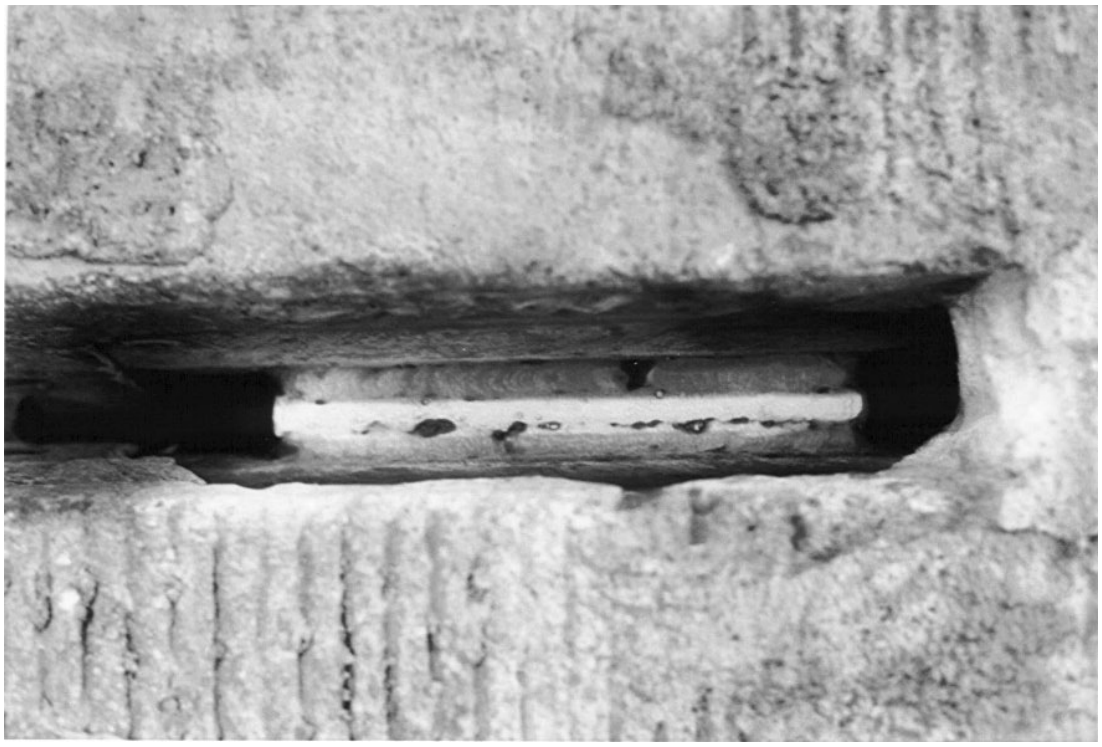

Figure 65. Bar/Plate Connection after Cyclic Loading.

Figure 66. Edge of Flange after Shear Key Removal.

Figure 67. Section of Shear Key.

given the quite smooth finish on the face concrete. A rougher surface on the flange edge would enhance the bond strength, although there was nothing in the tests conducted that would suggest more is needed.

ULTIMATE LOAD TESTS

The last test conducted was an attempt to apply a load of sufficient magnitude to cause distress or failure in the connection between adjacent beams, given the constraint that the loading system capacity was approximately 100 kips. The ram remained positioned at the location shown in Fig. 60. The ram load was increased to 94.7 kips when the capacity of the hydraulics was reached and the bridge had to be unloaded. Inspection of the tee flange, grout shear key, and the (closest) bar/plate connections showed no signs of distress or any evidence to indicate the loading had reached nearly 100 kips.

CHAPTER 6. APPLICATION TO TXDOT BRIDGES

Chapter 2 of this report recommended a new type of lateral connection for double tee bridges. Chapter 4 briefly reviewed the multi-beam bridge analytical model which predicts the forces in a multi-beam bridge subjected to truck loads, while Chapter 5 described the estimation of lateral connection stiffnesses needed to analyze TxDOT double tee bridges.

The purpose of this chapter is to develop design guidelines for double tee bridges incorporating the recommended lateral connection detail. Specifically, the bending moment to be used for beam design and the maximum forces acting on the lateral connection are addressed. This was accomplished by examining a selection of TxDOT bridge configurations that will form the basis of a new double tee bridge standard.

LIVE LOAD LATERAL DISTRIBUTION FACTOR

The live load lateral distribution factor (LF) is used to obtain a bending moment for sizing the double tees in a bridge. The beam design moment is obtained by multiplying LF times the maximum moment that can be produced along a simple beam by a single AASHTO HS-20 truck.

AASHTO [1994] provides an equation for estimating the LF for beams in several different types of bridge superstructures. For double tee bridges, it gives:

$$LF = S / D \qquad \text{(Eq 6.1)}$$

where

S = width of the double tee (ft.),

$D = 11.5 - 1.4 N_L (1 - 0.2C)^2$,

N_L = number of traffic lanes,

$C = K(S / L)$,

L = bridge span (ft.),

$K = \sqrt{\frac{(1+\mu)I}{J}}$

μ = Poisson's ratio for beam concrete,

I = moment of inertia of beam, and

J = torsional stiffness of beam.

TxDOT also has a "rule-of-thumb" expression for estimating the LF. It is shown below:

$$LF = S/10.5 \qquad \text{(Eq 6.2)}$$

where S is the tee beam width in feet. Multi-beam bridge analysis provides a more rigorous means of computing the lateral distribution factor LF in that it is based on theory which models, at a detailed level, the interactions between adjacent beams through the lateral connections which join them. As explained in Chapter 4, the (primary) bending moment M_y, moment M_z, shears, and torque can be computed at selected points along each tee in the bridge, together with the force components in all lateral connections. For a specific location of AASHTO truck on the bridge, the maximum M_y along each beam can be divided by the total truck moment to express it as a fraction of total truck moment.

The LF given in Eqs. (6.1) and (6.2) by their definition are an estimate of the largest fraction of truck moment occurring anywhere along any interior beam of a bridge due to any conceivable arrangement of AASHTO trucks complying with traffic lane definitions within AASHTO specifications [1986]. In applying the multi-beam bridge model, this means running multiple analyses, one for each conceivable truck position. Because the bridge is simple span, this task is not as daunting as it might first appear, and as explained in Jones [1999], reduces to a series of analyses in which a single truck is positioned longitudinally straddling mid-span in a well-known fashion and then moved laterally in discrete jumps across the width of each lane on the bridge. Results are then superimposed to capture the largest M_y occurring in each beam and from which the LF is computed. This process is coded into the software which implements the multi-beam bridge analysis and can thus produce "exact" values for lateral distribution factor.

Five different bridge geometries were examined to develop the LF recommendations presented in this chapter. Table 21 lists the arrangement of tees in each. These bridges correspond to those currently under development as TxDOT standards and range in roadway width from 24 to 44 ft. For a particular width of bridge, three standard TxDOT tees are available, and the choice of which to use is of course dependent on the span length. Consequently, for each

Table 21. Bridges Used in Analyses.

Roadway Width (ft.)	Tee Arrangement
24	6-7-7-6
28	6-6-6-6-6
30	6-7-6-7-6
38	6-7-7-7-7-6
44	6-7-7-6-7-7-6

of the three depths of available tees, three different span lengths were considered; a "short," a "medium," and a "longer" span. Table 22 summarizes these span lengths for the three tees.

The multi-beam analysis model (with automatic lateral load distribution factor calculations) was run on the 45 different bridges defined by Tables 21 and 22, resulting in a computed LF value for each beam in each bridge. These are all contained in the data of Table 23. Note that each line in the table refers to a particular arrangement of beams in the cross section and depth of tee used and that to obtain a design moment for all beams in the bridge section, one would simply take the largest value in the line. Because of symmetry, only the beams to the left of bridge centerline are listed, with beam no.1 being the leftmost in the bridge section.

The LF data in Table 23 is presented graphically in Figs. 68 through 70. Figure 68 was obtained by selecting from the 45 cases in Table 23, every one which had a 6 ft. wide tee positioned as the first (outside) beam. The plot shows variation in LF with span length for exterior beams. The points suggest a slight decrease in distribution factor with span length, which in fact is implied by Eq. (6.1). Also shown in the figure is the TxDOT formula, Eq. (6.2), which is seen to give a conservative estimate of distribution factor. Figure 69 addresses 6 ft. wide *interior* tees, and it can be seen that the TxDOT formula *underestimates* LF in any span less than about 40 ft. Figure 70 applies to 7 ft. wide interior tees, and the TxDOT expression appears conservative with the exception of a few very short spans. For comparison purposes, the graph in Fig. 71 plots the multi-beam theory LF values of Fig. 69 (interior 6 ft. tees) together with the values predicted by the AASHTO Eq. (6.1). The data suggest that the AASHTO formula also tends to underestimate the true distribution factor for spans under 40 ft.

These results indicate that for the five standard bridges considered, the current TxDOT rule of S/10.5 gives safe but somewhat overly conservative values except where 6 ft. wide

Table 22. Span Lengths Used in Analyses.

Nominal Tee Depth (in.)	Span Lengths (ft.) Short	Medium	Long
22	22	28	36
28	30	42	54
36	40	52	64

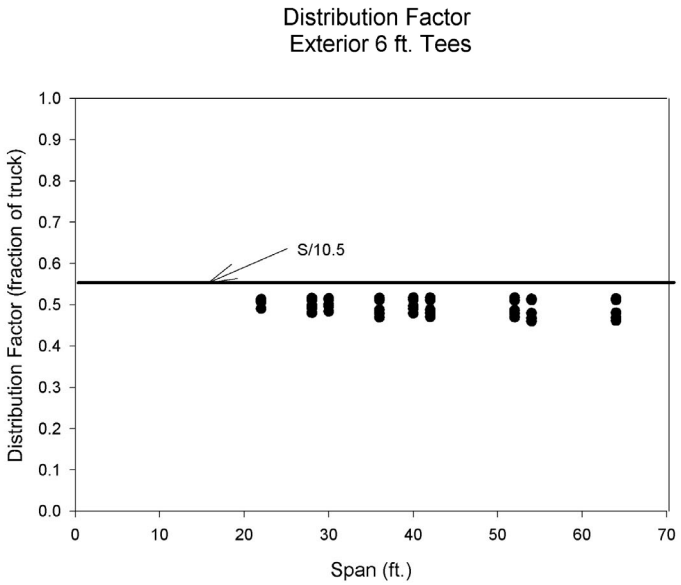

Figure 68. Load Distribution Factor for Exterior 6 ft. Tees.

Table 23. Computed Lateral Distribution Factors.

					Lateral Distribution Factor (fraction of truck)				Lateral Distribution Factor - S/xx.x Form			
Roadway Width (ft.)	Span Length (ft.)	Nominal Tee Depth (in.)	Number Traffic Lanes	Beam Layout	Beam Number 1	Beam Number 2	Beam Number 3	Beam Number 4	Beam 1	Beam 2	Beam 3	Beam 4
									xx.x Values			
24	22	22	2	6-7-7-6	0.51398	0.62263			11.7	11.2		
24	28	22	2	6-7-7-6	0.51654	0.58764			11.6	11.9		
24	36	22	2	6-7-7-6	0.51663	0.56158			11.6	12.5		
24	30	28	2	6-7-7-6	0.51588	0.59855			11.6	11.7		
24	42	28	2	6-7-7-6	0.51740	0.56220			11.6	12.5		
24	54	28	2	6-7-7-6	0.51451	0.54471			11.7	12.9		
24	40	36	2	6-7-7-6	0.51745	0.58510			11.6	12.0		
24	52	36	2	6-7-7-6	0.51767	0.55974			11.6	12.5		
24	64	36	2	6-7-7-6	0.51526	0.54619			11.6	12.8		
28	22	22	2	6-6-6-6-6	0.49114	0.50592	0.59901		12.2	11.9	10.0	
28	28	22	2	6-6-6-6-6	0.48065	0.47984	0.54910		12.5	12.5	10.9	
28	36	22	2	6-6-6-6-6	0.46979	0.45830	0.50289		12.8	13.1	11.9	
28	30	28	2	6-6-6-6-6	0.48408	0.48757	0.56596		12.4	12.3	10.6	
28	42	28	2	6-6-6-6-6	0.47092	0.45858	0.50651		12.7	13.1	11.8	
28	54	28	2	6-6-6-6-6	0.46022	0.44242	0.47145		13.0	13.6	12.7	
28	40	36	2	6-6-6-6-6	0.47956	0.47609	0.54292		12.5	12.6	11.1	
28	52	36	2	6-6-6-6-6	0.47013	0.45583	0.50037		12.8	13.2	12.0	
28	64	36	2	6-6-6-6-6	0.46183	0.44335	0.47310		13.0	13.5	12.7	
30	22	22	2	6-7-6-7-6	0.50677	0.58666	0.64640		11.8	11.9	9.3	
30	28	22	2	6-7-6-7-6	0.49273	0.53844	0.58393		12.2	13.0	10.3	
30	36	22	2	6-7-6-7-6	0.47951	0.50303	0.52581		12.5	13.9	11.4	
30	30	28	2	6-7-6-7-6	0.49676	0.54916	0.60463		12.1	12.7	9.9	
30	42	28	2	6-7-6-7-6	0.48045	0.50298	0.52969		12.5	13.9	11.3	
30	54	28	2	6-7-6-7-6	0.46770	0.47719	0.48491		12.8	14.7	12.4	
30	40	36	2	6-7-6-7-6	0.49087	0.52696	0.57612		12.2	13.3	10.4	
30	52	36	2	6-7-6-7-6	0.47925	0.49638	0.52201		12.5	14.1	11.5	
30	64	36	2	6-7-6-7-6	0.46939	0.47716	0.48707		12.8	14.7	12.3	
38	22	22	3	6-7-7-7-7-6	0.51280	0.62263	0.63672		11.7	11.2	11.0	
38	28	22	3	6-7-7-7-7-6	0.51234	0.58590	0.61522		11.7	11.9	11.4	

Table 23. Computed Lateral Distribution Factors (continued).

					Lateral Distribution Factor (fraction of truck)				Lateral Distribution Factor - S/xx.x Form			
Roadway Width (ft.)	Span Length (ft.)	Nominal Tee Depth (in.)	Number Traffic Lanes	Beam Layout	Beam Number 1	Beam Number 2	Beam Number 3	Beam Number 4	Beam 1	Beam 2	Beam 3	Beam 4
									xx.x Values			
38	36	22	3	6-7-7-7-7-6	0.51177	0.56293	0.59120		11.7	12.4	11.8	
38	30	28	3	6-7-7-7-7-6	0.51265	0.59454	0.62481		11.7	11.8	11.2	
38	42	28	3	6-7-7-7-7-6	0.51146	0.56187	0.59468		11.7	12.5	11.8	
38	54	28	3	6-7-7-7-7-6	0.51163	0.54731	0.57170		11.7	12.8	12.2	
38	40	36	3	6-7-7-7-7-6	0.51300	0.58083	0.61809		11.7	12.1	11.3	
38	52	36	3	6-7-7-7-7-6	0.51141	0.55912	0.59333		11.7	12.5	11.8	
38	64	36	3	6-7-7-7-7-6	0.51172	0.54815	0.57466		11.7	12.8	12.2	
44	22	22	3	6-7-7-6-7-7-6	0.50905	0.61704	0.67561	0.52007	11.8	11.3	10.4	11.5
44	28	22	3	6-7-7-6-7-7-6	0.49808	0.56106	0.62274	0.52219	12.0	12.5	11.2	11.5
44	36	22	3	6-7-7-6-7-7-6	0.48806	0.52603	0.57599	0.50821	12.3	13.3	12.2	11.8
44	30	28	3	6-7-7-6-7-7-6	0.50144	0.57387	0.63800	0.52705	12.0	12.2	11.0	11.4
44	42	28	3	6-7-7-6-7-7-6	0.48841	0.52447	0.57822	0.51294	12.3	13.3	12.1	11.7
44	54	28	3	6-7-7-6-7-7-6	0.48014	0.50317	0.54254	0.49364	12.5	13.9	12.9	12.2
44	40	36	3	6-7-7-6-7-7-6	0.49716	0.54846	0.61350	0.52713	12.1	12.8	11.4	11.4
44	52	36	3	6-7-7-6-7-7-6	0.48726	0.51763	0.57162	0.51265	12.3	13.5	12.2	11.7
44	64	36	3	6-7-7-6-7-7-6	0.48105	0.50173	0.54337	0.49606	12.5	14.0	12.9	12.1

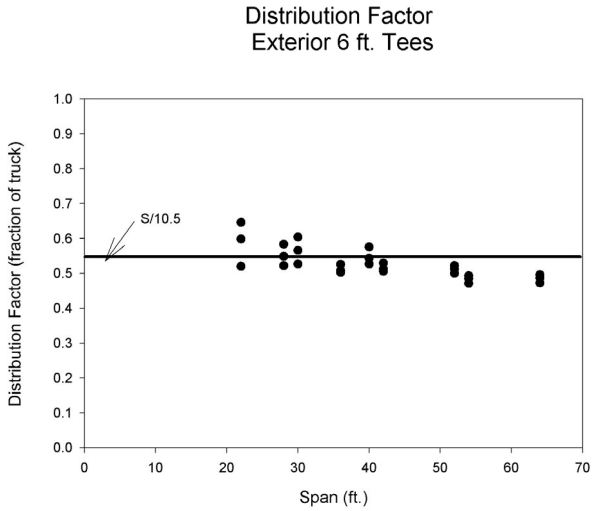

Figure 69. Load Distribution Factor for Interior 6 ft. Tees.

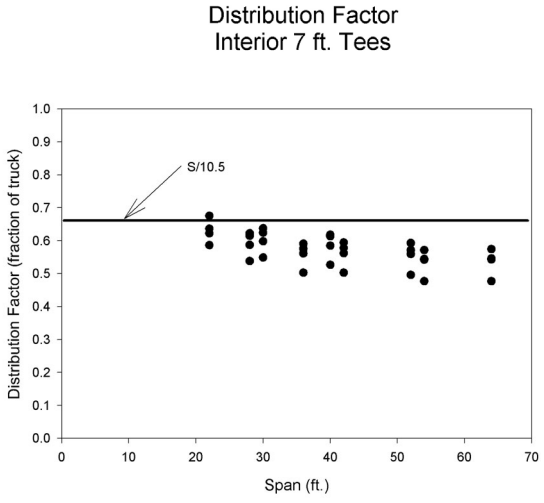

Figure 70. Load Distribution Factor for Interior 7 ft. Tees.

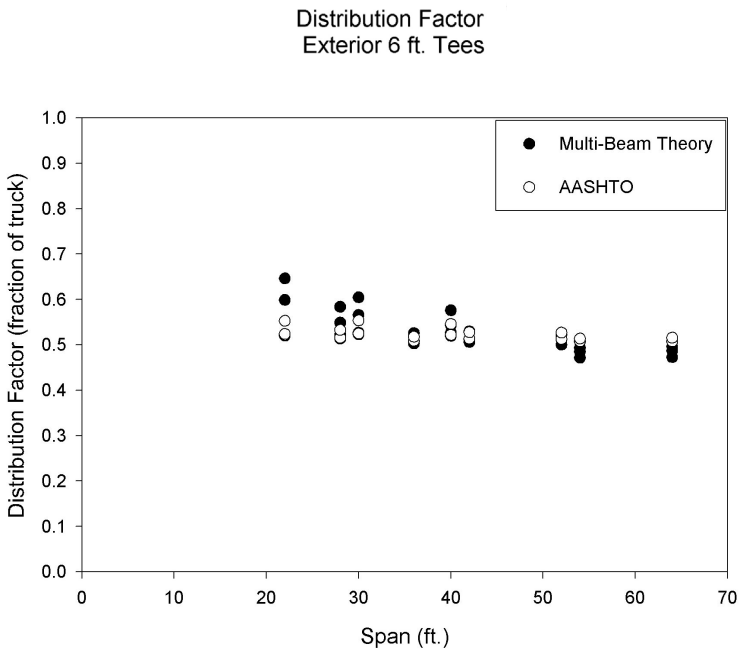

Figure 71. Comparison of AASHTO and Multi-Beam Theory Distribution Factors.

interior beams are used in spans shorter than 40 ft. In this case, the factor S/9.5 appears more reasonable.

LATERAL CONNECTION DESIGN FORCES

The lateral connection between the flanges of adjacent tees consists of a welded bar and embedded plate segment, and continuous, grouted shear key. The bar/plate discrete connection, which is spaced at 5 ft. intervals, will, in the multi-beam bridge model, develop the four force components introduced in Fig. 49 and repeated for clarity in Fig. 72. The continuous shear key portion of the lateral connection lying between the bar/plate locations is also modeled with the springs shown in Fig. 50 by lumping the stiffnesses of a 1 ft. length of key into the spring stiffnesses at points spaced at 12 in. intervals along the flange edge. The four force components are displayed in Fig. 73. Thus, the idealized lateral connection between adjacent tee flanges would consist of spring sets like those in Fig. 50 located every 12 in. along the flange, plus

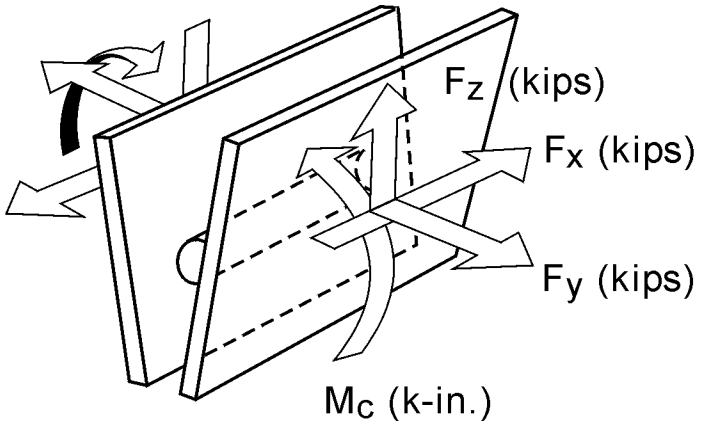

Figure 72. Force Components in Bar/Plate Discrete Connection.

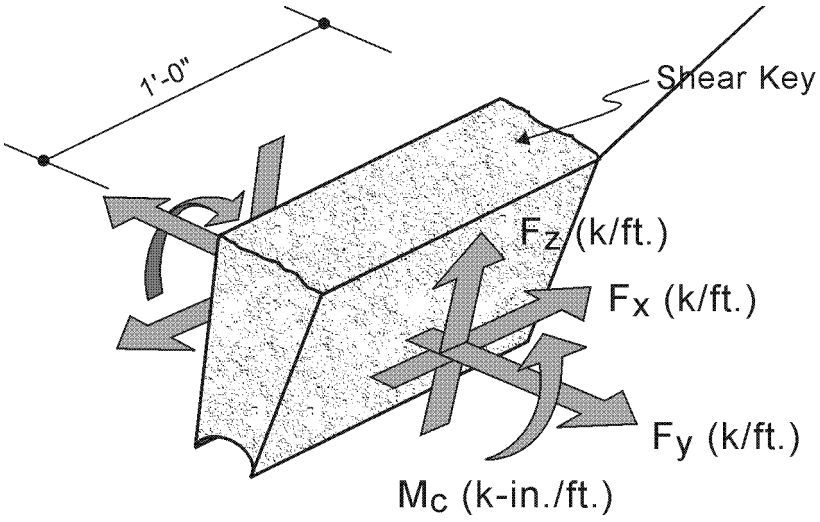

Figure 73. Force Components in Shear Key.

additional spring sets located every 5 ft. to mimic the bar/plate connection. The stiffnesses assigned to the two types of connecting elements would of course be different.

Figure 74 is a plot showing the typical variation of the moment component M_c of shear key force in Fig. 73, along the length of the span, while Fig. 75 shows the variation of F_z. The results are taken from the analysis of a 24 ft. roadway with 28 in. deep tees and 42 ft. span (see Table 21) with single HS-20 truck positioned on beam 2 as shown. Edge 1 refers to the joint between beams 1 and 2. As these plots suggest, the extreme value of transverse moment M_c on the shear key occurs around mid-span, while substantial shears on the key are found at the ends of the bridge and near wheel loads.

Forces in the bar/plate connection as well as in the shear key are dependent upon the placement of load, and an important question was what truck(s) positions lead to the largest possible connection forces. Numerical experimentation with various bridges from Tables 21 and 22 leads to the following observations:

(1) a 16 kip wheel must be adjacent to the bar/plate (discrete) connection or shear key location where maximum forces are sought,

(2) discrete connections closest to mid-span of the bridge and shear key zones at mid-span develop the largest forces,

(3) the wider the two beams connected, the greater the connection and shear key forces developed,

(4) placing two or more trucks on a structure produce connection forces negligibly larger than those resulting from a single well-placed truck,

(5) force components F_x and F_y are small in a double tee bridge.

Using these guidelines, representative structures were selected from among the 45 cases listed in Tables 21 and 22 and analyzed for maximum connection force. The results are summarized in Table 24. These same results are plotted in Figs. 76 through 79. Examination of these figures suggests the force components developed in both the shear key and the bar/plate connection are relatively small. For the range of conditions examined, recommended design forces in the shear key and the plate/bar connection should be taken as follows in Table 25.

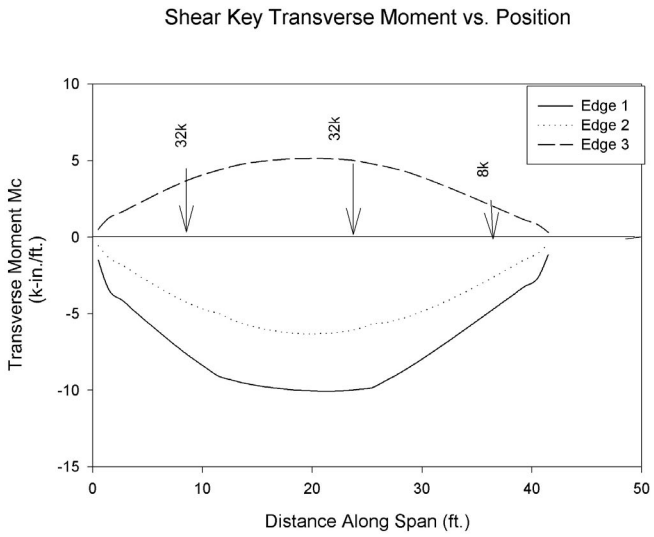

Figure 74. Shear Key Moment M_c along Span.

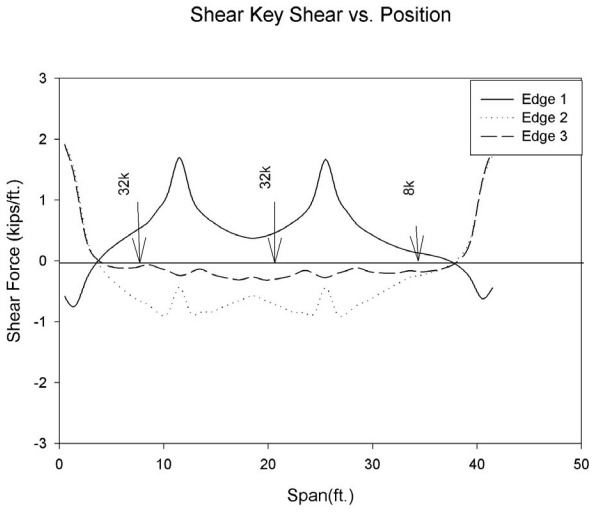

Figure 75. Shear Key Shear F_z along Span.

Table 24. Maximum Connection and Shear Key Forces.

Bridge Configuration	Tee Depth (in.)	Span Length (in.)	Maximum Connection Forces			Maximum Shear Key Forces		
			Mc (k-in.)	Fz (kips)	Fy (kips)	Mc (k-in)/ft.	Fz (kips/ft.)	Fy (kips/ft.)
6-7-6-7-6	22	28	0.063	0.80	0.101	8.0	1.69	0.10
6-7-6-7-6	36	64	0.198	0.60	0.080	12.4	1.28	0.34
6-7-6-7-6	28	42	0.167	0.37	0.115	10.5	1.65	0.13
6-7-7-6	22	28	0.125	0.80	0.096	7.8	1.70	0.10
6-7-7-6	28	42	0.160	0.37	0.113	10.1	1.70	0.12
6-7-7-6	36	64	0.193	0.61	0.067	12.0	1.29	0.09
6-7-7-7-7-6	22	28	0.132	0.83	0.102	8.3	1.77	0.10
6-7-7-7-7-6	28	42	0.189	0.64	0.123	11.9	1.48	0.20
6-7-7-7-7-6	36	64	0.226	0.48	0.152	14.3	1.19	0.11

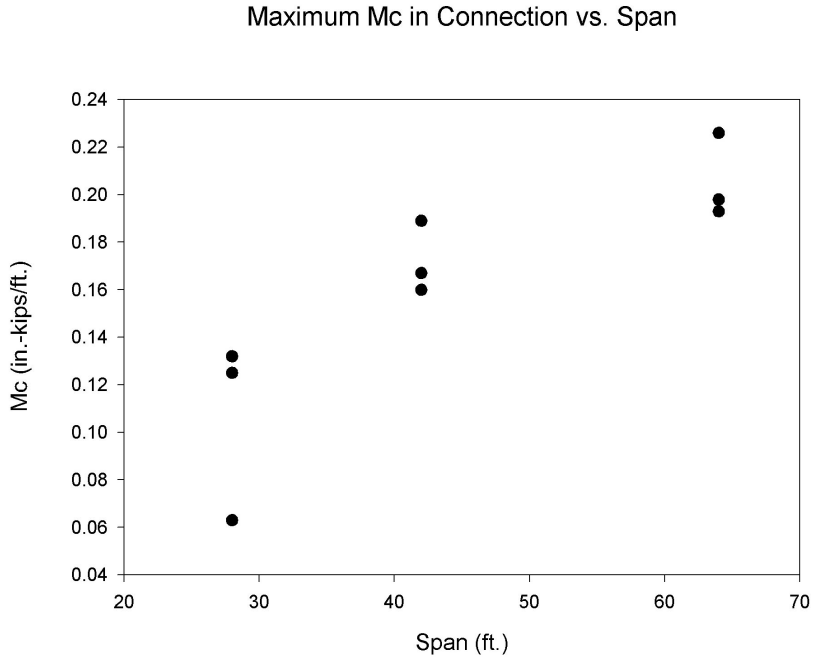

Figure 76. Maximum M_c in Connection Versus Span.

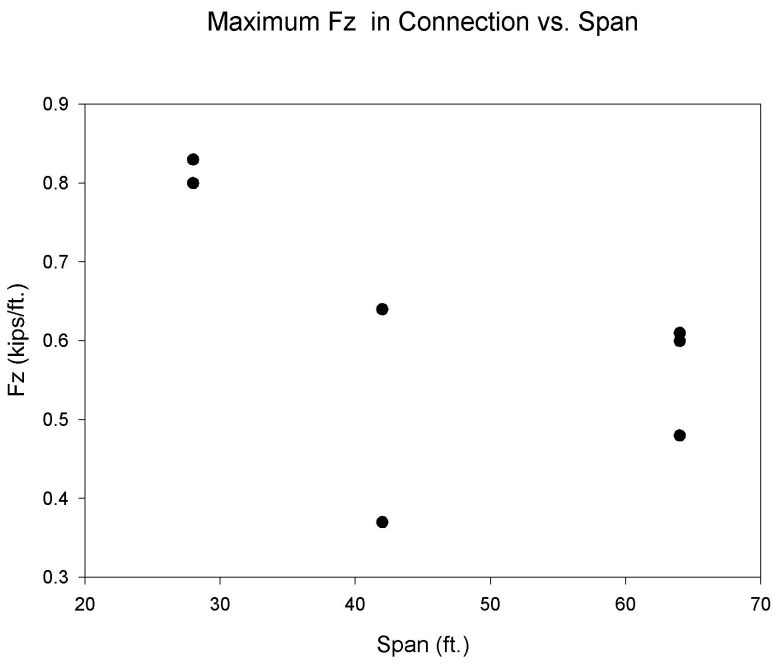

Figure 77. Maximum F_z in Connection Versus Span.

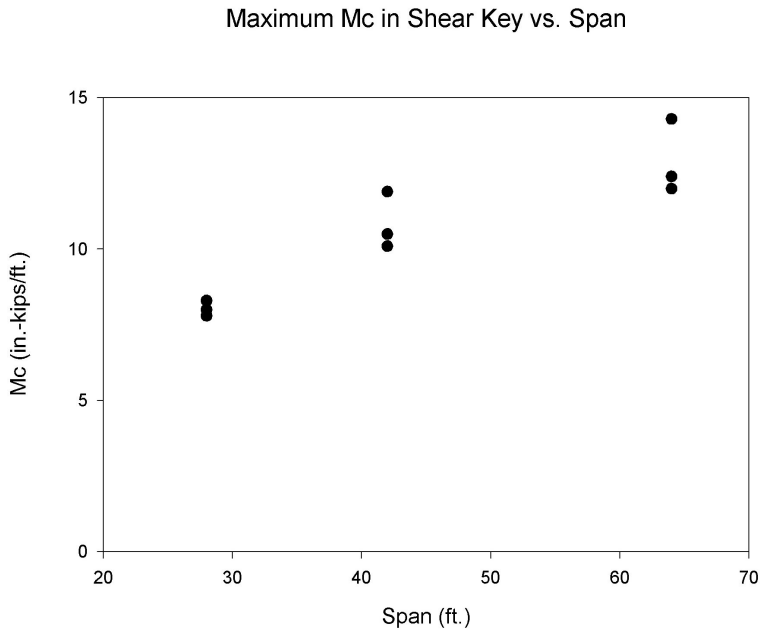

Figure 78. Maximum M_c in Shear Key Versus Span.

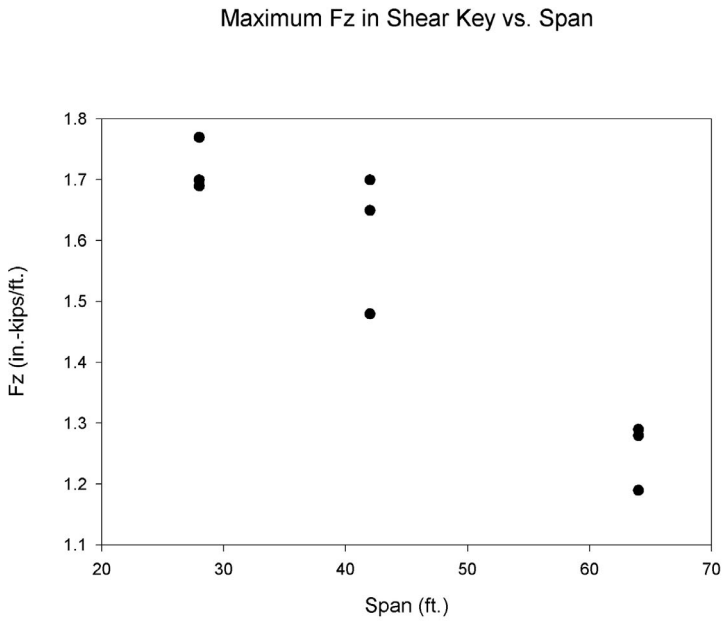

Figure 79. Maximum F_z in Shear Key Versus Span.

Table 25. Recommended Connection and Shear Key Design Forces.

	M_c	F_z	F_x	F_y
Shear Key	15 kip-in./ft.	1.8 kips/ft.	Negligible	Negligible
Bar/Plate	0.25 kip-in./ft.	0.9 kips/ft.	Negligible	Negligible

REFERENCES

American Association of State Highway and Transportation Officials, *Standard Specifications for Highway Bridges,* 14th Edition, 1986.

Arockiasamy, M., Badve, A. P., Rao, B. V., and Reddy, D. V., *Fatigue Strength of Joints in a Precast Prestressed Concrete Double Tee Bridge,* PCI Journal, January-February, 1991.

Cotham, J., *Double Tee Field Survey*, Internal Report, Design Division, TxDOT, 1997.

Duberg, J. E., Khachaturian, N., and Fradinger, R. E., *Method for Analysis of Multibeam Bridges*, Journal of the Structural Division, American Society of Civil Engineers, July 1960.

El Shahawy, M., *Feasibility Study of Transversely Prestressed Double Tee Bridges*, PCI Journal, September-October, 1990.

El Shahawy, M., and Issa, M., *Load Testing of Transversely Prestressed Double Tee Bridges,* PCI Journal, March-April, 1992.

Jones, H. L., *Multi-Box Beam Bridges with Composite Deck,* TTI Final Report 0-1709, April 1999.

Jones, H. L., and Boaz, I. B., *Skewed Discretely Connected Multi-Beam Bridges*, Journal of Structural Engineering, American Society of Civil Engineers, February 1986.

Martin, L. D., and Osburn, A. E. N., *Connections for Modular Precast Concrete Bridge Decks,* Federal Highway Administration, Report FHWA/RD-12/106, 1983.

PCI Committee on Connection Design, *Standard Precast Connections,* PCI Journal, July-August, 1998.

Powell, G. H., Ghose, A., and Buckle, I. G., *Analysis of Multibeam Bridges*, Journal of the Structural Division, American Society of Civil Engineers, September 1969.

Przemieniecki, J. S., *Theory of Matrix Structural Analysis,* McGraw-Hill, New York, 1968.

Stanton, J. F., and Mattock, A. H., *Load Distribution and Connection Design for Precast Stemmed Multibeam Bridge Superstructures*, NCHRP Report 287, Transportation Research Board, November 1986.